CCMS-92-16
VPI-E-92-15

CENTER FOR COMPOSITE MATERIALS AND STRUCTURES

IN-24-CR
10 54
P. 169

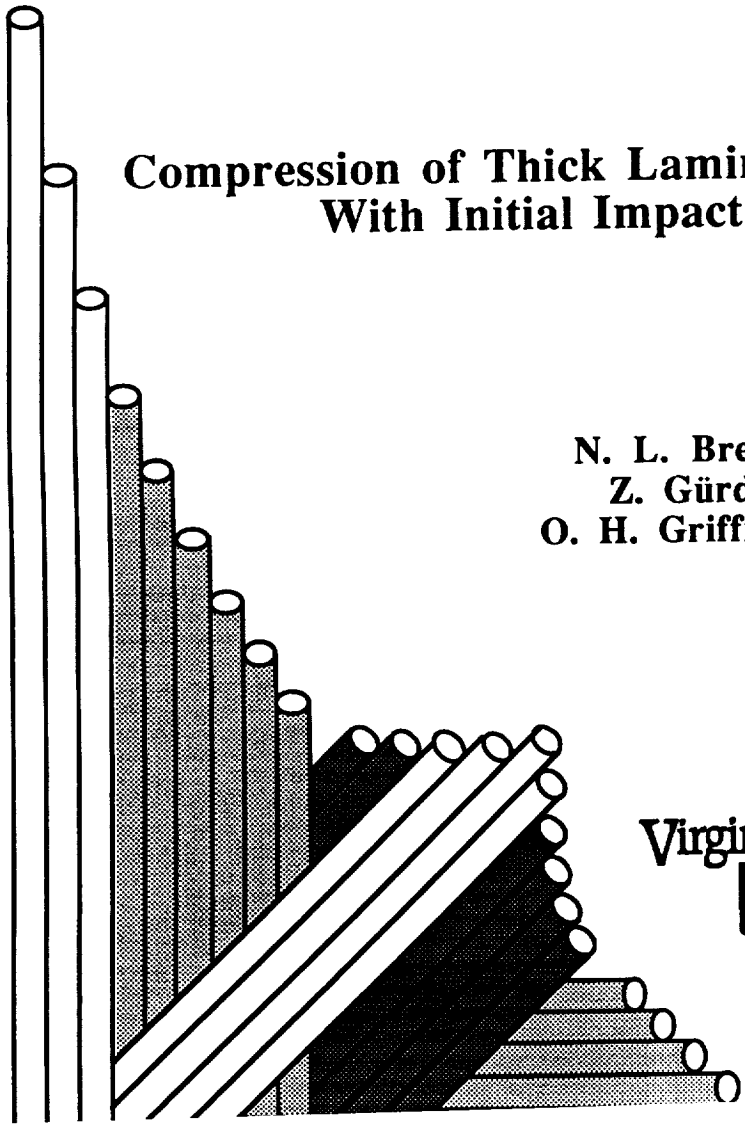

Compression of Thick Laminated Composite Beams With Initial Impact-Like Damage

N. L. Breivik
Z. Gürdal
O. H. Griffin, Jr.

Virginia Tech
VIRGINIA POLYTECHNIC INSTITUTE AND STATE UNIVERSITY

BLACKSBURG, VIRGINIA
24061

June 1992

College of Engineering
Virginia Polytechnic Institute and State University
Blacksburg, Virginia 24061

June 1992

VPI-E-92-15
CCMS-92-16

Compression of Thick Laminated Composite Beams With Initial Impact-Like Damage

N.L. Breivik[1]
Z. Gürdal[2]
O.H. Griffin, Jr.[3]

Performance period:
January 1990-December 1991

Grant: NAG-1-343

Prepared for: Mechanics of Materials Branch
National Aeronautics and Space Administration
Langley Research Center
Hampton, VA 23665-5225

---

[1] Graduate Student, Department of Engineering Science and Mechanics
Virginia Polytechnic Institute and State University

[2] Associate Professor, Department of Engineering Science and Mechanics
Virginia Polytechnic Institute and State University

[3] Associate Professor, Department of Engineering Science and Mechanics
Virginia Polytechnic Institute and State University

Compression of

Thick Laminated Composite Beams

With Initial Impact-Like Damage

ABSTRACT

While the study of compression after impact of laminated composites has been under consideration for many years, the complexity of the damage initiated by low velocity impact has not lent itself to simple predictive models for compression strength. The damage modes due to non-penetrating, low velocity impact by large diameter objects can be simulated using quasi-static three-point bending. The resulting damage modes are less coupled and more easily characterized than actual impact damage modes.

This study includes the compression testing of specimens with well documented initial damage states obtained from three-point bend testing. Compression strengths and failure modes were obtained for quasi-isotropic stacking sequences from 0.24 to1.1 inches thick with both grouped and interspersed ply stacking. Initial damage prior to compression testing was divided into four classifications based on the type, extent, and location of the damage. These classifications are multiple through-thickness delaminations, isolated delaminations, damage near the surface, and matrix cracks. Specimens from each classification were compared to specimens tested without initial damage in order to determine the effects of the initial damage on the final compression strength and failure modes. A finite element analysis was used to aid in the understanding and explanation of the experimental results.

It was found that specimens with multiple through-thickness delaminations experienced the greatest reduction in compression strength, from 50 to 75% below the strength of undamaged specimens. All the sublaminates formed by the delaminations failed at the same time. Individual sublaminate buckling was observed for isolated delaminations near the surface of the laminate.

Delaminations far from the specimen surface had little effect on the final compression strength. Damage occurring in the outside 0° plies caused a 10 to 20% strength reduction according to both analytical and experimental results. The effects of increased interlaminar stresses near the specimen edges caused a reduction in undamaged strength of $[0_5/45_5/-45_5/90_5]_{5s}$ specimens, while having little effect on the $[0_5/60_5/-60_5]_{7s}$ specimens.

Acknowledgements

This study was supported by grant NAG-1-343 as part of the NASA-Virginia Tech Composites Program. Support was provided through the Mechanics of Materials Branch at NASA-Langley Research Center under the guidance of grant monitor C.C. Poe Jr. Additional assistance was provided by Marc Portanova and Dr. John Masters. Tracy Bridges was instrumental in running the experiments.

Table of Contents

List of Figures

List of Tables

Chapter 1
Introduction

Composite laminates subjected to low velocity impact often develop damage which cannot be detected with visual inspection of the impact surface. Damage modes from non-penetrating low velocity impact by large diameter objects include combinations of fiber breaks, matrix cracks, and delaminations throughout the thickness of the material. The types of damage which occur in low velocity impact can be simulated using quasi-static loading, which results in damage modes which are less coupled and more easily characterized than low velocity impact damage. Of particular interest for laminated composite structures subjected to low velocity impact is the subsequent reduction in their compressive strength. By studying compression of specimens with well documented damage modes such as those induced by quasi-static loading, insight can be gained into the more complex problem of compression after impact.

This study is an extension of the work by Starbuck et al. [1] on the damage characterization of three-point bend beam specimens under quasi-static loading. The goal of that project was to develop a better understanding of damage states and damage susceptibility based on a combined experimental/analytical program. The objective also included the investigation of

damage tolerance, defined for that study to be the ability of the structure to carry the same type of load beyond the point at which some form of damage initiates. The analytical objective was to develop the necessary analytical tools to determine the sublaminate stress states near points of concentrated loading that were likely to initiate damage. The experimental objective, meanwhile, was to identify damage modes and damage initiation loads from an extensive testing program, which would also be used to verify the analysis.

The laminated beams that were used in the experimental study included various thicknesses, support spans, and lamination sequences. Additionally, grouped ply stacking sequences, consisting of 5 plies of the same angular orientation adjacent to each other, were compared to interspersed stacking sequences, where each adjacent ply has a different angular orientation. Experiments were conducted to determine both the final failure load and the load at which damage first initiated. Visual inspection was used to identify the damage modes for both specimens with initial damage only and failed specimens. A linear elastic solution based on a generalized plane deformation assumption was used to determine the stress distributions in the laminated beams. An elliptical traction distribution was used to model the contact at the load nose and support points.

Analytical results indicated that displacements and ply-level stress distributions were significantly affected by fiber orientation, length-to-depth aspect ratio, and whether a grouped or interspersed stacking sequence was used. Analysis was also used to predict damage initiation loads based on the four classifications of initial damage and failure criteria shown in Table 1.1. The coordinate axes according to Starbuck et al. are shown in Figure 1.1. In addition to the damage mode identification, experimental results also included observations on the damage susceptibility of the specimens. The quasi-isotropic [0/±45/90] type stacking sequences were found to be less damage tolerant than the [0/±60] type laminates. Likewise,

Table 1.1 - Initial damage modes according to Starbuck et al. [1]

Initial Damage Mode	Specimens Affected	Failure Criterion
crushing	aspect ratios < 1.0 in.	max. contact pressure
tensile or fiber breakage	0.24 in. thick specimens with 3.0 or 5.5 in. spans	max. tensile bending stress, back 0° plies
delamination	large aspect ratios, interspersed stacking	max. shear stress τ_{xz}, with consideration of compression normal stress
matrix cracking	grouped stacking	max. shear stress, xz plane

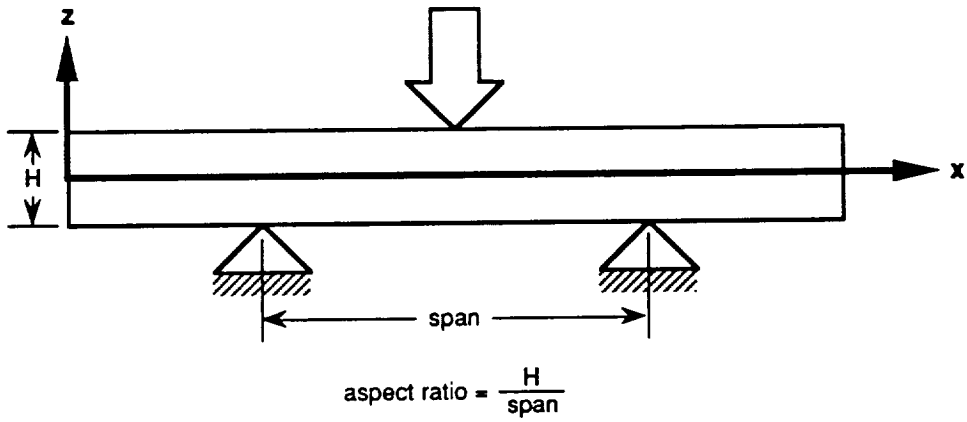

Figure 1.1 - Coordinate axes and specimen dimensions according to Starbuck et al. [1]

the grouped sequences were more susceptible to damage than the interspersed sequences. The linear elastic analysis predicted ply level stresses up to the load at which damage was initiated, but could not be used to predict damage tolerance and final specimen failure.

1.1 Objectives

The main objective of this project was to evaluate the effects of isolated damage modes on the compressive strengths and failure characteristics of laminated composite test specimens using an experimental and numerical approach. Most of the specimens were obtained from an earlier study on the damage characteristics of three-point bending [1]. Although Starbuck [1] examined the specimens and identified damage trends, more detailed damage descriptions were required for the present work. The first goal of the present study was to accurately identify and classify the damage states present in the specimens as obtained from Starbuck. Upon further examination, these specimens were found to have isolated damage modes which varied according to the type, location, and quantity of damage. These damages are hereafter referred to as initial damage states or classifications. The specimens were of various thicknesses ranging from 0.24 to 1.1 inches with quasi-isotropic stacking sequences of $[0/\pm60]_{ns}$, $[0/\pm45/90]_{ns}$, $[0_5/60_5/-60_5]_{7s}$ or $[0_5/45_5/-45_5/90_5]_{5s}$. Experimental determination of the compression strength was sought as a function of initial damage classification. Specifically, a relationship was sought between the mode and extent of initial damage, and the compression strength and failure mode. Numerical work in the form of finite element analysis was conducted to aid in the understanding of the experimental results.

1.2 Approach

The approach centered on an experimental program for compression testing of the initially damaged specimens, with supplemental analysis and literature review as needed to understand and interpret the experimental results.

A survey of the appropriate literature appears in Chapter 2. The topics covered include compression test fixtures, compression failure theories, experimental compression after impact work, and both experimental and analytical work on compression with initial damage. The procedure for the three-point bend testing conducted by Starbuck is reviewed in Chapter 3, which also includes the documentation of initial damage states and the selection of an appropriate compression test fixture and test method. Chapter 4 includes the experimental results, categorized according to the initial damage modes. These modes include multiple through-thickness delaminations, isolated delaminations, damage near the surface, and matrix cracks in grouped ply laminates. Numerical work is described in Chapter 5 beginning with a brief explanation of the finite element assumptions, initial damage representation, and applied failure criteria. The balance of the chapter is broken into two main sections. The first of these one addresses the problem of compression with initial damage in the form of isolated delaminations. The second focuses on the comparison between grouped and interspersed stacking sequences. The experimental and numerical work is summarized with the major conclusions of the project in Chapter 6.

Chapter 2
Literature Survey

Because this study involves aspects of many different topics in the mechanics of composites, the relevant literature also covers a variety of areas. Among these areas are the general topics of compression testing, compression failure theories, compression after impact testing, and analysis of compression response of composites with simulated damage. Although no attempt has been made to include all the papers on each of these subjects, the following represents the publications that relate most closely to the objectives of this study. A more complete review of compression test methods and compression failure theories was conducted by Camponeschi [2]. The review of compression failure theories by Shuart [3] is also very thorough for work prior to 1985.

2.1 Compression Testing

2.1.1 Fixture Designs

Numerous methods of compression testing are currently in use for composite laminates depending on the particular application. The basic types of compression testing include the sandwich beam method, side-face loaded method, end loaded method, and special purpose methods [4,5]. The different methods have evolved due to efforts to find a compressive strength for composite laminates as well as efforts to characterize compressive material properties in a reliable and efficient manner.

The sandwich beam compression test method is recognized by ASTM Standard D3410 [6] as a method to determine compressive material properties of unidirectional composite laminates. A composite specimen is used as the top face plate in a three part sandwich that includes a honeycomb core (hexagonal aluminum) and a back face made of some other material. The material for the back face is chosen such that the composite specimen will fail in compression before the back face fails. The specific material for the back face is not specified, although a thickness approximately twice that of the composite face plate is recommended. The basic concept of the sandwich test is to load this sandwich in four-point bending such that the composite specimen will be in compression between the two innermost load points. A schematic of a typical configuration is shown in Figure 2.1. The specimen size (top face plate)

as specified by ASTM Standard D3410 is a length of 22.0 inches, a width of 1.0 inch, and a thickness of 6 plies.

The other two recognized compression tests for material classification in ASTM Standard D3410 [6] use the side-face or shear loaded method [4,5]. A side-face or shear loaded method is characterized by load introduction to the specimen through of a pair of grips which hold the faces of the specimen at both ends. These grips are then restricted to remain aligned with respect to each other as they are brought together under compression loading. Due to the nature of the grips, the specimens must be protected from damage to their faces. Tabs are adhesively bonded to the specimens at each end with the gap between the grips becoming the effective gage length of the specimen. The two fixtures from ASTM Standard D3410 specify strict specimen dimensions. The total specimen length is 5.5 inches with a 0.5 inch gage length between tabs. The width of the specimen can range from 0.25 to 1.5 inches, depending of the fixture used. Thickness of the specimen is not specifically stated, however the total thickness of the specimen and tabs is restricted to 0.157 inches.

There is no recognized standard for end loaded compression test fixtures, although many are used for a variety of applications. A modified version of the method described in ASTM Standard D695 for the testing of plastics has been used by Boeing for material characterization [4,5]. This configuration requires end tabs to prevent brooming when testing to find the compressive strength. Since the specified gage length of 0.188 inches is so short, strain gage instrumentation cannot be used with end tabs. Therefore, to find material properties a test must be conducted without the end tabs and then stopped prior to end brooming.

Another end loading fixture, designed and used by Adams [4,7], is the Wyoming End-Loaded, Side Support (ELSS) fixture which uses an untabbed specimen. A pair of steel blocks bolted to each end of the specimen prevent buckling and end brooming, as shown in Figure 2.2. Flat

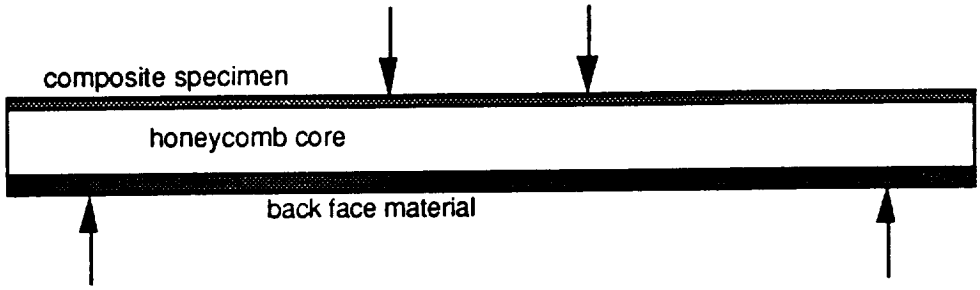

Figure 2.1 - Sandwich beam compression test configuration, ASTM Standard D3410 [6]

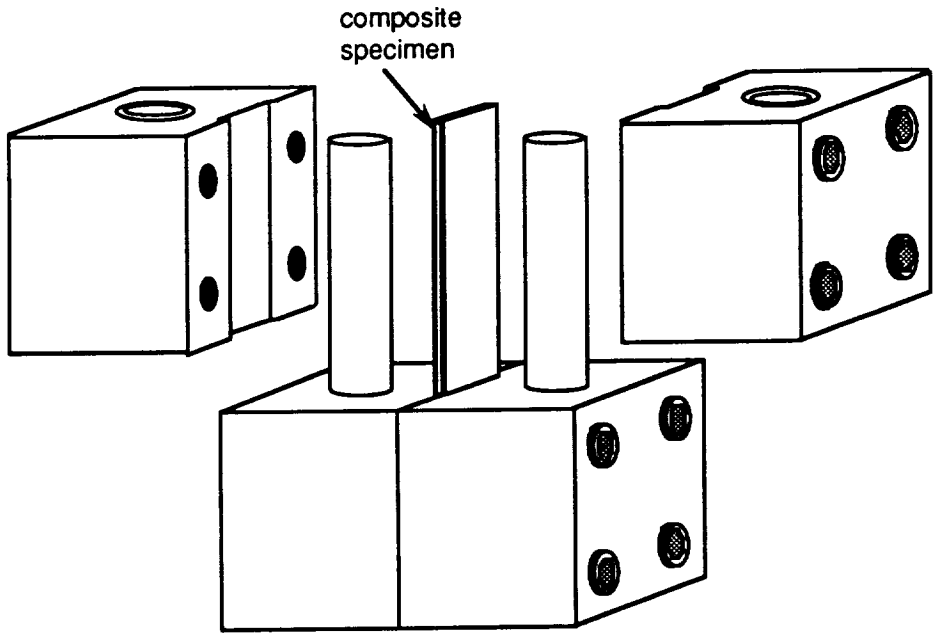

Figure 2.2 - Wyoming End-Loaded, Side-Support compression test fixture

steel platens are placed on both the top and bottom of the fixture to provide load bearing surfaces for the load frame. The specimen fits into a pair of grooves in the steel blocks which determine the specimen thickness and provide support to the sides of the specimen within the grips. The intended thickness is on the same order as the standard side-loaded (shear loaded) methods, with a total specimen length of 5.5 inches and a width of 0.5 inches. Specimen gage length is specified as 0.5 inches but may be varied from zero to 1.0 inches by changing the overall length of the specimen.

An end loaded fixture used at NASA-Langley Research Center [8] allows for specimens of different widths. This fixture consists of a pair of steel blocks to which the untabbed ends of the specimen are anchored. The blocks provide support to the front and back faces of the specimen and thus prevent failure by end brooming. The blocks are placed in a guide cylinder for alignment. Specimen length for the fixture is 1.5 inches with an unsupported gage length of 0.5 inches and a thickness equivalent to 16 plies of T300/5208 graphite/epoxy.

A modification of the NASA end-loaded fixture by Gürdal and Starbuck [9], shown in Figure 2.3, incorporates three important improvements. The first difference is that this modified fixture can accommodate specimens of different thicknesses by adding or subtracting shims located in the fixture grips at the ends of the specimen. These shims allow the specimen to be aligned directly under the load application even for different thickness specimens. Secondly, the boundary conditions at the ends are changed by creating a radius that slopes toward the specimen, thereby reducing the stress concentration due to Poisson expansion at the grips. Additionally, quarter-circle side supports the same thickness as the specimen are placed between the fixture grips to prevent expansion of the specimen in the width direction. Finally, side support pins are included so that longer specimens can be tested without buckling. Typical specimen

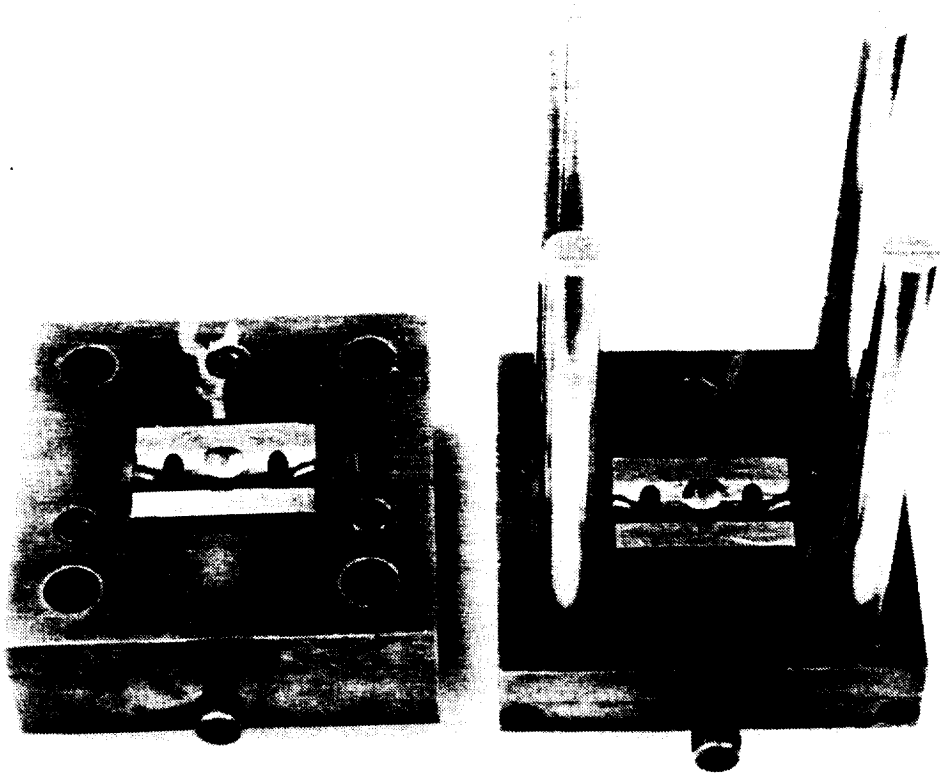

Figure 2.3 - Compression test fixture by Gürdal and Starbuck [9]

dimensions are 0.75 to1.0 inches wide by 1.5 inches long by 0.04 to 0.1 inches thick. The unsupported gage length is approximately the same as the specimen length.

The short block compression fixture shown in Figure 2.4 can also be used for specimens of different thickness. This simple fixture requires specimens to be of sufficient thickness, length, and width to prevent global buckling [10]. The fixture consists of a pair of flat platens with an adjustable width groove that secures the ends of the untabbed specimen. By using larger specimens, additional room is available for strain gages. A typical specimen size for this fixture is 1.75 inches long by 1.5 inches wide by 0.24 inches thick. Unlike many of the other fixtures mentioned, this fixture does not incorporate a means of alignment for either the fixture or the specimen. Thus, strain gages and other instrumentation are generally employed to assure proper specimen alignment with respect to the axis of loading.

A fixture designed by Camponeschi [2] specifically for the testing of thick section composites ranging from 0.25 to 1.0 inches thick, is shown in Figure 2.5. This fixture is based on the Wyoming End-Loaded, Side Support fixture discussed previously for the testing of 0.1 inch thick specimens. Steel blocks were again used to grip the top and bottom of the specimen, with flat steel platens inserted above and below the blocks to be used as load bearing surfaces. Because of the interlocking shape of the blocks, the specimens were supported on all four sides inside the grips. Camponeschi used tabbed specimens in order to retain similarity with the requirements of the fixtures in ASTM Standard D3410-87. Specimen geometries were designed to keep constant ratios of thickness to gage length and thickness to tab length. In order to accommodate these different specimen sizes, different fixtures were built and scaled accordingly. Alignment rods were not included in the design because the specimens were believed to be of sufficient thickness to provide stability for both the specimen and the fixture.

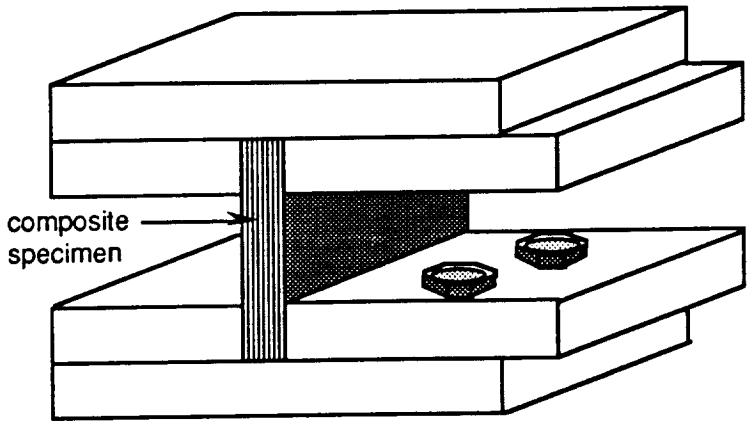

Figure 2.4 - End loaded, short block compression fixture, Shuart [10]

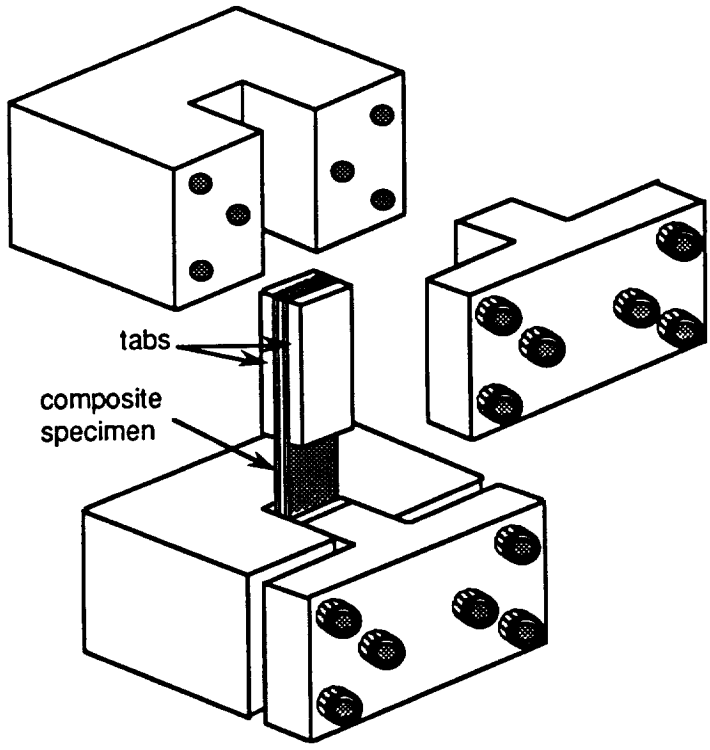

Figure 2.5 - End loaded fixture for thick section composites, Camponeschi [2]

Alignment of the specimen with respect to the loading axis was achieved by placing a self aligning spherical seat between the bottom platen and the load frame.

2.1.2 Specimen Geometry

Various studies have been conducted to study the effects of specimen length [11,12] and thickness [2] on compression strength. These studies have shown the importance of specimen geometry as it relates to ultimate compression strength.

A study conducted by Adams and Lewis [11] used 20-ply, unidirectional, AS4/3501-6, graphite/epoxy specimens to determine the effects of specimen gage length over a wide range of values. When specimen thickness is less than the specimen width, the slenderness ratio is defined as the ratio of gage length to width. No specimens with a thickness greater than the specimen width were tested. The compressive strength was found to be constant over a wide range of slenderness ratios, provided the specimen did not buckle globally. However, as the gage length was decreased to a level where the ratio of gage length to thickness was approximately equal to 1.0, compression strength decreased by 10-13%.

A similar study by Smoot [12] also showed an approximately constant compression strength when the slenderness ratio was below the value at which global buckling occurred. By varying the specimen gage length while holding the width and thickness constant, specimens were tested with slenderness ratios ranging from 15.2 to 163.2. The unidirectional specimens were made from AS1/3501-6 graphite/epoxy with a width of 0.25 inches and a thickness of 0.07 inches. Specimens with ratios of gage length to thickness on the order of 1.0 were not tested.

A study specifically addressing thick composites and the effects of increasing thickness on material properties and compressive strength was included by Camponeschi [2]. This study used two materials, AS4/3501-6 and S2/3501-6, and two stacking sequences, $[0_2/90]_{ns}$ and $[0]_n$. The three thicknesses tested were 0.25 inches, 0.5 inches, and 1.0 inches. Although the study found a decrease in compression strength for thicker specimens, this effect was later attributed to the fixture used (Figure 2.5). The effect of increased specimen thickness on compression strength was evaluated by defining the fiber exit angle. Fiber exit angle is defined as the angle of the outermost 0° fibers at the point in the specimen immediately after the edge of the compression test fixture grips, as shown in Figure 2.6. This angle exists due the Poisson expansion of the specimen in the unsupported gage length. The fiber exit angle was evaluated using a finite element analysis which led to the conclusion that the exit angle increases by 25% between the 0.25 inch thick specimen and the 1.0 inch thick specimen. The fiber exit angle was added to the initial fiber misalignment angle, and the resulting sum was used in two failure theories based on fiber kink band formation. The final compression failures predicted by this analysis were well matched to the experimental results, indicating that the increased exit angle was indeed the cause of the reduced strength. Finally, it was concluded that the compression strength for thick composites would be that same as the strength for thin specimens if the fixture restrictions were eliminated.

2.2 Compression Failure Theories

Camponeschi [2] includes an extensive literature review of both current and past theories for compression failure of laminated composite materials. The theories are divided into the general

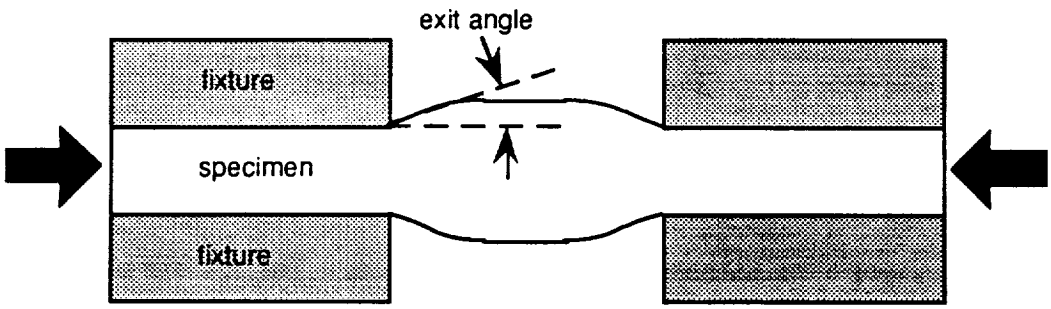

Figure 2.6 - Fiber exit angle, as defined by Camponeschi [2]

categories of fiber buckling, transverse tension, and fiber kinking. Fiber buckling theories (microbuckling) are usually based on the work by Rosen [13], for a two-dimensional stability model of unidirectional fiber columns on elastic foundations. An extensional mode (Figure 2.7) with fibers buckling out of phase was proposed for fiber volume fractions less than 30%, while a shear mode with fibers buckling in phase was proposed for fiber volume fractions greater than 30%. Other experimental findings since the publication of Rosen's work have found this model to provide an upper bound to experimentally determined compression failure strains. The lack of experimental agreement led to the development of other compression failure theories. The transverse tension theory attributes compression failure to the presence of transverse tensile stresses in laminates with low transverse strength. Interactive failure theories that include the effects of both transverse tension and uniaxial compression were proposed. Experimentally observed formation of kink bands led to theories for fiber kinking. Fiber kinking models are based on the assumption that the erroneous high estimate of compression failure given by the ideal fiber buckling models may be attributed to the presence of misaligned fibers.

In addition to the analytical failure theories reported in Ref. [2], a number of experimentally observed compression failure trends were also noted. For unidirectional composites, fibers which are weak in compression fail by uniaxial compression before fiber bucking occurs. For fibers that are not weak in compression, failure initiates as microbuckling at the free boundaries, delaminations, voids, or at points of stress concentration due to the test hardware. A compliant matrix leads to continued failure due to microbuckling, while a stiff matrix leads to failure by fiber kinking. For all of these unidirectional cases, final failure is in the form of kink bands. For quasi-isotropic laminates, failure is initiated in the 0° plies as kinking, which progresses differently depending on the toughness of the matrix. For brittle matrices, this progression is almost instantaneous.

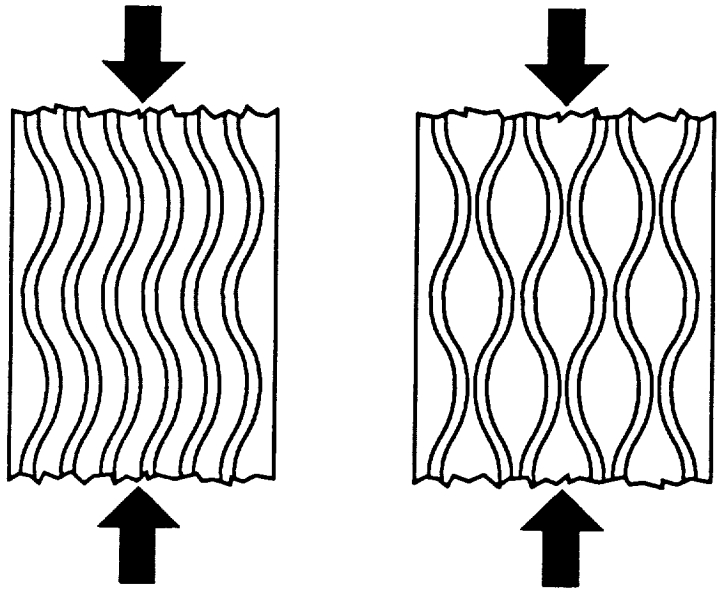

Figure 2.7 - Shear and extensional fiber buckling modes, according to Rosen [13]

Camponeschi [2] explained his experimental work by using the failure theories of Argon [14] and Budiansky [15] for fiber kinking. Argon attributes compression failure to kink band formation which initiates due to initial fiber misalignment. The misalignment produces shear stresses that eventually cause collapse of the misaligned fiber. The subsequent stress redistribution leads to the propagation of the collapse across the specimen. The expression developed for compression strength is a function of the initial angle of fiber misalignment and the shear strength of the matrix.

Budiansky proposes a more complete model for fiber kinking that reduces to the model by Argon for the case when the yield strain of the matrix is very low. Budiansky assumes perfect plasticity of the matrix beyond the yield strain. An expression is developed which gives the compression strength as a function of the initial fiber misalignment angle, the yield strain, and the shear modulus.

Another extensive literature review of compression failure theories was conducted by Shuart [3], although it includes only those works published before 1985. These theories are divided into short wavelength buckling failure and interlaminar shear failure due to lamina imperfections. For failure theories that included the effects of geometric and/or material nonlinearities, reasonable correlation with experimental data was achieved. Failure theories for multi-directional laminates in compression were found to be limited to buckling of the outermost layers. Buckling of interior, embedded layers had not been addressed. Shuart developed a set of failure criteria that includes a linear analysis to predict failure by outermost ply buckling, and a nonlinear analysis to predict failure by interlaminar shear strains and in-plane matrix shearing. A subsequent paper by Shuart [10] also included a maximum stress matrix compression criterion. It was found that the failure modes of angle ply $[\pm\theta]_s$ laminates depend of the orientation angle θ. For $0°\leq\theta<15°$, failure is due to outer lamina buckling or interlaminar shear strains, depending

on the level of imperfections in the lamina. For $15° \leq \theta \leq 75°$, failure is due to inplane matrix shearing, while for $\theta > 75°$, failure is due to compressive failure of the matrix.

In addition to those works cited by Camponeschi and Shuart, recent failure theories have included the effects of free edges and combined loading. Waas et al. [16] developed a model for straight, aligned fibers based on the observation that compression failure initiates at a free edge. The model, based on the work by Rosen [13], performs relatively well for low fiber volume fractions and gives failure strains lower than the Rosen model. The model is not as successful for higher fiber volume fractions, due to the interaction effects between multiple fibers and matrix. Better correlation is expected for fibers modeled in three rather than two dimensions. Other limiting assumptions include perfectly aligned fibers and perfect fiber/matrix bonding.

A microbuckling model for plates with a hole was proposed by Gürdal and Hafka [17]. The presence of both compressive and shearing stresses led to a modification of Rosen's theory to include shear effects. Experimental results for far-field failure strains of plates with a hole correlated well with the analysis.

2.3 Compression After Impact

The experimental study of compression after impact has been ongoing for many years. Some of the early work in this area was conducted by Starnes et al. [18] in 1979. They impacted 48-ply graphite/epoxy specimens (24.8 cm long by either 11.4 or 12.7 cm wide) with 1.27 cm diameter aluminum spheres with impact speeds ranging from 50 to 100 m/s. They concluded that

impact speeds between 50 and 60 m/s have little effect on compressive failure strain, although c-scans and sections taken through the impact site indicated the presence of interior damage. They also noted a significant strength loss at 100 m/s impact. The damage area and number of delaminations, as determined by sectioning some of the specimens through the impact site, were found to increase with increasing impact speeds.

A companion paper to the previous study was conducted by Rhodes et al. [19] to include further characterization of the specific damage caused by impact. The study by Rhodes again involved impact of graphite/epoxy specimens by 1.27 cm diameter aluminum spheres. Specimen dimensions were either 12.5 cm wide by 25.4 cm long or 83.1 cm wide by 25.4 cm long. Thicknesses ranged from 0.56 to 0.79 cm. Five stacking sequences were examined, all of which consisted of 45°, 0°, and 90° plies with 45° plies at the outer surfaces. The first visible damage was reported as a crack on the back surface of the specimen. At the same time, the front surface showed a shallow depression from the sphere. In the interior of the specimen, meanwhile, damage consisted of a v-pattern that began under the impact site at the top surface and extended outward and down. Low velocity impact caused matrix cracks and very short delaminations forming this v-pattern, while higher velocities caused the v-shape to fill in with further delaminations and matrix cracks. The damage was believed to be caused by internal stress waves that initiated in the specimen interior at the time of contact with the impact sphere. The presence of local out-of-plane deformation would then cause the damage to propagate. Under compression loading, three failure mechanisms were observed. These were local buckling of sublaminates, short wavelength out-of-plane deformation, and local shear failure. Sublaminate buckling was found to occur at a lower strain than the other two mechanisms. A third related paper by Starnes and Williams [20] presented sublaminate buckling results which were found to agree qualitatively with the analytical results by Chai, et al. [21]. In a study on the effects of different resin systems on impact damage tolerance, Williams and Rhodes [22] noted

two different compression after impact damage propagation modes, depending on the shear modulus of the resin. The first is a delamination mode that fails by sublaminate buckling. The second, referred to as transverse shear, is caused by shear instability and local fiber buckling. These two failure modes are shown schematically in Figure 2.8.

Guynn and O'Brien [23] conducted a study to identify the effects of stacking sequence and thickness on the distribution and size of delaminations due to impact, and the corresponding effects on residual compression strength. Specimens were made from T300/5208 graphite/epoxy with 16, 32, or 64 plies. Dimensions were either 4 inches by 13.75 inches for the 16-ply and 32-ply specimens, or 5 inches by 10 inches for the 64-ply specimens. Guynn and O'Brien concluded that delamination area due to impact damage area did not necessarily correlate with compression failure strain. Peanut-shaped delaminations were observed at almost every ply interface. The major axes of the delaminations were aligned with the fiber angle of the ply furthest from the impact point. The largest delaminations in thin laminates (16 plies) were located in the interface next to the back ply, causing this ply to buckle early in the post-impact compression test. More uniform delamination distribution through the thickness was found in thicker laminates (32 or 64 plies). For the same impact energy per unit thickness, the thicker laminates were found to have higher compression failure strains.

A more recent paper by Dost, et al. [24] also discussed the effects of stacking sequence on compression after impact response. Specimens were either 24 or 32 plies thick, with lengths of 15.2 cm and widths of 10.2 cm. This study involved quasi-isotropic stacking sequences with a constant change in angle in the repeating sequence. Stacking was chosen such that the difference between adjacent angles added to a sum of zero ($[45/90/-45/0]_{ns}$, for example). Impact of such a stacking sequence was shown to result in a spiral staircase damage pattern (Figure 2.9), as was documented earlier by Gosse and Mori [25]. The staircase pattern is actually

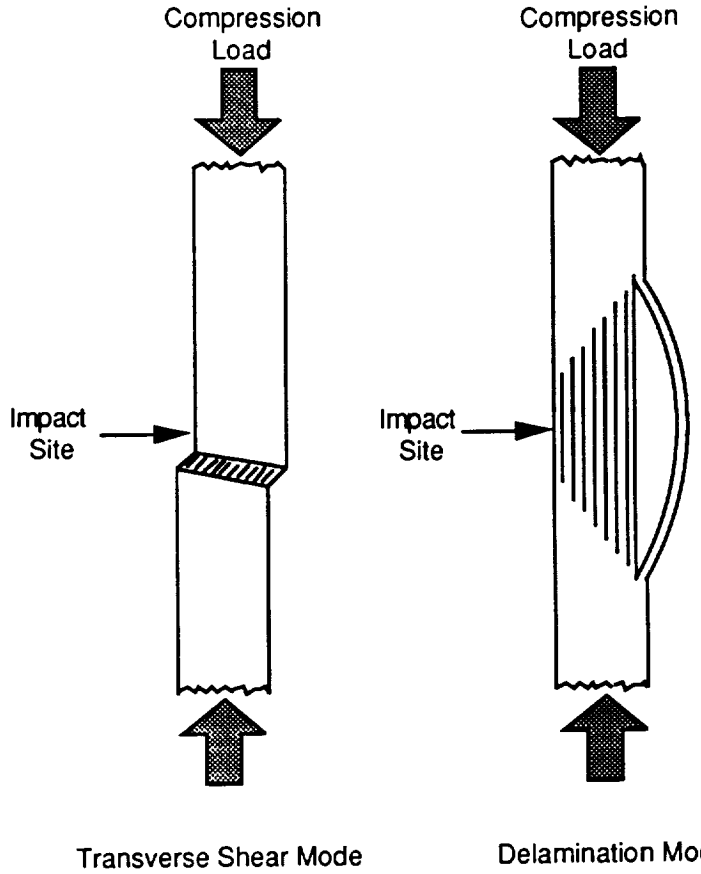

Figure 2.8 - Compression after impact failure modes, Williams and Rhodes [22]

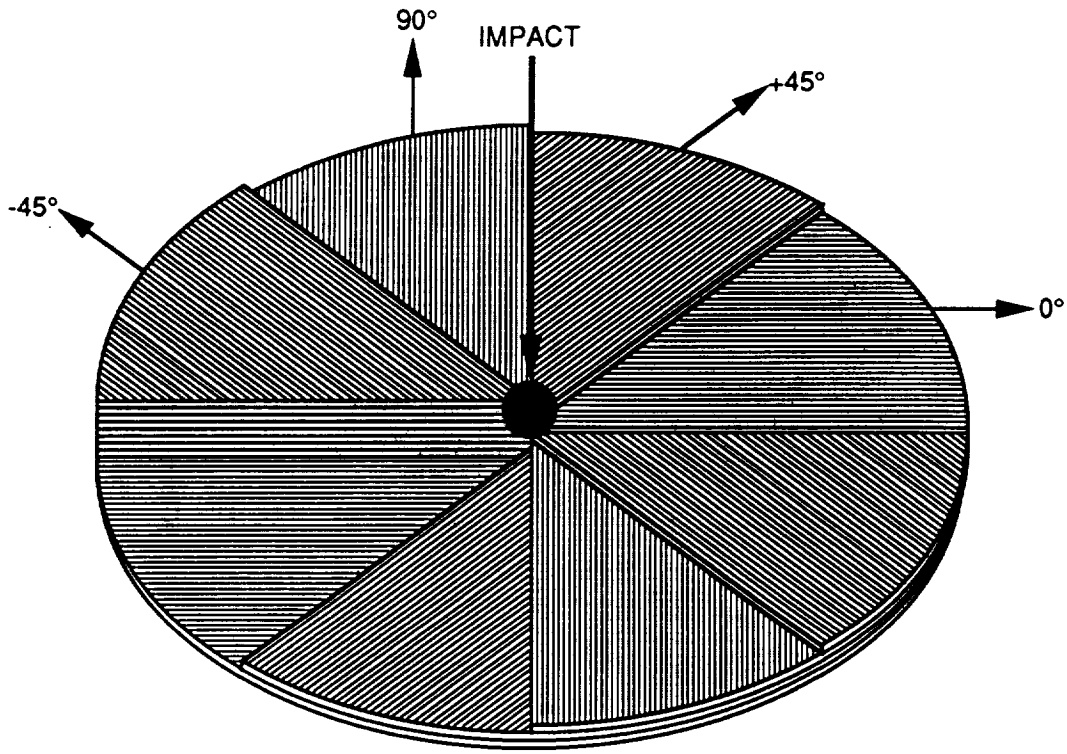

Figure 2.9 - Spiral staircase pattern of impact damage in quasi-isotropic laminate, Avery [26]

made up of delaminations which occur at each ply interface, connected to the delaminations at neighboring interfaces by transverse matrix cracks. Fiber damage was also noted to occur for some impact energies, with a concentration at the impact site. The maximum diameter of the fiber damage zone was found to be the size of a hole that the impacter would form if it penetrated the composite. The same v-pattern noted by Starnes, et al. [18] was noted to occur for these stacking sequences. A series of laminates with increasing effective ply thickness, $[45/90/-45/0]_{3s}$, $[45_2/90_2/-45_2/0_2]_{2s}$ and $[45_3/90_3/-45_3/0_3]_s$ was also tested. It was concluded that increasing the ply group thickness had an overall negative effect on compression after impact performance for a given impact energy. It was suggested that the failure mechanism may be different for these grouped ply laminates, rather than sublaminate stability as was assumed for the interspersed ply laminates. Specimens with a $[30/60/90/-60/-30/0]_{2s}$ stacking sequence were found to have higher compression after impact strengths, due to the thicker sublaminates that occurred in these specimens versus the $[45/90/-45/0]_{3s}$ specimens.

2.4 Compression With Simulated Impact Damage

In order to gain a clearer understanding of compression after impact failure mechanisms, several researchers have conducted compression studies on specimens with damage initiated through some means other than impact. Experimental studies generally focus on preimplanted delaminations, while analytical work is concerned with the analysis of plates with carefully

selected forms of delamination. Unlike compression after impact studies, the effects of fiber damage and additional matrix cracking are generally neglected.

2.4.1 Experimental Studies

A number of studies have been conducted which incorporate the use of implanted delaminations and/or small holes to simulate the impact damage. Among such studies is a paper by Wang and Whitcomb [27] that includes both pre-implanted artificial delaminations and small holes. Delaminations with 1.5 inch diameters were implanted between layers 4 and 5 in $[90/0_2/90]_{6s}$ stacking sequences of AS4/3502 and AS4/PEEK(APC-2). The delaminations divided the laminates into a sublaminate and base laminate. The holes were drilled in the base laminate to simulate possible base laminate damage. The diameters of the holes ranged from 0.75 to 1.25 inches. The conclusion of this study was that the strain required for delamination growth decreased with the presence of a hole compared to the laminate without a hole. This implies that damage in the base laminate would also reduce the strain necessary for delamination growth.

A study by Davidson [28] was conducted on specimens with pre-implanted delaminations in order to provide verification of a subsequent sublaminate buckling analysis. A comparison to actual impact damaged specimens was included. The 24-ply specimens with pre-implanted delaminations showed clear indications of sublaminate buckling according to the strain gages and shadow moire techniques used. However, the specimens with actual delaminations exhibited a slow steady increase in out-of-plane deflection with no apparent bifurcation point.

In reference [29], Davidson reports additional experimental data for panels with a $[\pm45/90/0/\pm45/0_2/\pm45/0_2]_s$ stacking sequence and pre-implanted delaminations. For circular

delaminations located 4 plies down from the top surface, delamination buckling was observed prior to final failure. Loading was always coincident with the x-axis of the panel. When the delamination was elliptical with its major axis coincident with the y-axis of the panel, no delamination buckling occurred prior to final failure. Elliptical delaminations were placed both 4 plies down and 8 plies down from the top surface. A comparison was made between 2 circular delaminations with one located 4 plies from the top and the other located 4 plies from the bottom, and the same configuration with a third delamination located at the midplane of the panel. It was found that these configurations have the same initial buckling load, although the final failure load is about 18% lower for the three delamination case. Further comparisons can be drawn between one, two, and three circular delamination cases. All three configurations experience the same initial buckling load with the one and two delamination cases also sharing the same final failure load.

Also working with pre-implanted delaminations for sublaminate buckling verification, Pavier and Chester [30] selected a carbon fiber reinforced PEEK material. Delaminations were implanted 3 or 5 plies down in a $[45/\text{-}45/0_3/45/\text{-}45/0_2]_s$ stacking sequence. With the aid of a 3-dimensional finite element analysis they concluded that initially flat delaminations gave identical results to undamaged coupons. This was at first unexpected since the sublaminates were unsymmetric, however it was noted that the bend-stretch coupling effects were negated by the fact that the ends of the sublaminate were not free to rotate. When an initial out-of-plane deflection of 0.1-0.2 mm was included, failure loads that matched experiments could be attained. The failure criterion used was Tsai-Hill. The authors concluded that the presence of delaminations had a measurable effect on compression strength, although the data they presented listed only 1 of 8 specimens with greater than a 7% reduction in compression strength. Experimentally, the delaminated sublaminates were observed to buckle prior to compression failure.

2.4.2 Analytical Studies

Analysis of damaged composites under compression loading currently includes the study of buckling phenomena, postbuckling delamination growth, and delamination growth due to static loading. Chai, et al. [21] used an analysis based on a three term Rayleigh-Ritz approximation to find the buckling load of a delaminated, one-dimensional, isotropic, homogeneous, linearly elastic plate. One delamination was assumed such that the damage area was large compared to the laminate thickness but small compared to the size of the plate. This analysis gave the buckling strain of the delaminated region. Postbuckling delamination growth was predicted by comparing the strain energy release rate to the fracture energy (energy required to produce a new unit of delamination). It was found that delamination growth may be either stable or unstable depending on the dimension of the delamination and the magnitude of the fracture energy.

Sallam and Simitses [31] and Yin,et al. [32] used a similar buckling analysis for one-dimensional, cross-ply, delaminated beam/plates. The boundary conditions on the beam/plate were either hinged or clamped. An unsymmetric cross-ply beam/plate was also studied to determine the effects of bend/stretch coupling. Following the buckling analysis, the strain energy release rate was computed to determine the stability of delamination growth. It was found that buckling occurs at low values of applied load for long thin delaminations, and delamination growth is a strong possibility. The load required to sustain delamination growth was found to decrease as growth continued. For short thick delaminations, the buckling load served as a lower bound estimate of the ultimate failure load for the beam.

Shivakumar and Whitcomb [33] were interested in the buckling of near surface, embedded, elliptical, anisotropic sublaminates with a quasi-isotropic base laminate. Buckling strains were determined by both a finite element program and a Rayleigh-Ritz approximation. It was found that 0° sublaminates buckle only by remote compression strain, while 90° sublaminates also buckle by remote tension strain (Poisson contraction in the y-direction due to remote tension in the x-direction causes buckling of 90° sublaminates). The buckling strains of $[0]_4$ and $[90]_4$ sublaminates were found to form the upper and lower bounds of the buckling strains for $[0/90]_{2s}$, $[\pm 45]_{2s}$, and $[0/\pm 45/90]_T$ sublaminates.

Shaw and Tsai [34] studied the one-dimensional delamination growth problem for a $[\theta/\pm 45/-\theta]_T$ stacking sequence with the delamination located between the +45° and -45° plies. The moment and force resultants from the bucking analysis were used in a finite element model of the crack tip region (at the end of the delamination). The finite element model was then used to find the strain energy release rates. It was found that the G_{III} component of the strain energy release rate (delamination growth by scissoring) was negligible compared to the G_{II} (growth by sliding) and G_I (growth by crack opening) components. The total strain energy release rate was found to increase as the applied load increased. As the load was increased, the crack length for unstable crack growth was found to decrease, a trend which had been previously noted by Sallam et al. [31] for cross-ply laminates. The specific delamination failure mode (mode I or mode II) was found to change as the angle θ changed in the stacking sequence $[\theta/\pm 45/\theta]_T$.

Jones and Callinan [35] studied through-the-width delaminations using a three-dimensional finite element model. Static loading was used with calculations of the strain energy release rate and strain energy density to predict delamination growth. Specimens considered had a $[\pm 45/0_2]_{2s}$ stacking sequence and a single delamination of varying width and length. Load was introduced at the center of the ends of the specimens. For this loading condition,

antisymmetric sublaminates were found to exhibit bending and twisting. Values of the strain energy release rate and strain energy density increased slightly with increasing delamination length and width.

Whitcomb [36] compared near surface, embedded delaminations to near surface, through-the-width delaminations. The analysis was conduced with geometrically non-linear, three-dimensional finite elements. A $[0/\pm45/90]_s$ stacking sequence was used with simplified "homogeneous quasi-isotropic laminate" material properties which consisted of an averaged C_{ij} matrix for the laminate. The G_I, G_{II} and G_{III} components of the strain energy release rate were calculated after sublaminate buckling occurred and G_{III} was found to be negligible. For through-the-width delaminations and embedded elliptical delaminations, the G_I component at the top of the delamination (coincident with the x-axis) followed a similar trend but with a reduced magnitude for the embedded delamination. The circular delamination had no G_I component at the top of the delamination. However, both of the embedded delaminations had an additional G_I contribution on the side of the delamination coincident with the y-axis. Therefore, it was concluded that embedded and through-the-width delaminations grow differently under uniaxial compression.

Dost, et al. [37] and Ilcewicz, et al. [38] extended the work of Shivakumar and Whitcomb [33] for embedded delaminations using a Rayleigh-Ritz approximation. The effects of bending-extension coupling were included by using a reduced bending stiffness approximations (the [D] matrix was reduced by $[B][A]^{-1}[B]$). The effect of a finite width plate was accounted for by using a finite element analysis to determine a finite width correction factor. Multiple delaminations were handled by reducing the moduli of each sublaminate as it buckled, and continuing the analysis. Experiments on an impacted, quasi-isotropic plate with a spiral array of interconnected matrix cracks and delaminations [24,25] (Figure 2.8) were used to verify the analysis.

Delaminations were modeled as individual circles creating four ply thick repeating sublaminates. The buckling load for each the the four possible stacking sequences was calculated and averaged for use in the progressive analysis. As each sublaminate buckled and its moduli were reduced, a maximum strain failure criterion was monitored to determine the ultimate plate failure load. The analysis compared well to the experimental results.

In a similar analysis to Dost, et al. [37] and Ilcewicz, et al. [38], Avery [26] used the same reduced moduli concept to represent buckled sublaminates. However, rather than modifying the [D] matrix to account for bend/stretch coupling, Avery used the full ABD matrices with fully coupled partial differential equations for anisotropic elasticity. This method is compared to the same experimental data as [37,38] and found to give an upper bound for laminate failure, while [37,38] give a lower bound.

Davidson [28,39] considered compression failure, global buckling, and local delamination buckling failure modes in order to predict the initial failure load and mode. Up to three embedded, elliptical delaminations are considered. A buckling analysis was used similar to Ref. [37,38] in that bend/stretch coupling was modeled using the reduced bending stiffness approximation. In addition, analysis included effects of Poisson ratio mismatch between sublaminates. Initial failure is determined by checking each of the failure criteria and finding the lowest failure load. Compression failure is determined using the maximum strain failure criterion. It is noted that both compression failure and global buckling correspond to ultimate laminate failure. Delamination buckling, meanwhile, allows continued analysis of the remaining, unfailed sublaminates. The results compared well to experiments with implanted delaminations. The experimental results were also compared to analysis by Shivakumar and Whitcomb [32] and Chai, et al. [21]. These two analyses were found to over predict the initial buckling load.

In order to find the buckling loads and modes for multiple through-the-width delaminations, Lee, et al. [40] used a one-dimensional finite element model based a layer-wise plate theory. The specific cases examined included a symmetric half model (no u displacement at x=0) and an antisymmetric half model (no w displacement at x=0). The notation used to define the specimen and delamination dimensions and buckling modes is shown in Figure 2.10 and 2.11. For two delaminations near the surface (t/h = 0.25), symmetric sublaminate buckling dominates. The addition of a delamination at the midplane does not change the buckling load or mode. When the delaminations are farther from the surface (t/h = 0.5), and the delamination length ratio is between a/L=0.1 and a/L=0.4, the buckling mode is local symmetric. However, when a delamination is added at the midplane, the buckling mode changes to global antisymmetric, with a correspondingly lower buckling load. Multiple, uniform length delaminations were also examined and compared with a single delamination and non-uniform length (triangular) delaminations as shown in Figure 2.10. Multiple uniform length delaminations were found to have a lower buckling load than the single delamination case. This is due to the antisymmetric buckling mode, which becomes dominant as the number of delaminations increases. For multiple delaminations with a triangular distribution, the buckling mode and load is local symmetric, the same as for the one delamination case.

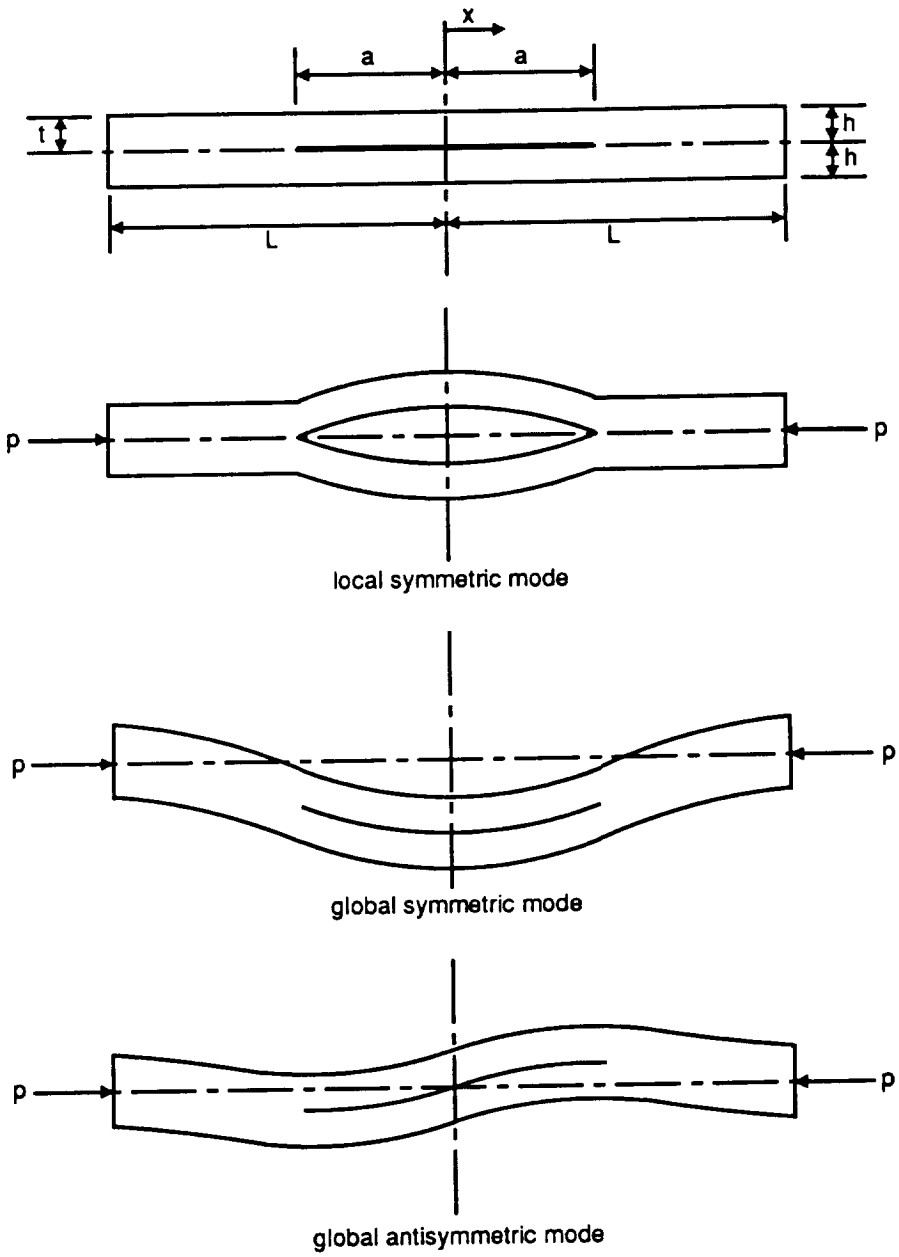

Figure 2.10 - Buckling mode shapes for one delamination at midplane, Lee et al. [40]

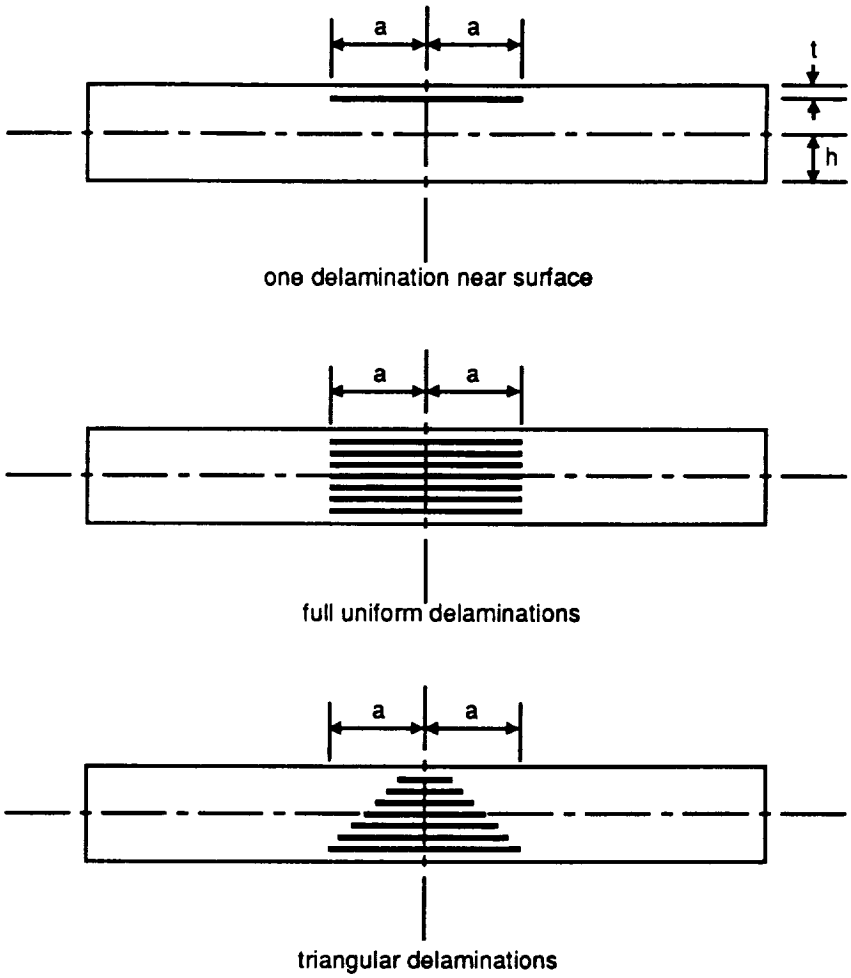

Figure 2.11 - Delamination locations, Lee et al. [40]

Chapter 3
Experimental Procedure

Details of the experimental procedure, beginning with the 3-point bend testing conducted to initiate impact-like damage, are included in this chapter. The first section includes a summary of the 3-point bend testing procedure and an explanation of the chosen stacking sequences. The next section begins with a description of the documentation procedure for classifying the damage states after 3-point bend testing. A table of all the specimens tested in compression along with their initial damage classification is included. The four initial damage classifications are described with photos of typical specimens exhibiting each classification. The final section shows the compression fixture used and the instrumentation placement. Details of the compression testing procedure and recorded data are also included.

3.1 Flexure Testing, 3-Point Bending

Most of the specimens used in this work were inherited from a previous study by Starbuck et al. [1]. The 9 by 12 inch panels used in this previous study were fabricated from Hercules AS4/3501-6 graphite/epoxy material. Ten specimens with dimensions of 6.0 by 1.0 inches were cut from each panel , with the thickness varying according to the stacking sequence.

The goals of Starbuck's experimental work were to study the effects of stacking sequence, specimen thickness, distance between support points, and effective layer thickness on damage characteristics under 3-point bend loading. He sought to determine the loads at which damage initiated in the specimens and the modes of this damage. The fixture he used is shown in Figure 3.1. It allowed a finite radius (0.25 inches) for the load and support points and the flexibility to change the span by changing the distance between the lower supports.

Loading was accomplished using a 100 kip hydraulic load frame operating under displacement control at a rate of 1.3 mm/min. Two tests were conducted for each stacking sequence and span configuration, with one stopped after damage initiation and the other tested to ultimate failure. Damage initiation was determined either by noting a drop in the load/displacement curve, or by hearing an audible crack from the specimen. The specimens which were stopped after damage initiation became the initially damaged specimens used in this study.

Two quasi-isotropic layups were chosen for the original study in order to determine the effects of specimen thickness, layer thickness and stacking sequence. Thickness effects were studied by testing 48-ply, 120-ply, and 200-ply or 210-ply laminates. Both [0/±45/90] and [0/±60]

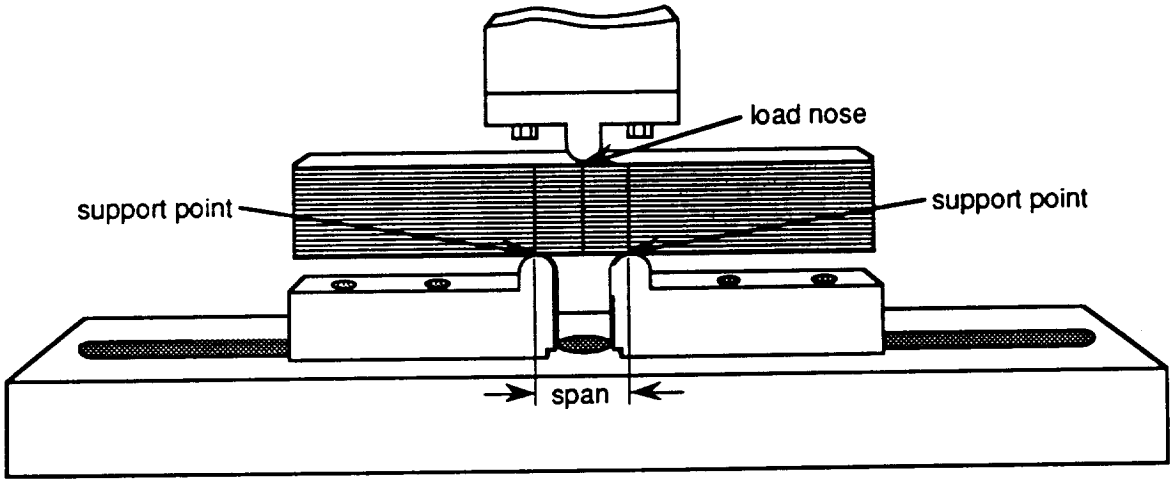

Figure 3.1 - Test fixture, three-point bending

sequences were used, yielding the six stacking sequences of $[0/\pm45/90]_{6s}$, $[0/\pm45/90]_{15s}$, $[0/\pm45/90]_{25s}$, $[0/\pm60]_{8s}$, $[0/\pm60]_{20s}$, and $[0/\pm60]_{35s}$. The effect of layer thickness on failure mode and load was studied by comparing two additional laminates, $[0_5/45_5/-45_5/90_5]_{5s}$ and $[0_5/60_5/-60_5]_{7s}$, to the 200-ply and 210-ply laminates with interspersed sequences. Specimens were labeled Q6, Q15, Q25, Q8, Q20, Q35, Q5 and Q7 according to the number of repeats of the sequence above the plane of symmetry. In order to study the effects of changing the distance between the support points, four spans of 5.5 inches, 3.0 inches, 1.0 inches, and 0.5 inches were employed. This brought the number of specimens tested under three-point bend to eight per panel for eight panels, one at each span tested to damage initiation and one at each span tested to ultimate failure.

In addition to the specimens used by Starbuck, two more panels of the same material and dimensions were fabricated with stacking sequences of $[0/\pm45/90]_{25s}$ and $[0_5/45_5/-45_5/90_5]_{5s}$. These additional panels were used for a study on the effects of initial damage extent on compression strength. The panels were cut into 6.0 by 1.0 inch specimens and tested under three-point bend loading with displacement control and a span of 1.0 inches. However, rather than stopping the tests at the perceived damage initiation loads, tests were stopped at predetermined load levels based on the initiation and failure loads reported by Starbuck. By selecting load levels between these two loads, the amount of damage due to 3-point bending could be varied. Specimens from these two panels were labeled A and B for the interspersed and grouped sequences respectively.

3.2 Initial Damage Documentation

The next stage of the current project involved documenting the damage states in the specimens after three-point bend testing. This was accomplished by first polishing the edges of each specimen, then making edge replicas using cellulose acetate replication film and regent grade acetone. Duplicate replicas were taken of each edge in order to assure that no details were missed and to provide a permanent record that could be referred to after compression testing. X-rays enhanced with a zinc iodide solution were taken through the specimen faces in order to see how the damage was distributed across the width. Examination of the x-rays and replicas led to the classification of four different initial damage modes based on the extent, location, and type of damage.

The mechanisms of failure include fiber breakage, matrix cracks, and interlaminar delamination. None of these actually occurs separately from the others, but instead occurs as part of a damage region. The specimens are listed in Table 3.1 according to their various initial damage classifications. The numbers in parentheses are three-point bend spans, given in inches. The specimen numbers consist of Q (for quasi-isotropic) followed by the number of symmetric repeats for the panel. The number after the dash refers to the specific specimen within the panel. Since some specimens were completely failed during the three-point bend study, the specific specimen numbers are not consecutive. Specimens from panels A and B are numbered A1 through A5 and B2 through B7 to identify individual specimens within the A and B panels, respectively.

Table 3.1 - Initial damage classifications, with three-point bend spans in parentheses

	Undamaged	Multiple Through-Thickness Delams.	Isolated Delams.	Damage Near Surface	Matrix Cracks (Grouped Ply Stacking Sequences)
$[0/\pm45/90]_{6s}$	Q6-10	Q6-3 (1.0) Q6-4 (0.5) Q6-8 (0.5)	Q6-7 (1.0)	Q6-5 (5.5) Q6-6 (3.0)	
$[0/\pm60]_{8s}$		Q8-4 (0.5) Q8-8 (0.5)	Q8-3 (1.0) Q8-7 (1.0)	Q8-1 (5.5) Q8-6 (3.0)	
$[0/\pm45/90]_{15s}$	Q15-9	Q15-3 (1.0)	Q15-2 (3.0) Q15-6 (3.0) Q15-7 (1.0)	Q15-10 (3.0)	
$[0/\pm60]_{20s}$	Q20-9 Q20-11	Q20-3 (1.0)	Q20-7 (1.0)	Q20-5 (5.5)	
$[0/\pm45/90]_{25s}$	Q25-9 Q25-10 A5	A4 (1.0)		Q25-5 (5.5) Q25-6 (3.0) Q25-7 (1.0) A1 (1.0) A2 (1.0) A3 (1.0)	
$[0_5/+45_5/-45_5/90_5]_{5s}$	Q5-10 Q5-11 B7				Q5-4 (1.0) Q5-6 (5.5) Q5-7 (3.0) Q5-8 (1.0) Q5-9 (0.5) B2 (1.0) B3 (1.0) B4 (1.0) B5 (1.0) B6 (1.0)
$[0/\pm60]_{35s}$	Q35-10 Q35-11 Q35-9		Q35-2 (3.0)	Q35-5 (5.5) Q35-6 (3.0) Q35-7 (1.0)	
$[0_5/+60_5/-60_5]_{7s}$	Q7-10				Q7-2 (3.0) Q7-6 (3.0) Q7-7 (1.0)

In the first classification of initial damage states, a combination of delaminations and matrix cracks is found to occur within each [0/±45/90] or [0/±60] ply set through the specimen thickness. This classification was referred to as multiple through-thickness delaminations, since the delamination and matrix crack combinations are distributed evenly from the top to the bottom of the specimens. This classification is most prevalent for the shorter spans (0.5 to 1.0 in.) and thinner specimens (48 or 120 plies). Examples of this type of damage can be seen in Figure 3.2, where the top photo is taken from the edge replica. Only delaminations are included in the sketch, rather than delamination and matrix crack combinations, due the the resolution of the drawing.

The second classification is also made up of matrix crack and delamination combinations. However, this damage occurs in only one or two ply groups per specimen with the overall length of each combination from 0.75 to 3.5 inches long. This damage classification is referred to as isolated delaminations, and occurs primarily with moderate spans (1.0 to 3.0 inches) and thin specimens (48 or 120 plies). A typical edge replica and x-ray are shown in Figure 3.3.

A larger classification which includes all three failure mechanisms is that of damage near the surface, as shown in Figure 3.4. This damage generally occurs in the first five ply groups beneath the load nose and up to five additional groups above the support points. Thick specimens (200 or 210 plies) with short spans (0.5 to 1.0 inches) and thin specimens (48 plies) with long spans (3.0 to 5.5 inches) commonly contain initial damage that falls into the classification of damage near the surface.

The final classification is primarily matrix crack dominated. It is the only damage classification which occurred for specimens with grouped ply stacking sequences. Although the matrix cracks may be restricted to the first few ply groupings, the damage mechanism is sufficiently

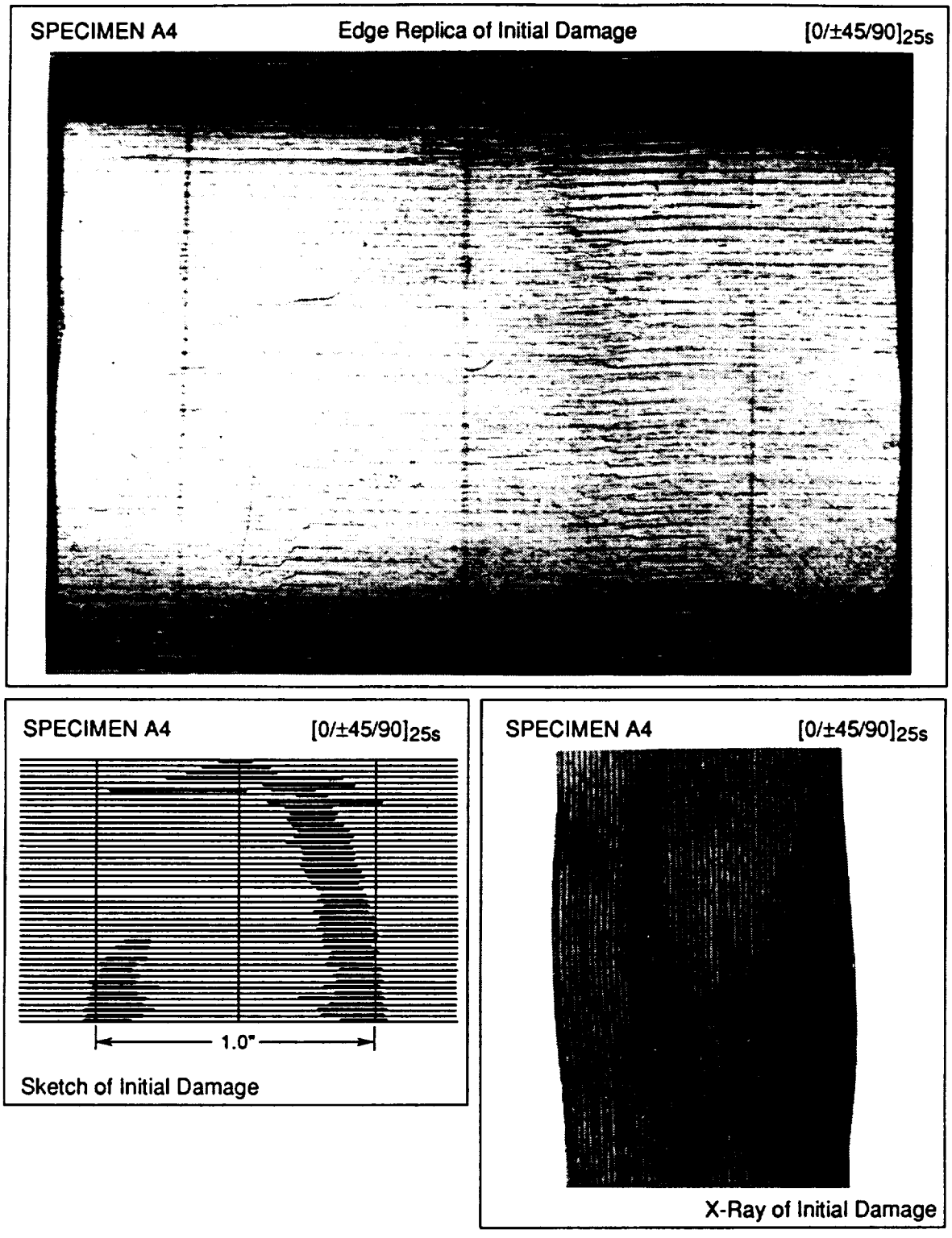

Figure 3.2 - Typical damage for multiple through-thickness delaminations

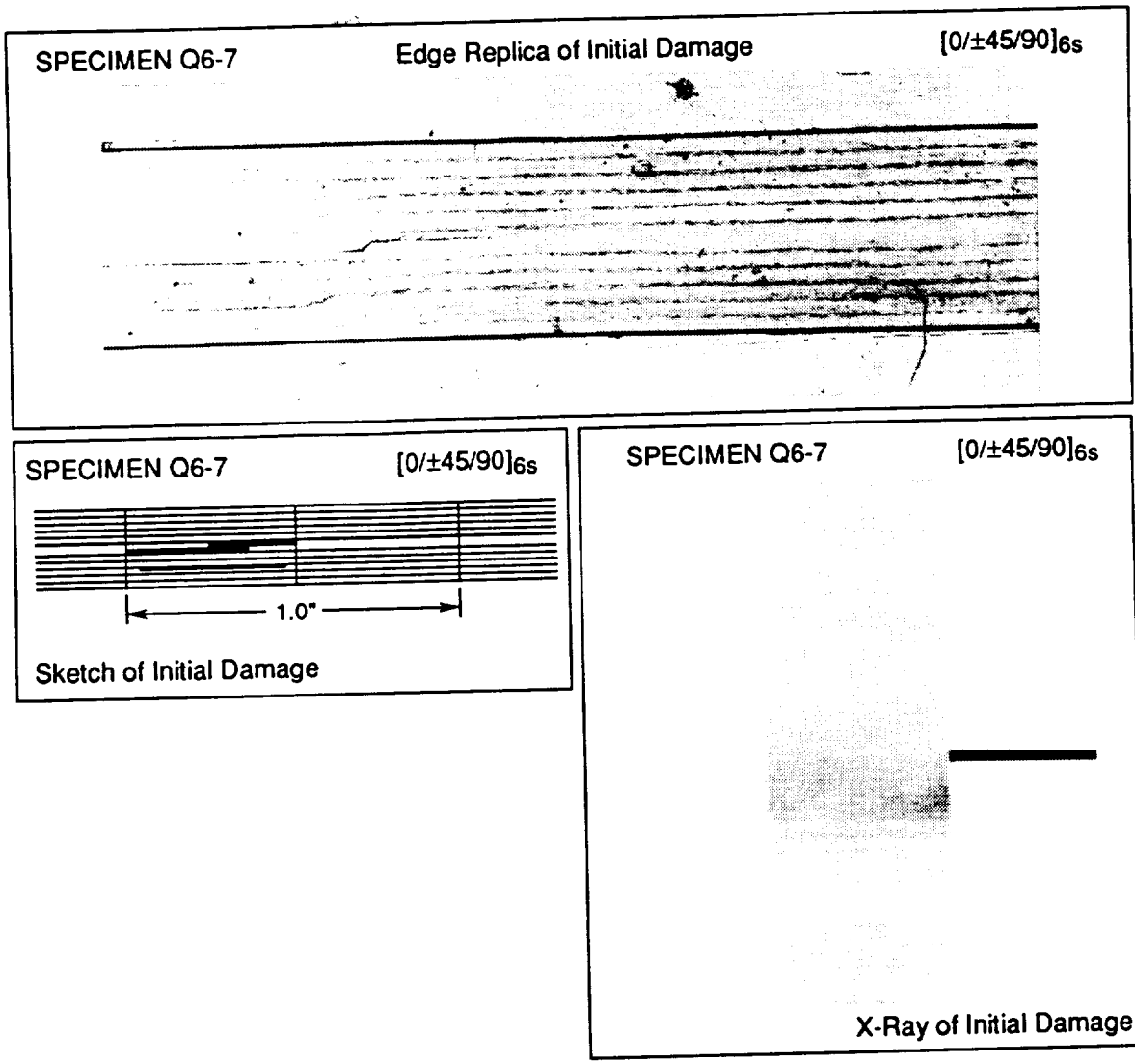

Figure 3.3 - Typical damage for isolated delamination classification

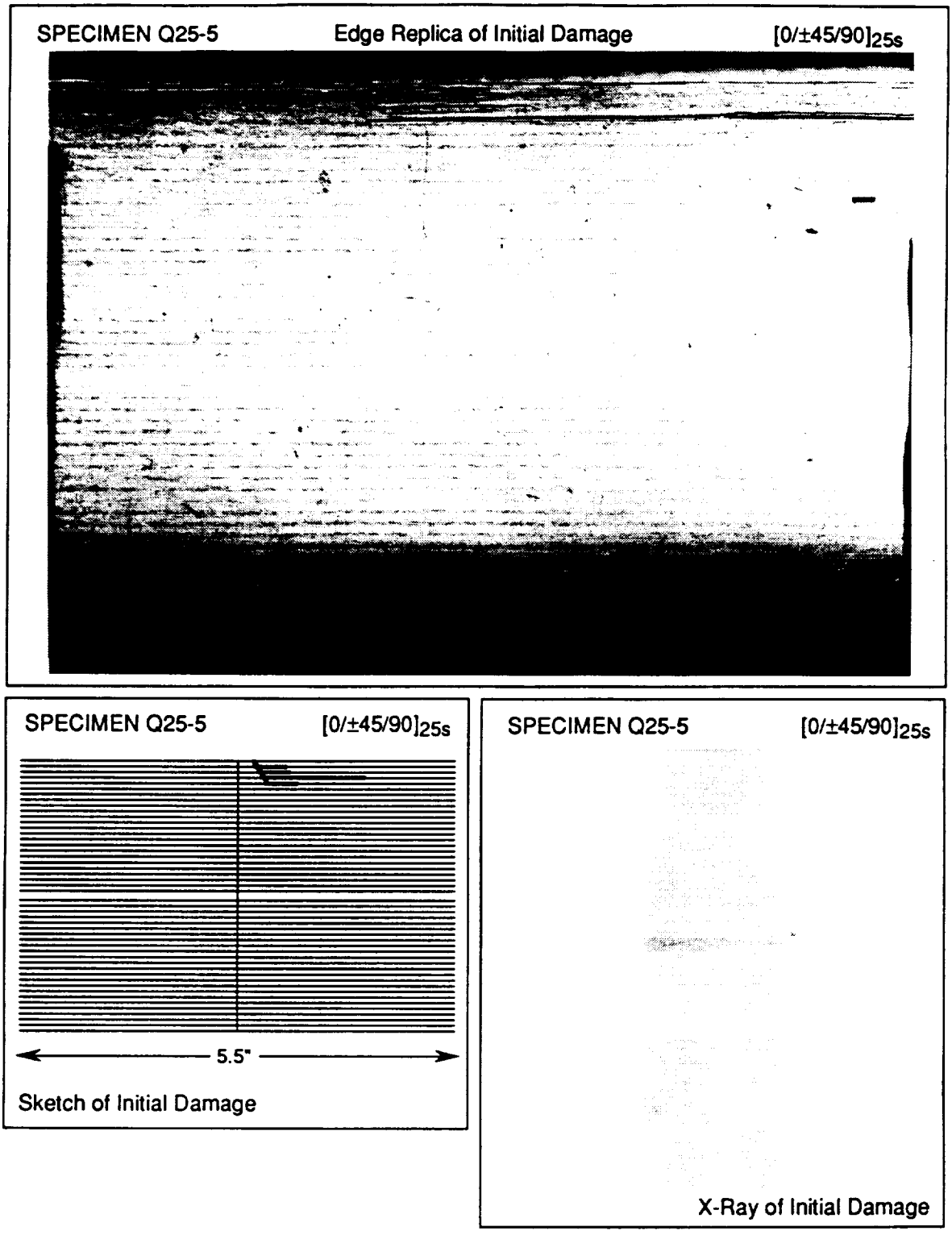

Figure 3.4 - Typical damage near the surface classification

different to warrant a separate classification. An edge replica and x-ray of a typical specimen are shown in Figure 3.5. Note from the x-ray of panel B that numerous matrix cracks in 90° layers are present along the entire length of the specimen. These matrix cracks appear in the center 90° plies prior to any testing, with panel B showing a significantly higher density than panel Q5. Panel Q7 does not have this problem since the middle plies are not oriented at 90°.

The remaining specimens listed in Table 3.1 are the undamaged specimens that were not tested in the three-point bend study. These specimens were included in the compression testing program in order to provide a base from which to compare the strengths of the damaged specimens.

Fiber volume fractions which were calculated according to the procedure in ASTM D-3171 are shown in Table 3.2. The fiber volume fractions were needed to assure that strength comparisons between panels were appropriate, particularly for undamaged specimens. Based on the findings, a slight difference in undamaged compression strength was expected between panels Q25 and A ($[0/\pm45/90]_{25s}$ stacking sequence) and between panels Q5 and B ($[0_5/+45_5/-45_5/90_5]_{5s}$ stacking sequences).

3.3 Compression Testing

In order to load these specimens of with different thicknesses in compression, a compression test fixture was needed. Besides the requirement that the fixture accept specimen thicknesses ranging from 0.24 to 1.1 inches, the fixture must also prevent global buckling. Since all the specimens were 6.0 inches long, a maximum unsupported gage length of 1.5 inches was

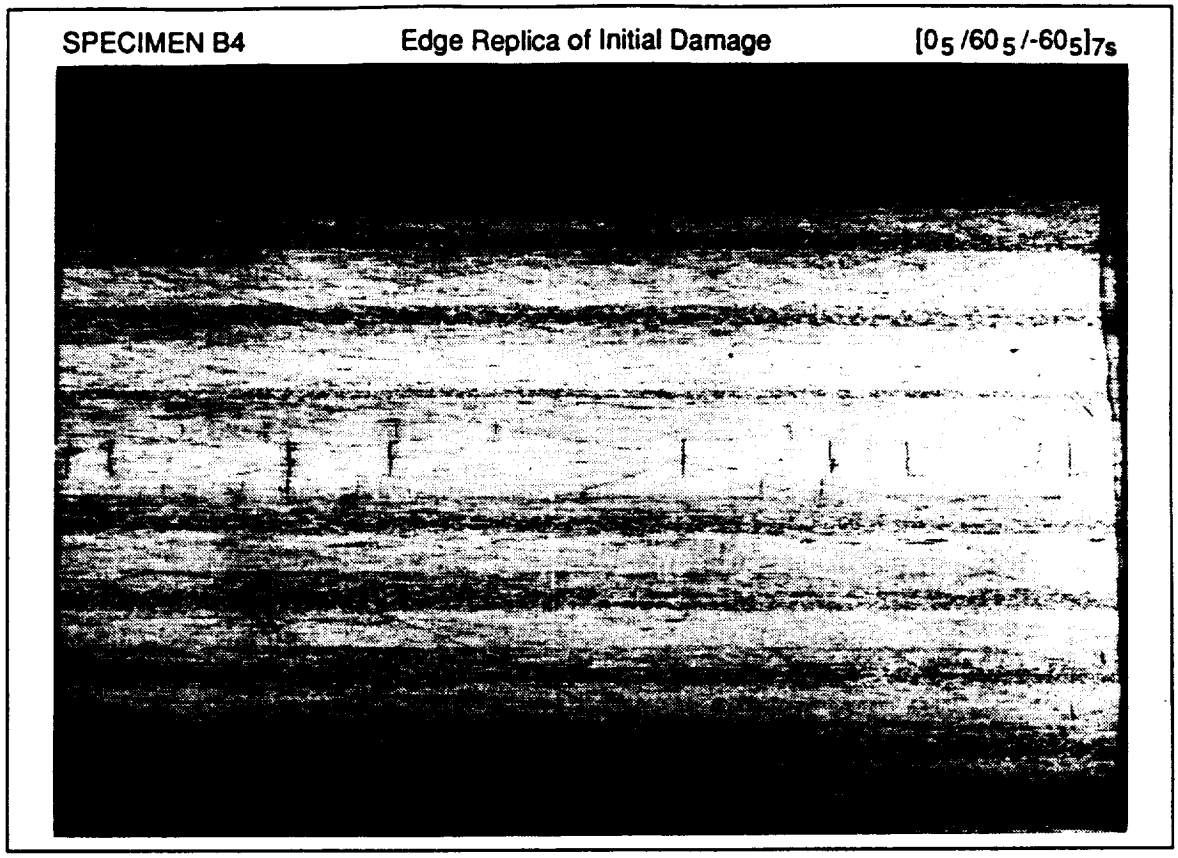

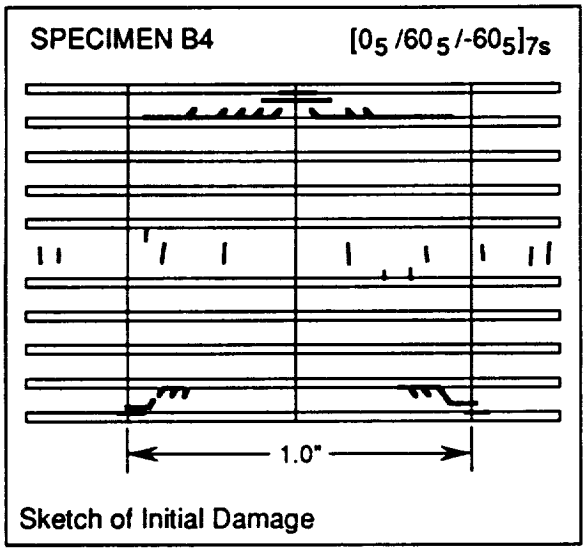

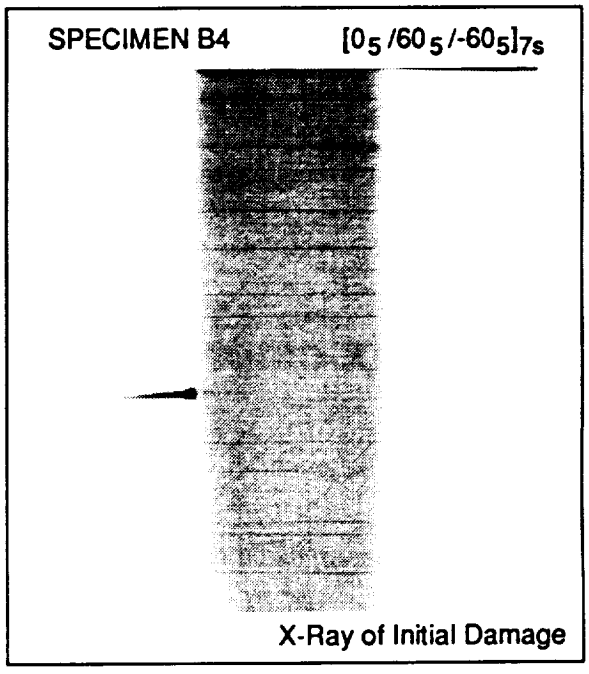

Figure 3.5 - Typical damage for matrix crack (grouped ply) classification

Table 3.2 - Fiber volume fractions for each of the ten panels

	Panel	Fiber Volume Fraction
$[0/\pm45/90]_{6s}$	Q6	0.677
$[0/\pm60]_{8s}$	Q8	0.640
$[0/\pm45/90]_{15s}$	Q15	0.629
$[0/\pm60]_{20s}$	Q20	0.627
$[0/\pm45/90]_{25s}$	Q25 A	0.632 0.551
$[0_5/+45_5/-45_5/90_5]_{5s}$	Q5 B	0.641 0.602
$[0/\pm60]_{35s}$	Q35	0.593
$[0_5/+60_5/-60_5]_{7s}$	Q7	0.580

determined for the thinnest specimens (48 plies) based on Euler column buckling as explained in the appendix of ASTM Standard D 3410-87 [4]. Thus the compression fixture had to maintain this effective gage length for all of the specimens. The specimens were much thicker than those used in shear loaded applications [2-7], where load is introduced to the specimen through tight clamps on the specimen faces as explained in Section 2.1. Loading a thick specimen with a shear loading fixture would require high clamping forces so that all of the layers would move together. If insufficient clamping forces were used, the outside layers of the specimen may move independently of the middle layers. Since the clamping forces required to keep all the layers of a thick specimen together would likely damage or destroy the specimen, a fixture which employed end loading was chosen.

The fixture used by Camponeschi [2], shown in Figure 2.5, was studied as a base from which to construct a fixture specific to the specimens at hand. Like Camponeschi's fixture, the current fixture, as shown in Figure 3.6, uses interlocking steel blocks to provide support to the ends of the specimens. These blocks allow for different specimen thickness while preventing end brooming and reducing the effective gage length. Additional alignment rods were included to ease the test set-up and insure that the specimen was being compressed along its axis. The often unsymmetric distribution of initial damage was expected to cause some undesirable global specimen bending. The alignment rods were expected to reduce this phenomenon. In order to reduce the stress concentration at the point in the specimen adjacent to the edge of the grips, a radius of 0.25 inches was included around the inside edges of the fixture. Since the specimens were sufficiently thick to allow a significant end loading area, end tabs were not used. The torque on each of the 12 bolts was 5 ft lbs. The entire fixture rested between two steel platens through which the compressive load was applied.

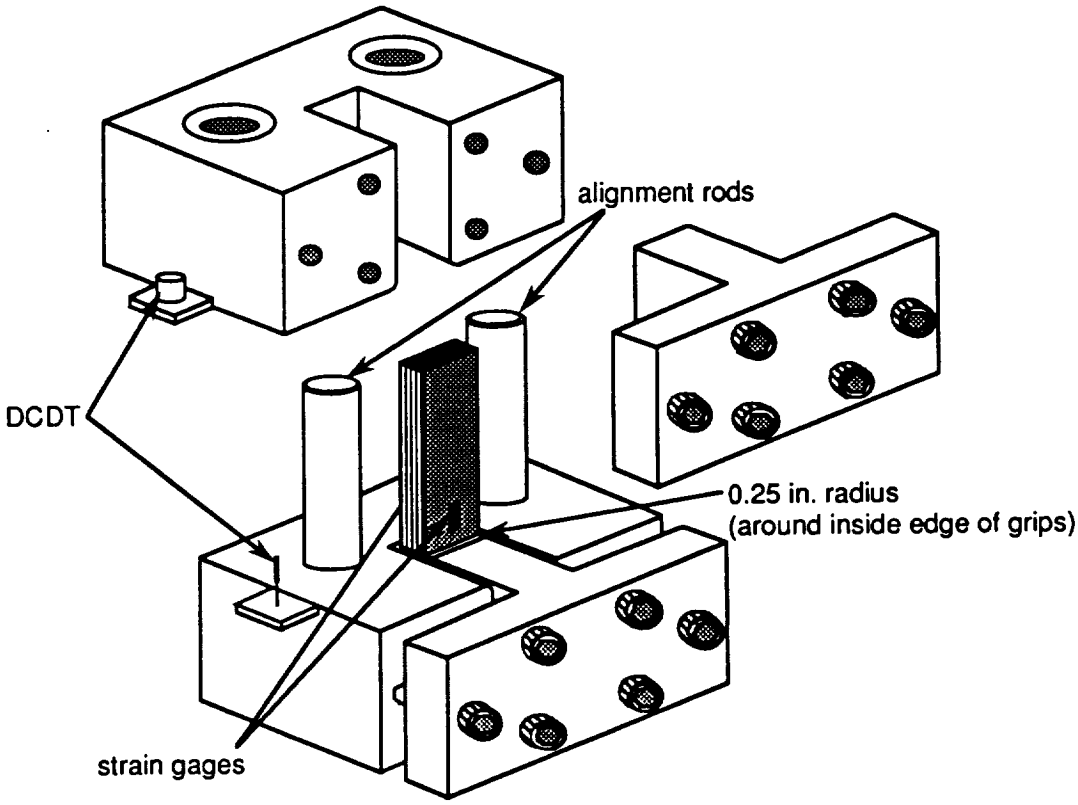

Figure 3.6 - Compression fixture for end loaded thick specimens

Also shown in Figure 3.6 is the location of the DCDT displacement transducer and the longitudinal strain gages. One strain gage was placed on each face of the specimen at the center to monitor specimen alignment during testing and determine whether or not global buckling occurred. The DCDT was placed on the outside of the blocks to measure the change in length of the unsupported gage section. Because the specimen may slip somewhat in the steel block grips, the change in length measure by the DCDT also includes the change in length of the gripped portions of the specimen.

A Micromeasurements System 4000 data acquisition system was used to record output from the two strain gages, the DCDT, and the load and crosshead displacement from the load frame. Three different load frames were used based on the thickness and expected maximum failure loads of the specimens. All were MTS hydraulic load frames. The 48-ply, 0.24 inch thick specimens were tested with a 50 kip frame, the 120-ply, 0.6 inch thick specimens were tested in a 100 kip frame, and the remaining specimens were tested in a 300 kip frame, which is shown in Figure 3.7. Loading was conducted under displacement (stroke) control with a ramp rate of 0.00025 in./sec, with data from all five channels recorded every second.

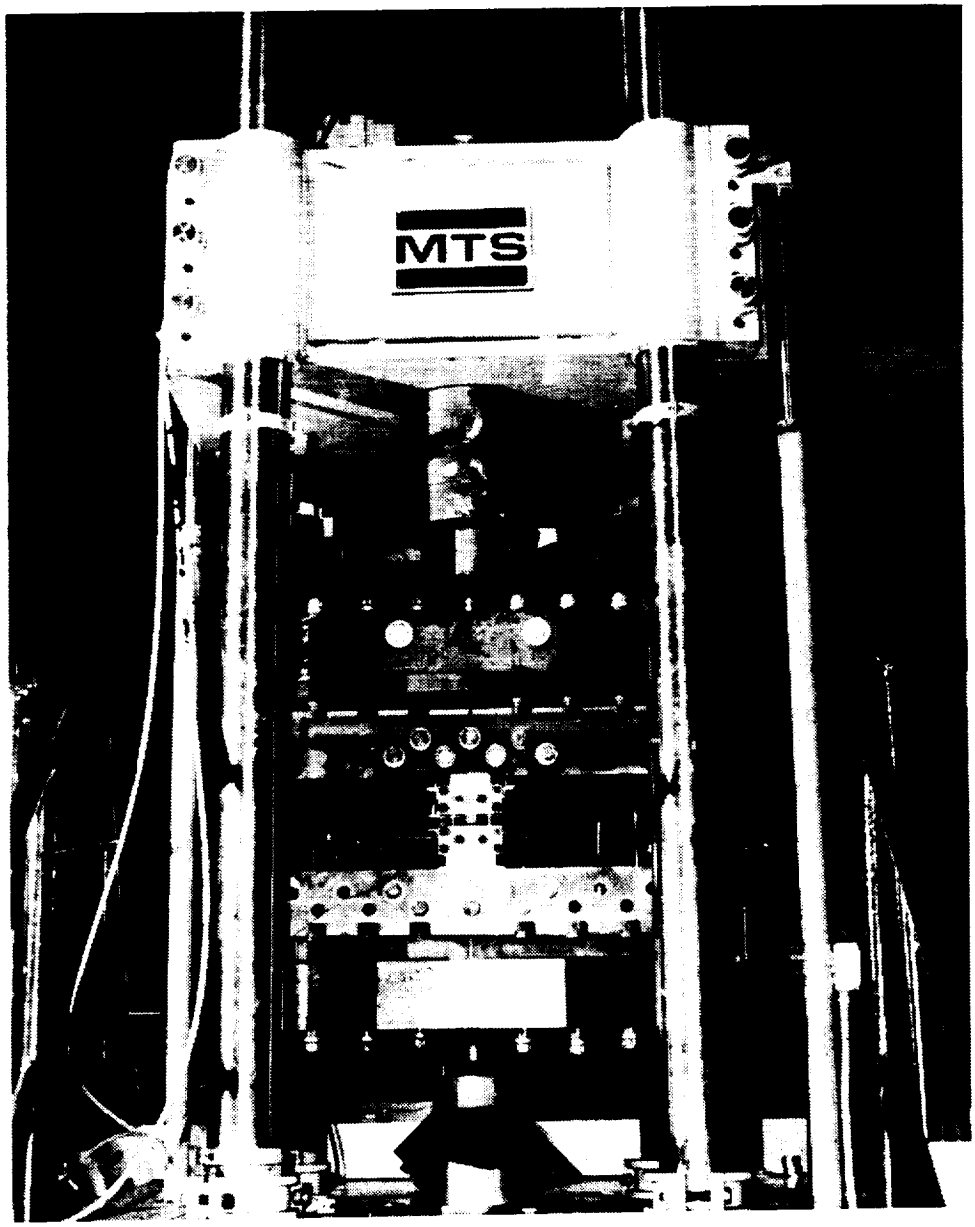

Figure 3.7 - MTS 300 kip hydraulic test stand with compression fixture

Chapter 4
Experimental Results

The experimental results are divided into five sections according to the initial damage mode of the specimens and their final compression failure modes. The first section discusses the results of compression tests conducted on undamaged specimens, which are later used as a baseline to ascertain the strength reduction effects of the different initial damage failure. This is followed by a section on specimens with an initial damage mode of multiple short delaminations distributed though the thickness. The third section includes those specimens with relatively isolated, longer delaminations. Specimens with damage concentrated near the top and bottom surface are covered in the fourth section. Finally, those specimens with grouped ply stacking sequences are included in the final section. Both the initial damage modes and compression failure characteristics of the grouped ply laminates are sufficiently different than those in the interspersed stacking sequences to warrant a separate consideration.

All of the graphs in Chapter 4 represent experimental compression data, with both stress and strain plotted as positive quantities. The stress values are an average stress obtained from

dividing the applied load by the specimen cross sectional area. The strain measurements were obtained by dividing the DCDT readings by the total length of the specimens. For strains below 4000 μ, the values from the DCDT readings very nearly matched the strain gage readings. Strain gages, although accurate for measuring surface strain, do not give a reliable measure of the average strain in the specimen beyond 4000 μ because surface strains are no longer representative of average strain beyond this level. The DCDT reading was divided by the total length of the specimen rather than the gage length because this gave the best agreement with the initial strain gage readings. However, because the inside of the grips were not frictionless, the longitudinal strain was likely higher in the gage section and lower within the gripped portions. This may explain some of the discrepancy between the experimental and numerical results, as discussed in Chapter 5.

4.1 Compression of Undamaged Specimens

A limited number of specimens which had not undergone the three point bend test were tested in compression in order to determine the amount of strength loss that could be attributed to initial damage. These specimens were cut from the same panels as the initially damaged specimens. There were generally one to three specimens tested from each panel. For panel Q8, with a $[0/\pm60]_{8s}$ stacking sequence, no representative undamaged specimen was available.

4.1.1 Stacking Sequence Effects

The strengths for the thin specimens, those with thicknesses less than 1.0 inches, are shown as compression stress-strain relations in Figure 4.1. These relations are obtained from the testing procedure described in the last section of Chapter 3. All four of these specimens failed at approximately the same stress, even though they include three different stacking sequences. Although a representative specimen from panel Q8 is missing, it is safe to assume that the compression strength of a specimen with a $[0/\pm60]_{8s}$ stacking sequence would not differ appreciably from the strength of specimens with $[0/\pm60]_{20s}$, $[0/\pm45/90]_{6s}$, and $[0/\pm45/90]_{15s}$ stacking sequences.

Although the compression strength seems to be relatively constant, the mode of failure differs. All of 0.24 inch thick specimens with 48 plies failed catastrophically. However, specimens with 120 or more plies failed either catastrophically or progressively depending on the stacking sequence. Thick specimens with a [0/±60] type stacking sequence tended to fail in their outer plies first while the bulk of the plies in the center of the specimen remained in tact. Failure load was defined, for the purposes of this study, as the maximum load carried by the beam. Thus, the failure mode is the damage state corresponding to the failure load. As a result of this definition, the failed [0/±60] type specimens appear able to carry additional load, and this may be the case. However, further loading beyond the first load drop did not result in higher loads. Therefore, the initial load drop corresponds to both the failure load and the failure mode. The progressive failure mode for the [0/±60] type specimens can be seen in comparison to the catastrophic failure mode for the [0/±45/90] type specimens in Figure 4.2.

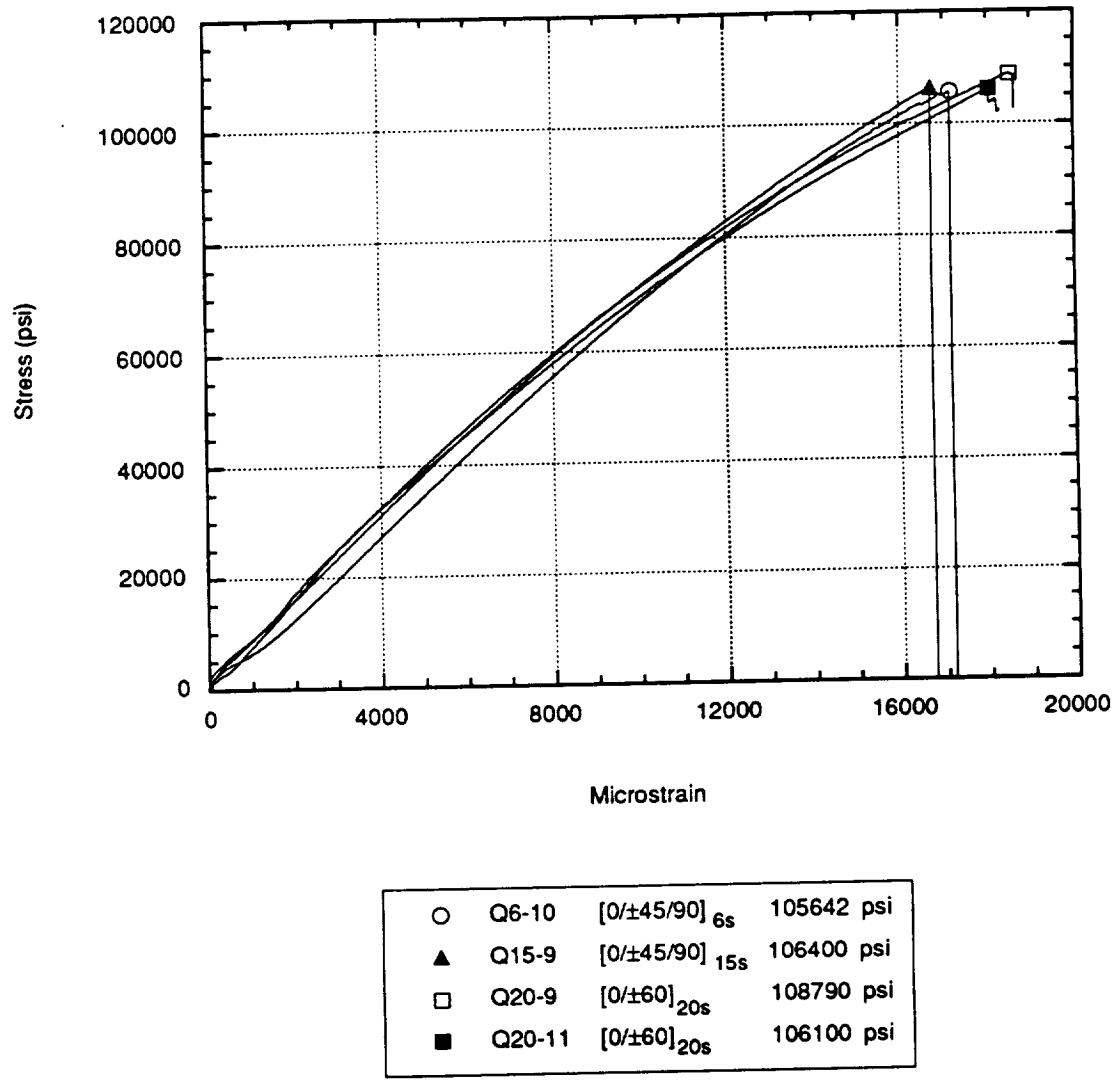

Figure 4.1 - Experimental compression relations for undamaged specimens, thickness less than 1.0 inch, $[0/\pm45/90]_{6s}$, $[0/\pm45/90]_{15s}$, and $[0/\pm60]_{20s}$

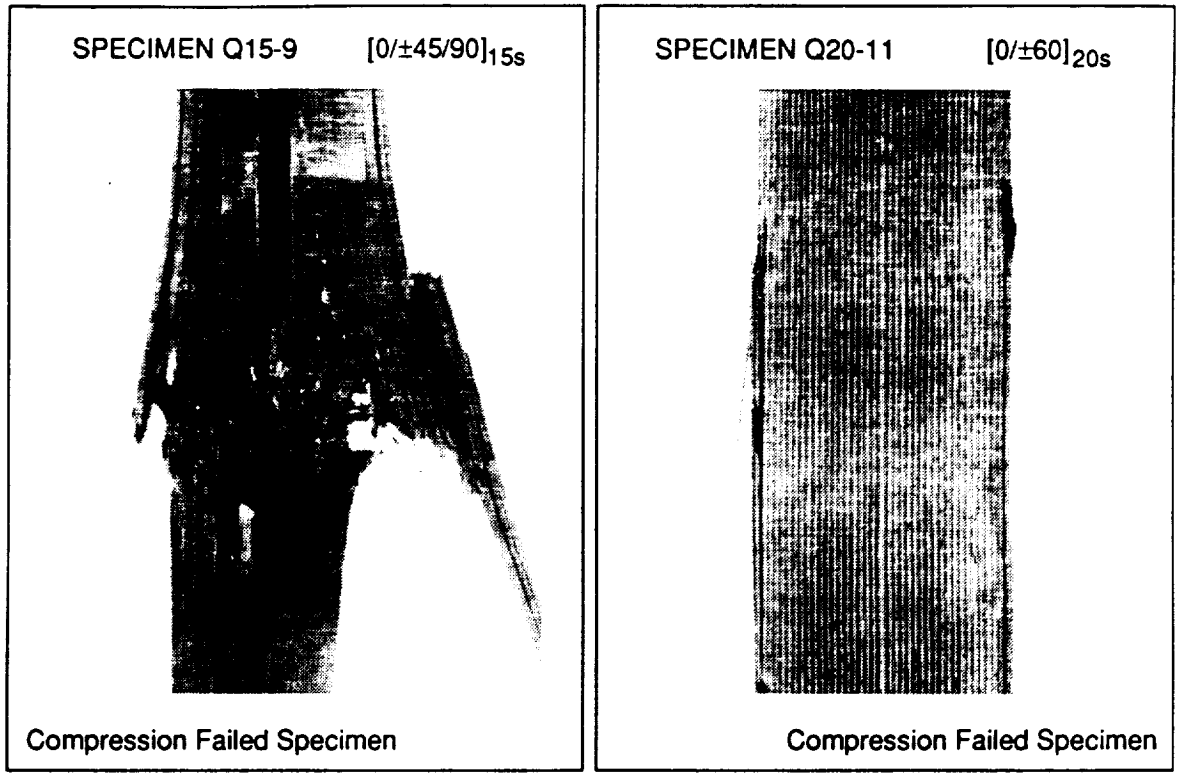

Figure 4.2 - Typical compression failed specimens, $[0/\pm45/90]_{15s}$ and $[0/\pm60]_{20s}$

4.1.2 Specimen Thickness Effects

Camponeschi [2] noted that the compression strength of thick composites appeared to decrease as the thickness increased: a behavior which was attributed to end effects in the fixture. That fixture, like the fixture used for the present testing program, restricts the thickness and width expansion of the specimen in the grips. This provides support to the ends and prevents end brooming. However, the unsupported gage length of the specimen tends to expand in the thickness direction due to Poisson's expansion. As the thickness of the specimen increases, so too does the magnitude of the fiber exit angle (out of plane fiber angle with respect to the axis of loading in the outer 0° ply at the edge of the grips, shown in Figure 2.6). By using compression failure theories by Argon [14] and Budiansky [15] based on initial fiber misalignment angle, Camponeschi was able to show that an increased fiber exit angle results in a decreased compression strength. This exit angle was calculated for thicknesses ranging from 0.25 to 1.0 inches using a finite element technique. When the compression strengths were corrected for the effects of exit angle, it was concluded that the compression strength of thick composites was actually no different than the strength reported for thinner composites.

Although the fixture used in this study (Figure 3.6) has rounded corners on the inside edges of the grips adjacent to the specimen, the exit angle still exists but with a lower stress concentration due to the grips themselves. It was not possible to observe the thickness effect noted by Camponeschi for the specimens with a 0.6 inch thickness because only one undamaged specimen with a thickness less than 0.6 inches was tested. However, as the thickness was increased to 1.0 inches and beyond, compression strength did appear to

decrease. The compression failure relations for the thick specimens along with the compression failure strengths from the previous plot for the thin specimens are shown in Figure 4.3. Notice that the three specimens with $[0/\pm45/90]_{25s}$ stacking sequences, Q25-9, Q25-10 and A5, all have very nearly the same compression strengths. However, the Q35 series specimens with a $[0/\pm60]_{35s}$ stacking sequence show more scatter. This may be because specimen Q35-11 was only 0.976 inches wide in a 1.002 inch wide grip opening, whereas specimens Q35-9 and Q35-10 were 1.000 inches wide. The extra 0.024 inches for width-wise expansion in the grips may have slightly reduced the magnitude of the exit angle in specimen Q35-11, as compared to the wider specimen Q35-9 and Q35-10. A reduced exit angle, according to Camponeschi's [1] explanation, would increase the specimen failure load, as observed for specimen Q35-11.

As with the 0.6 inch thick specimens of Figure 4.2, the 1.0 inch thick $[0/\pm45/90]_{25s}$ specimens failed catastrophically while the 1.1 inch thick $[0/\pm60]_{35s}$ specimens failed in their outside plies first, as shown in Figure 4.4. Notice that the failure mode for specimen A5 shows evidence of kink band formation. Although other specimens may also have failed due to kink band formation, the final condition of the specimens after testing prevented any conclusions about the nature of their failure initiation.

Since testing was conducted under displacement (stroke) control, a failure in the specimen could be detected when the load experienced a drop while the displacement continued to rise. Specimens Q35-9 and Q35-10 ($[0/\pm60]_{35s}$ stacking sequence) were tested beyond the first load drop in order to determine if higher strengths could be attained. Testing of specimen Q35-9 was stopped after the first load drop, the specimen was removed from the fixture for examination, then returned to the fixture and reloaded until the next load drop. The second load drop occurred at 86497 psi, below the compression strength of 93650 psi attained for the

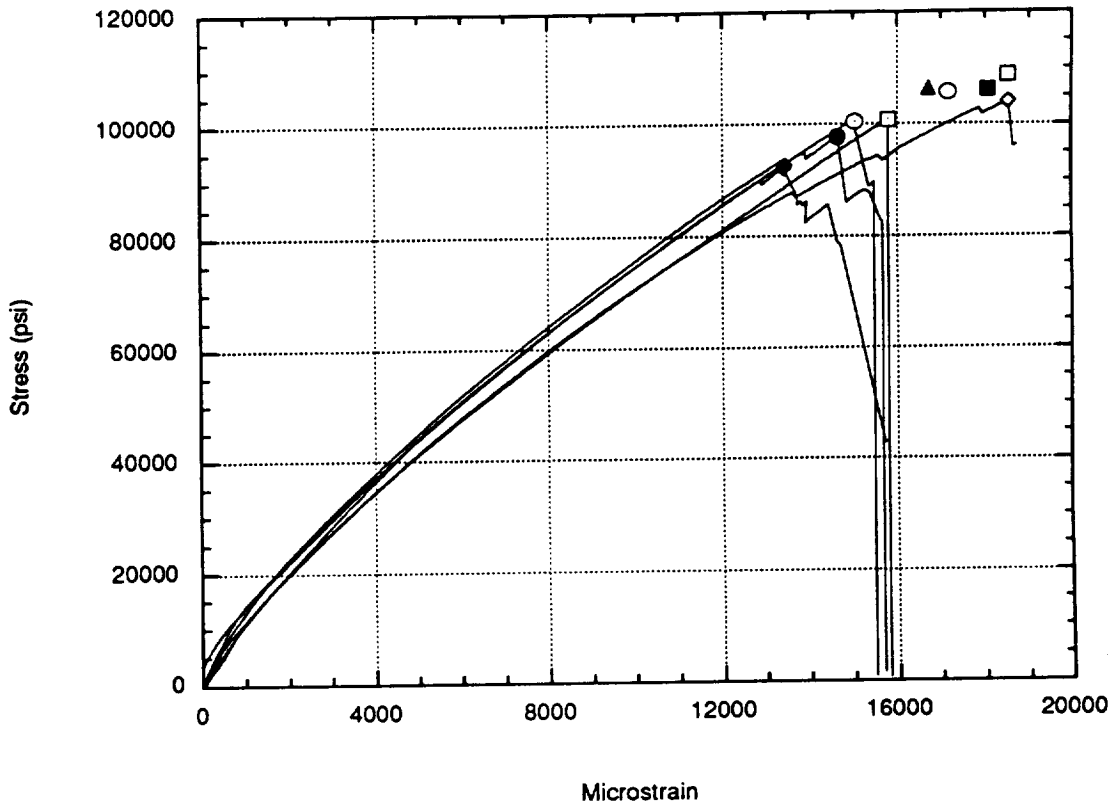

●	Q25-10	$[0/\pm45/90]_{25s}$	97711 psi	□	A5	$[0/\pm45/90]_{25s}$	100825 psi
⊙	Q25-9	$[0/\pm45/90]_{25s}$	100437 psi	■	Q20-11	$[0/\pm60]_{20s}$	106100 psi
◆	Q35-9	$[0/\pm60]_{35s}$	93650 psi	□	Q20-9	$[0/\pm60]_{20s}$	108790 psi
◆	Q35-10	$[0/\pm60]_{35s}$	92222 psi	▲	Q15-9	$[0/\pm45/90]_{15s}$	106400 psi
◇	Q35-11	$[0/\pm60]_{35s}$	104044 psi	○	Q6-10	$[0/\pm45/90]_{6s}$	105642 psi

Figure 4.3 - Experimental compression relations for undamaged specimens, thickness 1.0 inches or greater, $[0/\pm45/90]_{25s}$ and $[0/\pm60]_{35s}$

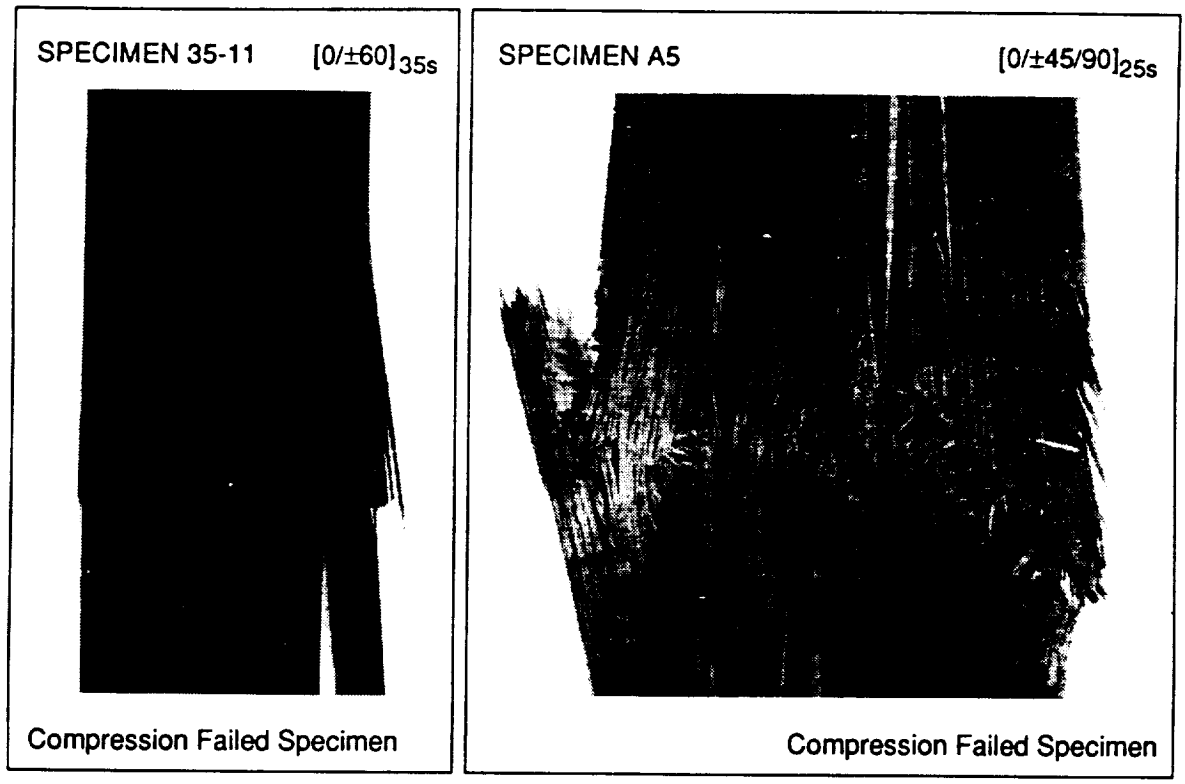

Note: Photos not to same scale

Figure 4.4 - Typical compression failed specimens, $[0/\pm45/90]_{25s}$ and $[0/\pm60]_{35s}$

first loading, suggesting that no additional load could be carried after the initial failure which caused the first load drop. Specimen Q35-10 was loaded continuously after the initial load drop until the failure extended through the thickness of the specimen. After the initial load drop at 92222 psi, further straining showed that the specimen was still capable of carrying load, but not of exceeding the compression strength reported at the first load drop. Therefore, it can be concluded that the first significant load drop in [0/±60] type specimens corresponds to the magnitude of the ultimate compression strength.

4.1.3 Grouped Stacking Sequence

The specimens with grouped stacking sequences failed at much lower loads, as shown in Figure 4.5. An examination of the plot suggests that the $[0_5/45_5/-45_5/90_5]_{5s}$ specimens failed at a lower load than the $[0_5/60_5/-60_5]_{7s}$ specimen. Although the cause of this will be discussed further in Chapter 5, it is interesting to note the corresponding difference in compression failure modes, as shown in Figure 4.6.

Specimen Q7-10, with the $[0_5/60_5/-60_5]_{7s}$ stacking sequence, began failure at the outer plies just as the other [0/±60] type specimens did. Likewise, the specimens with $[0_5/45_5/-45_5/90_5]_{5s}$ stacking sequences failed through the thickness, as did the other [0/±45/90] type specimens. However, failure of the grouped $[0_5/45_5/-45_5/90_5]_{5s}$ specimens included fiber breaks in the 0° plies at a 45° angle to the x-axis. The fiber breaks follow the same angle as the adjacent +45° layers. As compression continued, the broken 0° plies shifted to the side in the width direction. Failure is primarily in the form of extensive matrix cracks and fiber breaks, with no apparent evidence of fiber kinking. Meanwhile, the specimen with a $[0_5/60_5/-60_5]_{7s}$ stacking sequence

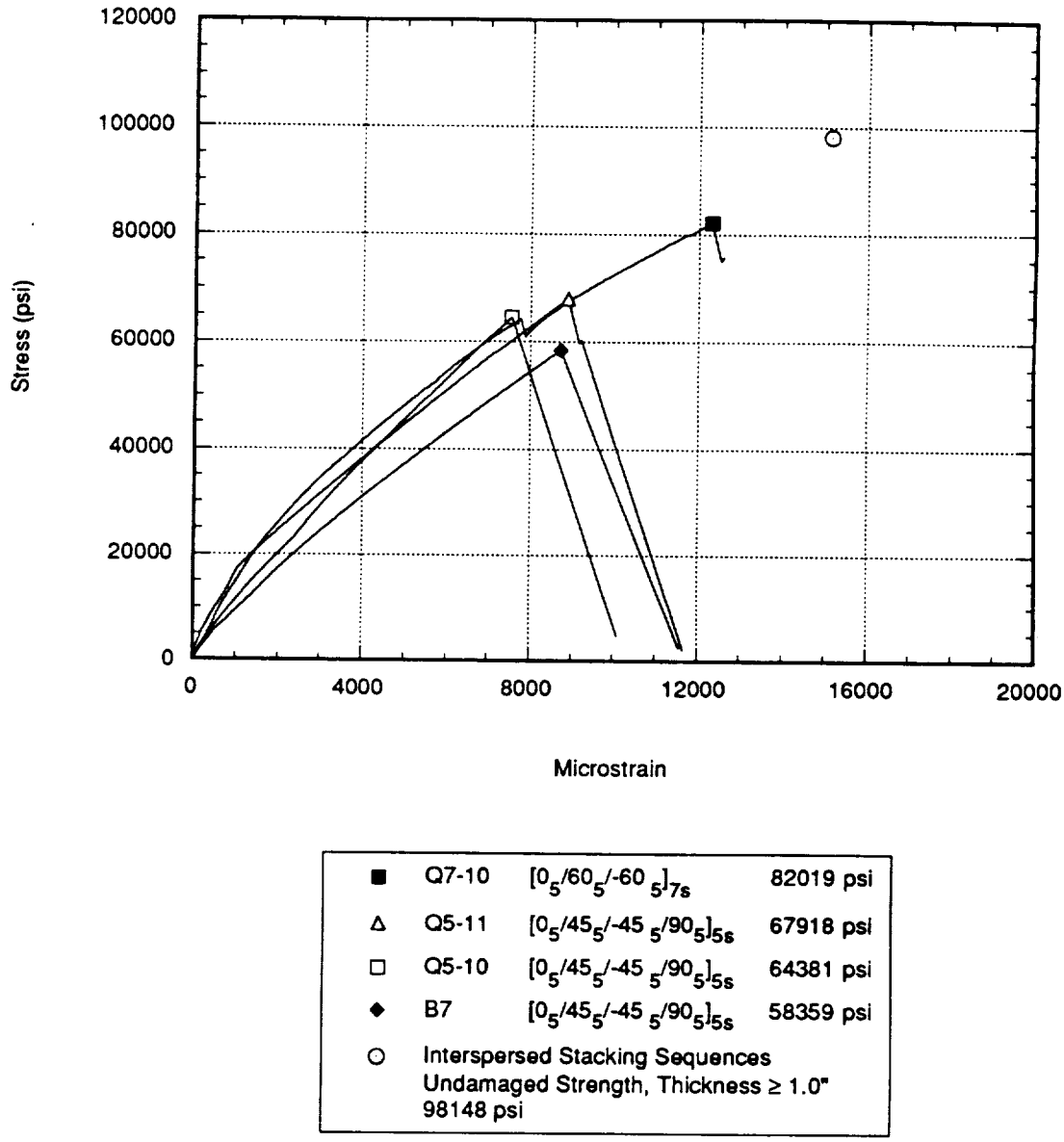

Figure 4.5- Experimental compression relations for undamaged specimens with grouped ply stacking sequences, $[0_5/45_5/-45_5/90_5]_{5s}$ and $[0_5/60_5/-60_5]_{7s}$

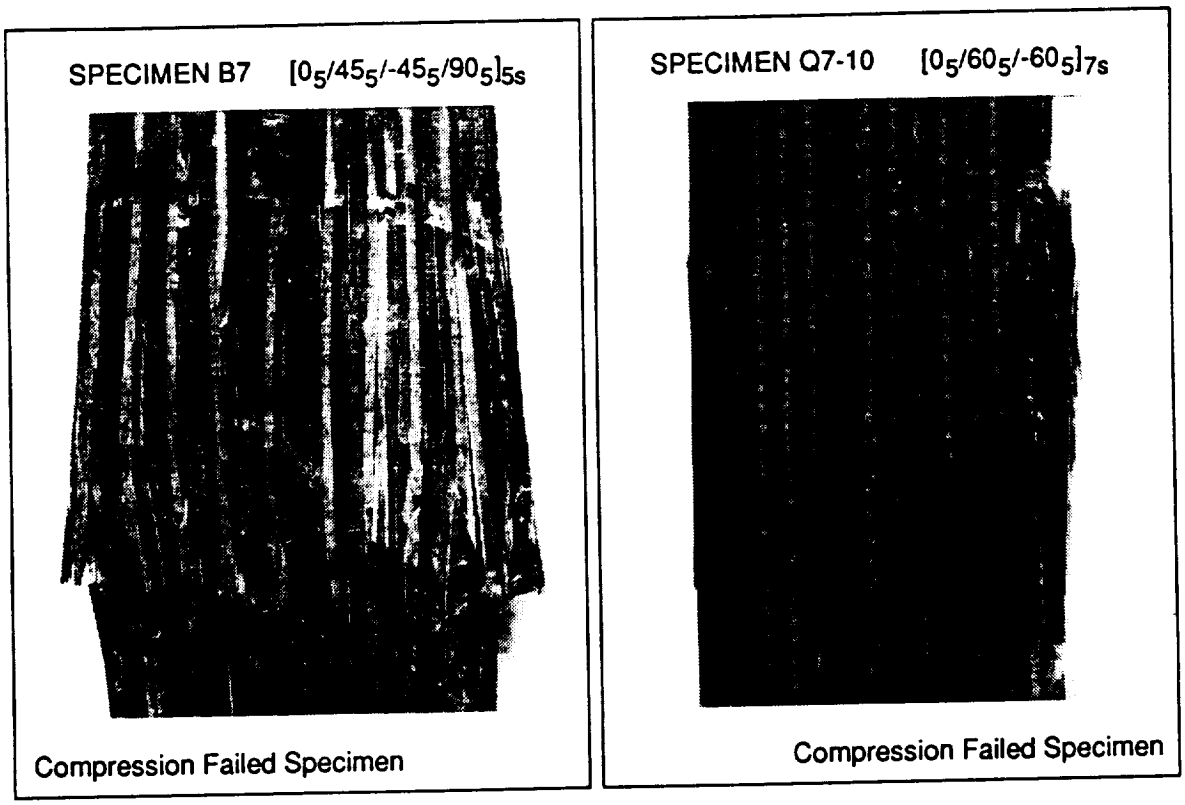

Figure 4.6 - Typical compression failed specimens, $[0_5/45_5/-45_5/90_5]_{5s}$ and $[0_5/60_5/-60_5]_{7s}$

shows evidence of matrix cracks and delaminations in the outer plies but again no kink bands. With this sequence, however, the 0° fibers do not break at any discernable angle.

4.2 Multiple Through-Thickness Delaminations

Specimens with interspersed stacking sequences and three point bend spans of 0.5 or 1.0 inches often exhibited an initial damage state consisting of short delaminations distributed through the thickness (see Figure 3.2). Each delamination exists as part of a set that includes a delamination, one or more matrix cracks, then further delamination. These delamination sets occurred within each [0/±60] or [0/±45/90] ply set, but seldom crossed through the 0° plies. The length of the delamination sets varied according to the three-point bend span, with the 0.5 inch span yielding sets approximately 0.2 inches long and the 1.0 inch span giving sets approximately 0.4 inches long. Different variations of delamination location, delamination length, and matrix crack density gave different variations of a compression failure mode. This initial damage state was quite similar to the impact damage documented in Refs. [19,22,23]. The initial three-point bend damage and resulting failure mode agree qualitatively with the transverse shear failure mode documented by Williams and Rhodes [22], shown in Figure 2.8.

4.2.1 Compression Failure Modes

Eight specimens with multiple through-thickness delaminations were tested. The final compression failure mode for each of these specimens can be described as a combination of

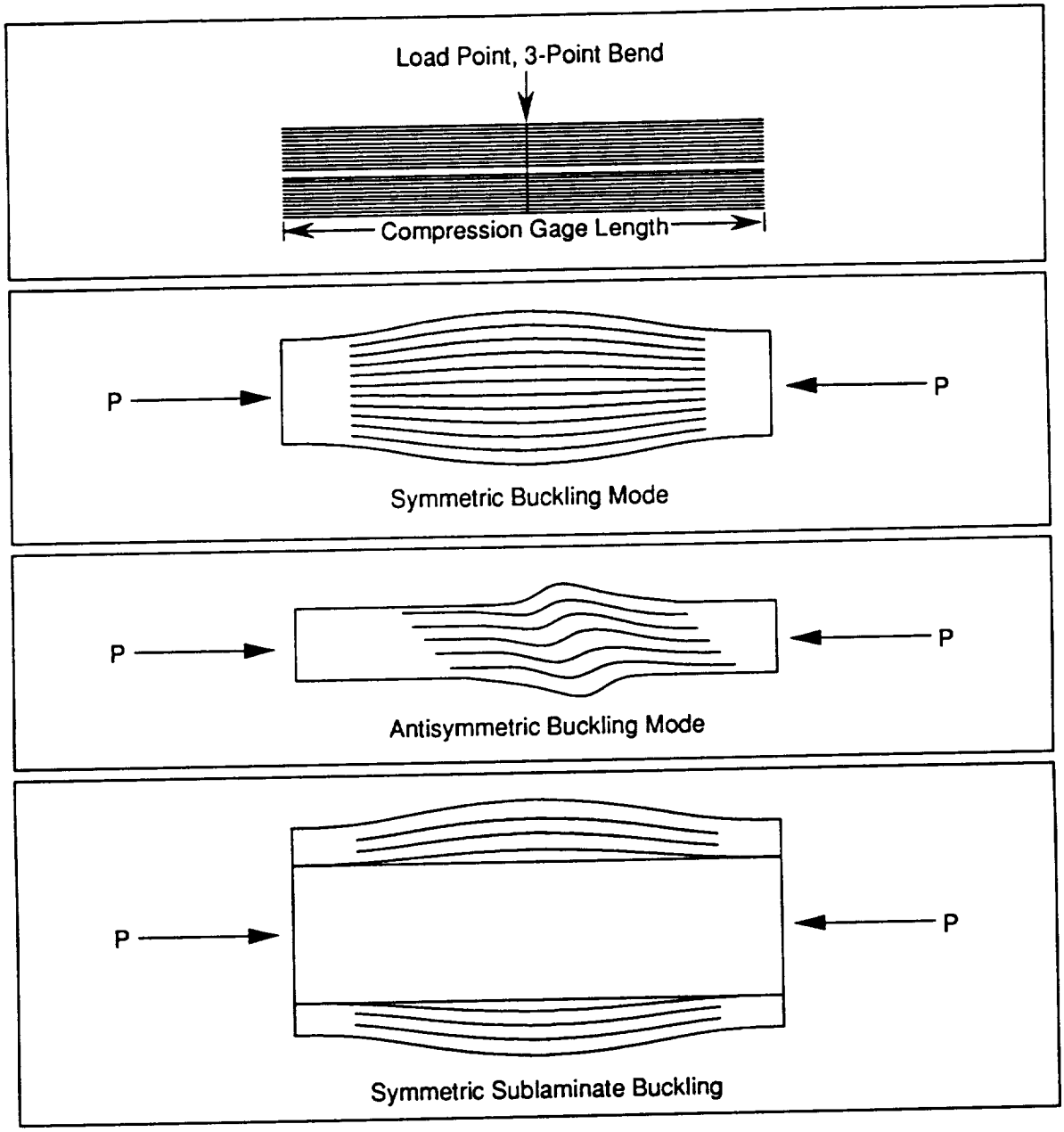

Figure 4.7 - Typical failure modes for multiple through-thickness delaminations

symmetric, antisymmetric, and sublaminate buckling, as shown in Figure 4.7. The first observed buckling shape is symmetric with respect to the loading axis and consists of both faces of the specimen moving out from the midplane. The next buckling shape is antisymmetric and actually looks much like the second buckling mode for a thin column with clamped end conditions. Many specimens did not fail in either of these classifications uniquely, but instead showed some portions, or sublaminates, which buckled separately. As illustrated by the example in Figure 4.7, for some cases the center sublaminate did not buckle at all when the other sublaminates gave way. In other cases, all of the sublaminates buckled simultaneously, with some sublaminates appearing symmetric while others in the same laminate buckled in an antisymmetric mode.

The compression stress-strain relations for the eight specimens with multiple through-thickness delaminations are shown in Figure 4.8. Rather than failing as separate sublaminates with different buckling loads, the entire laminate fails together, as exemplified by the abrupt drops in the stress-strain relations. Only specimen Q20-3, with a $[0/\pm60]_{20s}$ stacking sequence, continues to carry load after failure. This appears in the stress-strain curve as a small increase in the stress after the final load drop. All other specimens in this category lose all load carrying capability at failure. The reduction in compression strength for specimens with multiple through-thickness delaminations, when compared to undamaged specimens, ranges from 50% to 75%, depending on the quantity and length of the delaminations.

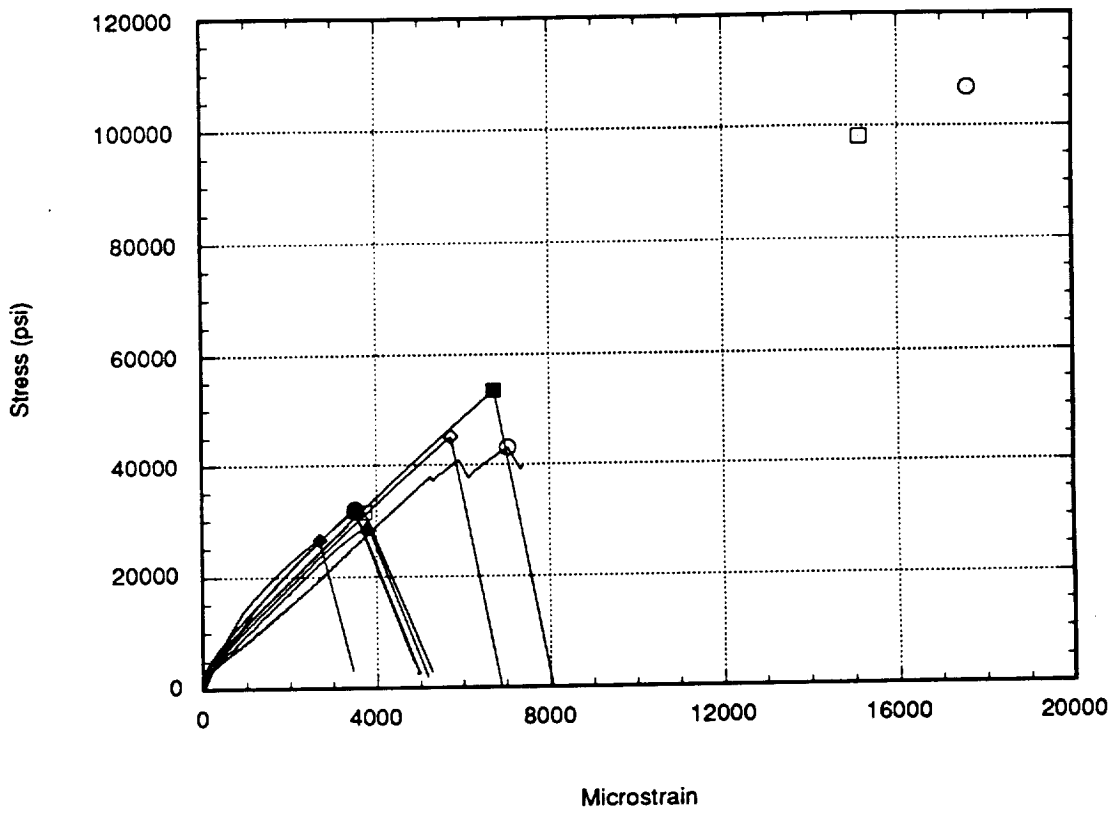

●	A4	$[0/\pm45/90]_{25s}$	32052 psi	■	Q6-4	$[0/\pm45/90]_{6s}$	53378 psi
●	Q8-8	$[0/\pm60]_{8s}$	31646 psi	◆	Q6-3	$[0/\pm45/90]_{6s}$	26568 psi
□	Q8-4	$[0/\pm60]_{8s}$	31517 psi	◇	Q6-8	$[0/\pm45/90]_{6s}$	45138 psi
▲	Q15-3	$[0/\pm45/90]_{15s}$	29076 psi	○	Undamaged Strength, Thickness < 1.0" 106730 psi		
○	Q20-3	$[0/\pm60]_{20s}$	43115 psi	⊡	Undamaged Strength, Thickness ≥ 1.0" 98148 psi		

Figure 4.8 - Experimental compression relations for specimens with multiple through-thickness delaminations, $[0/\pm45/90]_{6s}$, $[0/\pm45/90]_{15s}$, $[0/\pm45/90]_{25s}$, $[0/\pm60]_{8s}$, and $[0/\pm60]_{20s}$

4.2.2 Failure of 48-Ply Specimens

The $[0/\pm60]_{8s}$ specimens with 0.5 inch spans show a clear example of antisymmetric buckling, as seen in Figure 4.9. These two specimens, Q8-4 and Q8-8, contain delaminations of approximately equal length distributed in such a way as to break the 48-ply laminate into 16 sublaminates containing between 2 and 3 plies each. At failure, these sublaminates fail simultaneously to form an antisymmetric shape. Likewise, the $[0/\pm45/90]_{6s}$ specimens with 0.5 inch span lengths show a similar antisymmetric buckling shape. Again referring to Figure 4.9, the initial damage and failure mode for specimen Q6-8, with a $[0/\pm45/90]_{6s}$ stacking sequence, appears the same as for specimens Q8-4 and Q8-8. The actual failure stress is higher for Q6-8 because the $[0/\pm45/90]_{6s}$ specimens are divided into 12 sublaminates containing between 3 and 4 plies each rather than 16 sublaminates containing between 2 or 3 plies each for the $[0/\pm60]_{8s}$ specimens. The failure stresses can be found in Figure 4.8.

The failure mode for specimen Q6-4, with a $[0/\pm45/90]_{6s}$ stacking sequence, looks slightly different because the delaminations near the midplane do not extend all the way across the width of the specimen. Examination of the edge replicas (not pictured here) reveals midplane delaminations which appear only on one edge of the specimen with no apparent damage on the opposite edge. The result is a failure mode which is actually made up to two antisymmetric buckling shapes which occur at the same stress. For specimen Q6-3, with a $[0/\pm45/90]_{6s}$ stacking sequence and a 1.0 inch span length, the buckling mode is symmetric. Thus comparing Figures 4.9 and 4.10, it can be concluded that short delaminations on the order of 0.2 inches long lead to an antisymmetric buckling mode while longer delaminations on the order

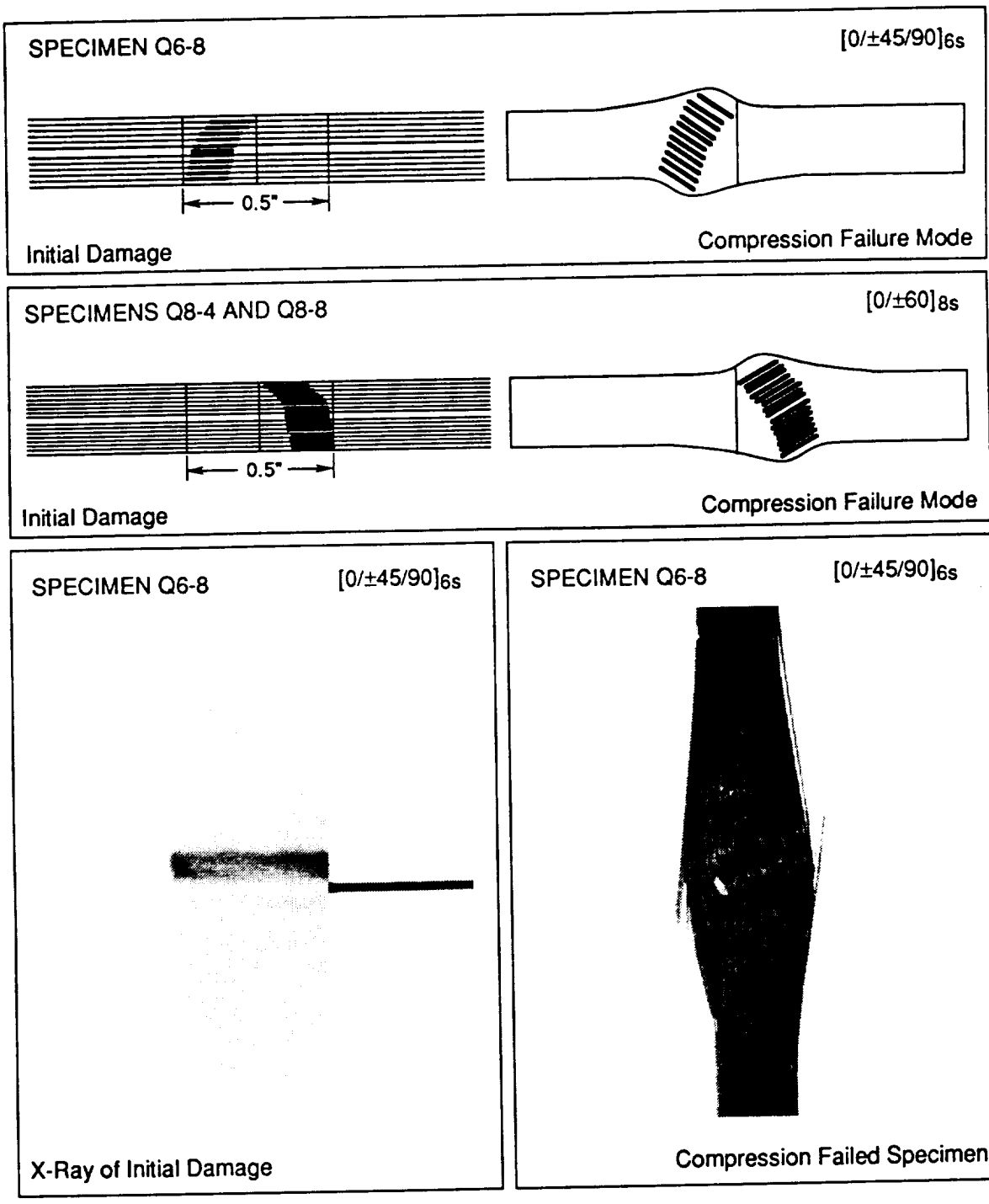

Figure 4.9 - Initial damage and failure modes for specimens with multiple through-thickness delaminations, $[0/\pm60]_{8s}$ and $[0/\pm45/90]_{6s}$

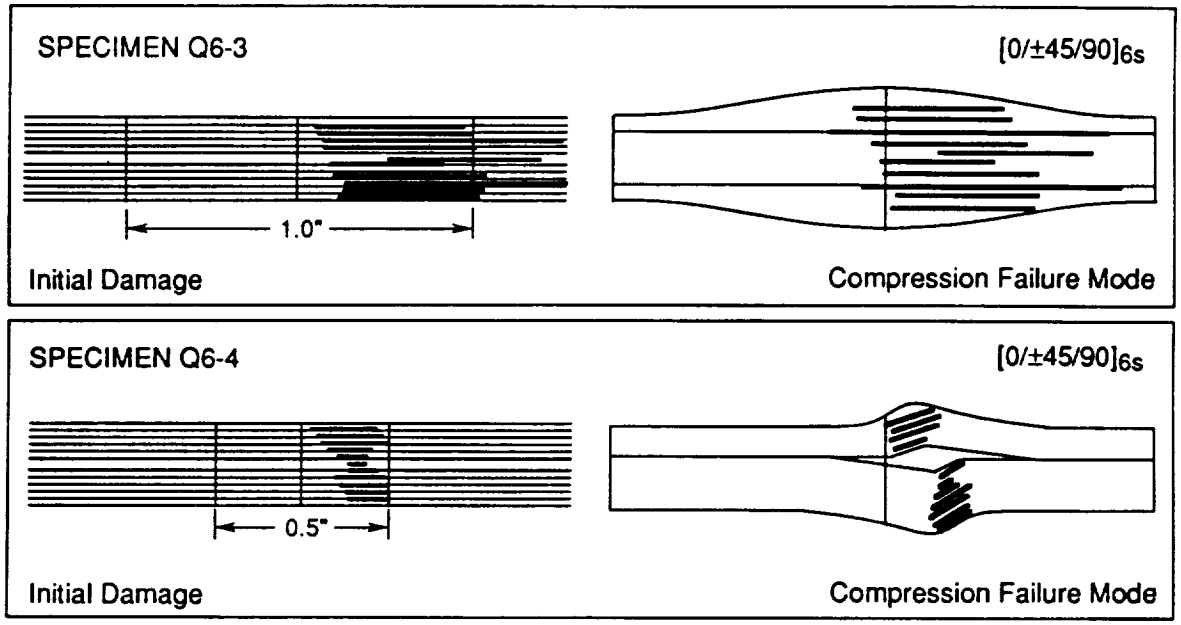

Figure 4.10 - Initial damage and failure modes for specimens with multiple through-thickness delaminations, $[0/\pm45/90]_{6s}$

of 0.4 to 0.6 inches long lead to a symmetric buckling shape. The compression strength is lower for the longer delaminations with a symmetric buckling shape.

4.2.3 Failure of 120-Ply and 200-Ply Specimens

The next two stacking sequences discussed are $[0/\pm45/90]_{15s}$ and $[0/\pm60]_{20s}$ with 120 plies each. Specimen Q15-3 can best be compared with specimen Q6-3 since both have a [0/±45/90] type stacking sequences with a 1.0 inch span. As illustrated in Figure 4.8, these two specimens do indeed have similar compression strengths. Referring to Figures 4.10 and 4.11, note that the upper 90 plies of specimen Q15-3 behave much like specimen Q6-3 in that both fail with a symmetric buckling shape. Specimen Q15-3 can be seen to split into two different buckling shapes around ply 90 where numerous matrix cracks occur. The lower portion of the specimen, which contains slightly shorter delaminations, then buckles in an antisymmetric shape.

The initial damage and failure mode of specimen Q20-3 with a $[0/\pm60]_{20s}$ stacking sequence is slightly different than the [0/±60] type specimens discussed earlier. Unlike the thinner specimens, Q20-3 does not contain a delamination in every ply set, and the three-point bend span is now 1.0 inches rather than 0.5 inches. Near the midplane of the specimen, there is only one delamination for every two or three ply sets, as shown in Figure 4.11. This yields sublaminates that range in thickness from 2 or 3 plies near the front and back faces, to a maximum of 12 plies near the midplane. The failure mode for this specimen can thus be seen as the sum of three parts. The front and back sections buckle symmetrically (symmetric sublaminate buckling), as was noted previously for delaminations of this length and approximate density. The section around the midplane, meanwhile, does not show any change

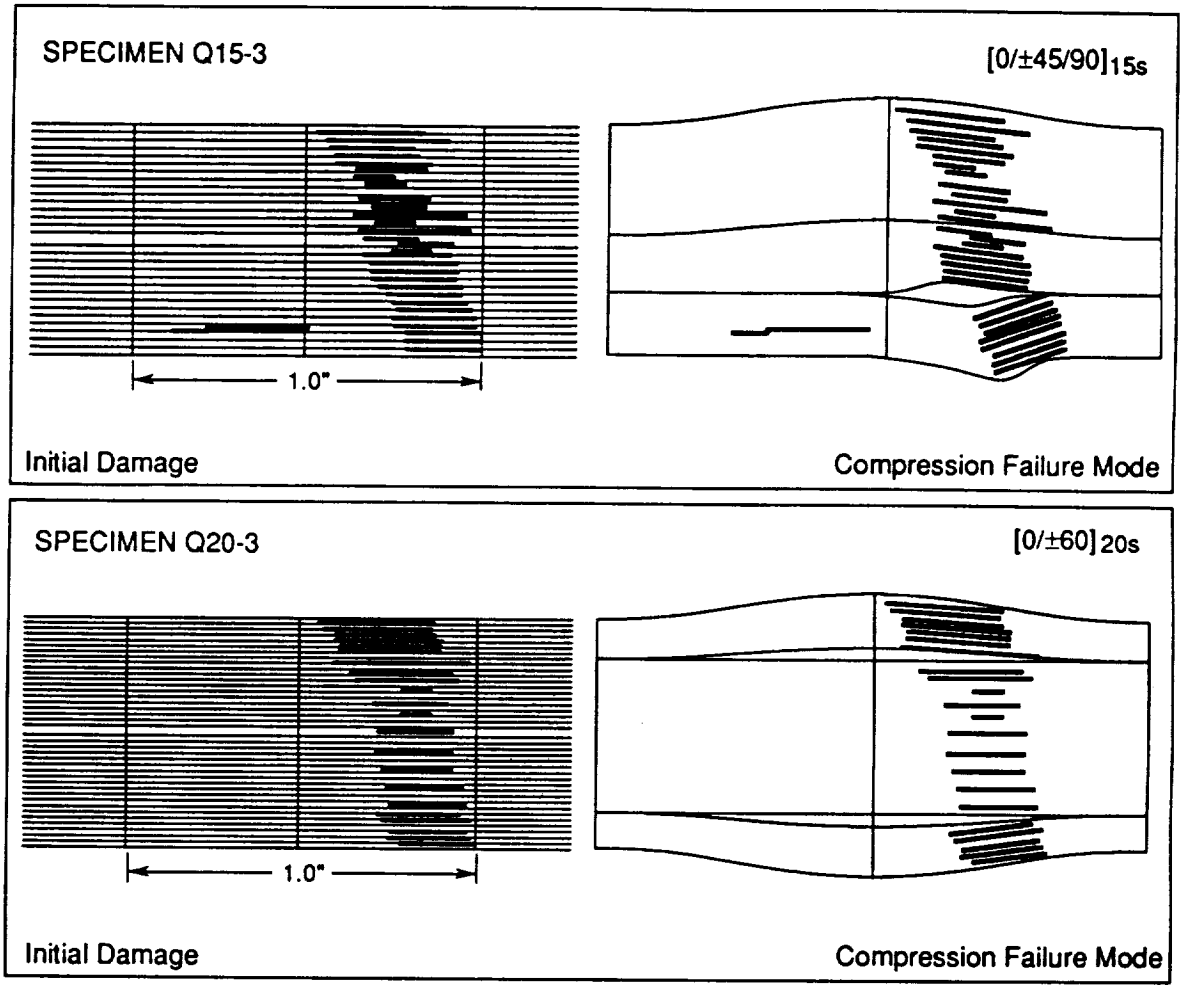

Figure 4.11 - Initial damage and failure modes for specimens with multiple through-thickness delaminations, $[0/\pm45/90]_{15s}$ and $[0/\pm60]_{20s}$

from its initial damage state. In addition to the different appearance of the failure mode, the compression stress-strain curve is also different as seen in Figure 4.8. Unlike the other specimens with multiple through-thickness delaminations, specimen Q20-3 failed in distinct steps. This can be attributed to the fact that the midplane section continued to carry load after the front and back sections buckled separately.

For the thickest types of specimens, only the $[0/\pm45/90]_{25s}$ specimen with a 1.0 inch span exhibited initial damage in the form of multiple through-thickness delaminations. It should be noted that this specimen was part of a study which involved specimens with increasing amounts of initial damage. The goal was to study the effects on increasing damage quantity on the final compression strength. Of the five specimens tested with this stacking sequence and span, only specimen A4 fit the classification of multiple through-thickness delaminations. Specimen A4 contained approximately one delamination every ply group with delaminations on both sides of the centerline in the last 60 plies. The failure mode for this specimen, as shown in Figure 4.12, appears as a combination of an antisymmetric buckling shape for the upper portion of the specimen and a symmetric shape for the lower 60 plies.

Referring to Figure 4.8, the compression strengths for specimens Q15-3 and Q6-3 are quite similar to the strength of specimen A4, all of which have [0/±45/90] type stacking sequences and contain delaminations every 3 to 4 plies. This implies that the thickness of the sublaminates, and not the thickness of the specimens, determines the value of the compression strength for multiple through-thickness delaminations of similar length.

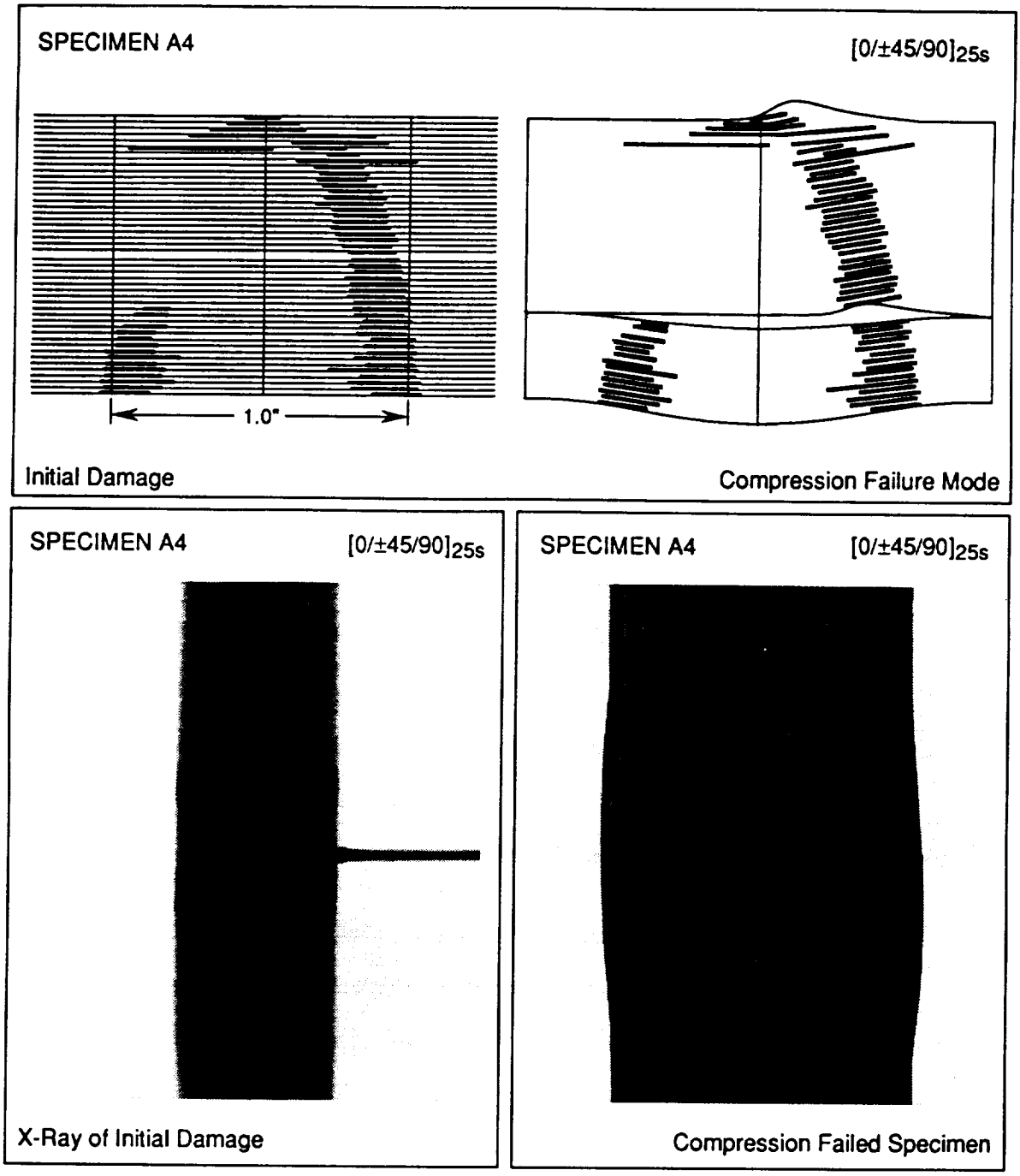

Figure 4.12 - Initial damage and failure mode for specimen with multiple through-thickness delaminations, $[0/\pm45/90]_{25s}$

4.3 Isolated Delaminations

Isolated delaminations tend to occur with three-point bend spans of 1.0 or 3.0 inches and interspersed stacking sequences. The delaminations are isolated in that each set of delaminations and matrix cracks is separated from other sets by several repeating ply units. Each set is contained in a repeating ply unit of either [0/±45/90] or [0/±60] plies, without crossing through the 0° plies. These delamination sets divide the original specimen into one of two possible patterns. First, delaminations may occur dispersed though the thickness creating two or more unsymmetric sublaminates of similar thickness. Alternately, these delaminations may occur near the surface and thus divide the laminate into one or more thin unsymmetric sublaminates and a significantly thicker base laminate. These two different patterns result in distinctly different failure modes.

4.3.1 Compression Failure Modes

Of the nine specimens tested with isolated delaminations, four had delaminations near the surface and five had delaminations dispersed through the thickness (far from the surface). When a delamination occurs near the surface, causing the specimen to behave like a thin sublaminate and a base laminate, the specimens tend to fail by sublaminate buckling. After failure of the sublaminate, the base laminate remains relatively intact and is capable of carrying additional load. By contrast, failure of the specimens with delaminations far from the surface

occurs abruptly with a complete loss of load carrying capability. The failed specimen often appears in two parts divided by a delamination which propagated to both ends of the specimen. The difference in failure modes suggests that different mechanisms may govern the compression failure depending on the location of the delaminations.

4.3.2 Delaminations Far From the Surface

The compression stress-strain relations for the five specimens with delaminations near the midplane are shown in Figure 4.13, while their damage states prior to compression testing are shown in Figures 4.14 and 4.15. Examining the 48-ply specimens first, note that specimens Q8-3 and Q8-7, with $[0/\pm60]_{8s}$ stacking sequences, differ only in the location of their delaminations with respect to the specimen thickness. Specimen Q8-3 contains twodelaminations which divide the laminate into three sublaminates. The two outer sublaminates are unsymmetric while the center sublaminate is nearly symmetric. Specimen Q8-7 meanwhile is divided into just two unsymmetric sublaminates of roughly equal thickness. However, an examination of Figure 4.13 reveals that these two specimens failed at roughly the same stress. Specimen Q6-7, with its $[0/\pm45/90]_{6s}$ stacking sequence and two delaminations, also failed at roughly the same stress.

Turning attention to the 120-ply specimens Q15-6 and Q15-2, with $[0/\pm45/90]_{15s}$ stacking, note that both contain delaminations near the midplane. The main difference between the two is the addition of matrix cracks in the first 12 plies of specimen Q15-6. Although the relations shown in Figure 4.13 do not make it explicitly clear, these thicker specimens experience two load drops prior to failure. By stopping specimen Q15-6 after each of these drops, it was determined that the drops are due to failure of the first 12-16 plies. After the first drop, the first three 0°

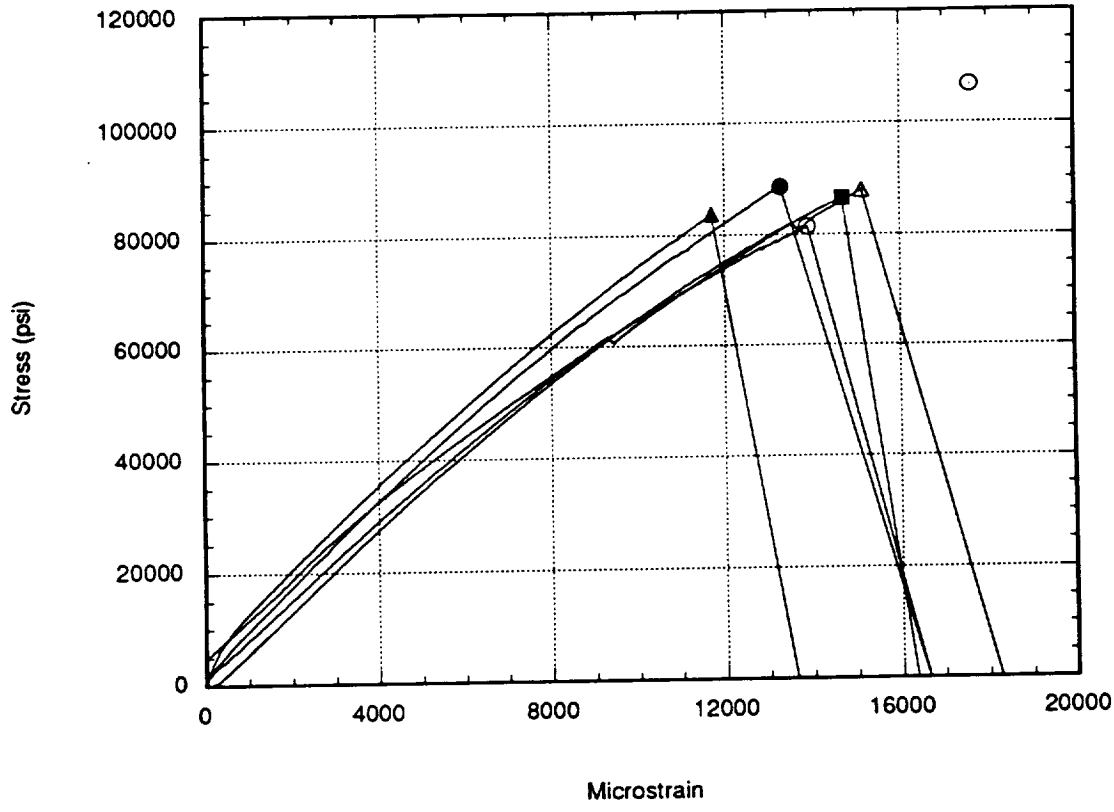

Figure 4.13 - Experimental compression relations for specimens with isolated delaminations near the midplane, $[0/\pm60]_{8s}$, $[0/\pm45/90]_{6s}$, and $[0/\pm45/90]_{15s}$

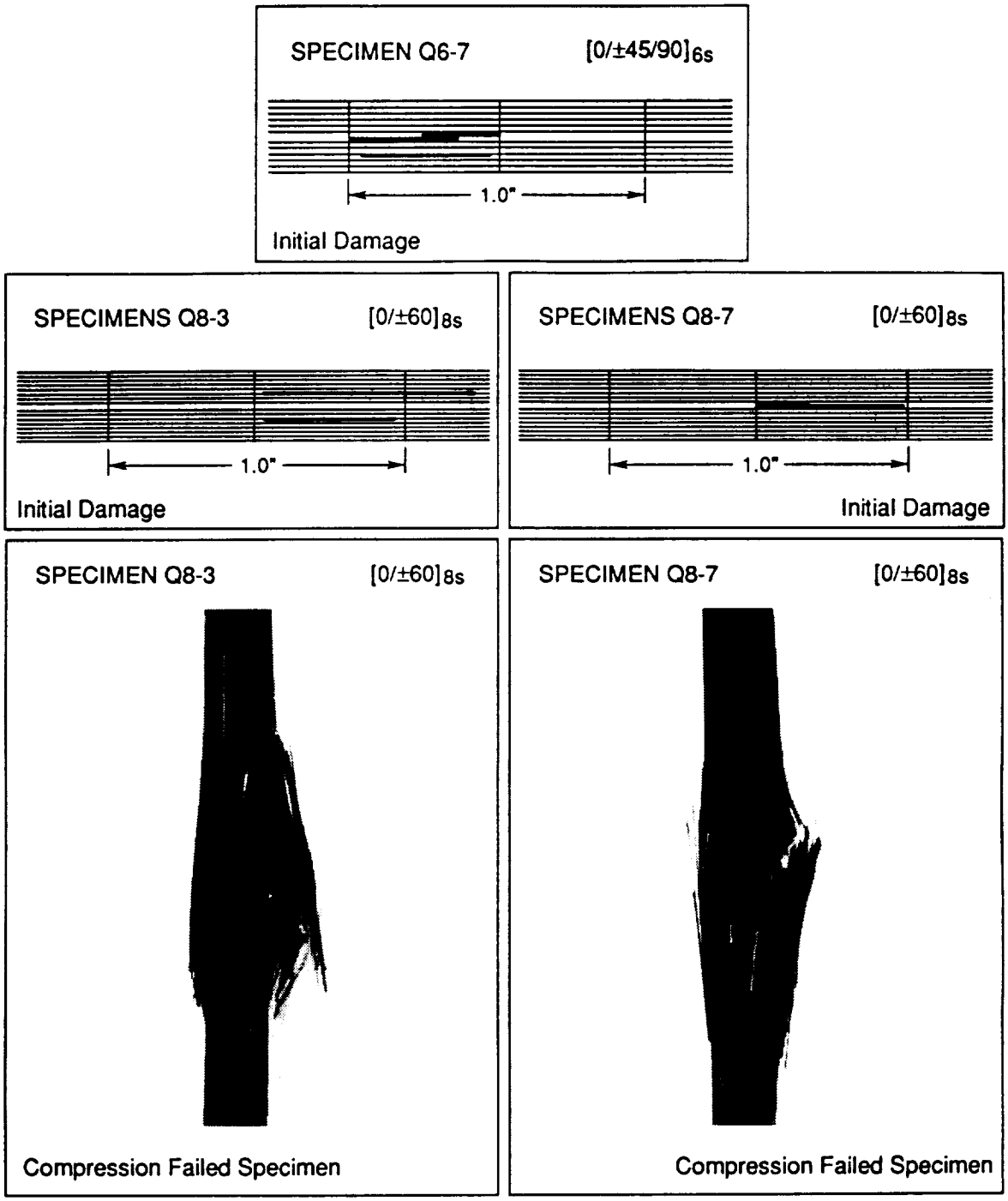

Figure 4.14 - Initial damage and failed specimens for isolated delaminations, $[0/\pm45/90]_{6s}$ and $[0/\pm60]_{8s}$

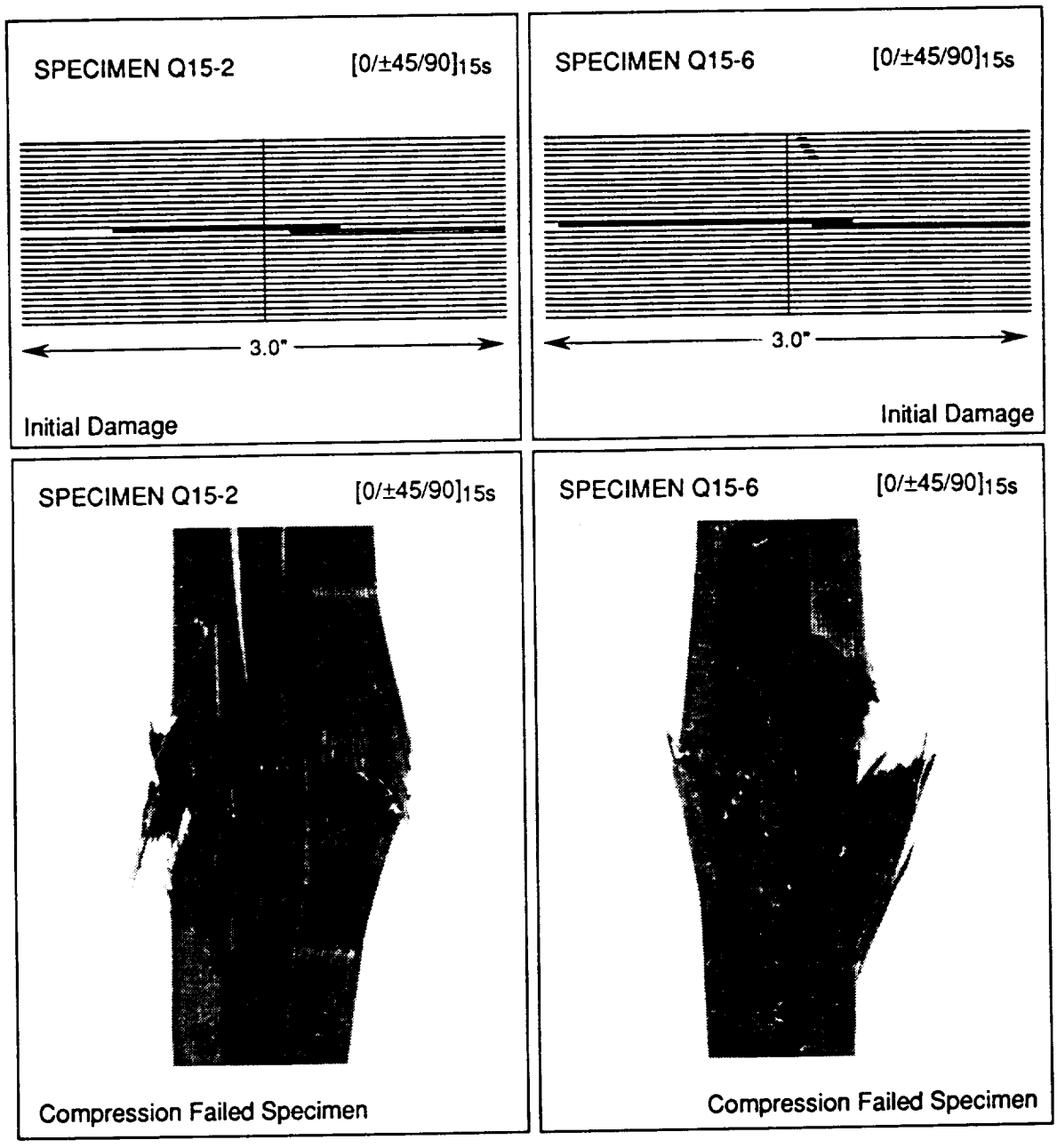

Figure 4.15 - Initial damage and failed specimens for isolated delaminations, $[0/\pm45/90]_{15s}$

layers had failed due to broken 0° fibers. The second load drop occurred after the next two 0° plies failed. However, like the 48-ply specimens, final failure occurred abruptly and completely and at approximately the same stress as all the other specimens with delaminations far from the surface. The reduction in compression strength associated with localized fiber breaks in the first 0° ply, and delaminations far from the surface, was approximately 20%.

4.3.3 Delaminations Near the Surface

The compression stress-strain relations of four different specimens with delaminations near the surface are shown in Figure 4.16. Specimen Q15-7, with a $[0/\pm45/90]_{15s}$ stacking sequence and 1.0 inch span, contains a delamination after the eighth ply, as shown in Figure 4.17. When tested in compression, a load drop corresponding to failure of the first eight plies occurred at a stress of 54793 psi. Specimen Q20-7, with a $[0/\pm60]_{20s}$ stacking sequence and 1.0 inch span, contained a delamination after the twelfth ply. The load drop it experienced at 69114 psi corresponded to the failure of the first 12 plies. Following this developing trend, specimen Q35-2, with a $[0/\pm60]_{35s}$ stacking sequence and a delamination after the first 15 plies, experienced a drop in load at 83206 psi. This corresponded to the failure of the first 15 plies. Specimen Q35-6 had the same damage near the surface as specimen Q35-2, a delamination after the fifteenth ply. The first load drop occurred at 83986 psi, very close to the stress at load drop for specimen Q35-2. Unlike the specimens with the delaminations far from the surface, these specimens tend to follow the trends suggested by a sublaminate buckling theory. That is, thinner sublaminates fail as a result of buckling at lower loads than thicker sublaminates. All four specimens were capable of carrying additional loads following this initial load drop.

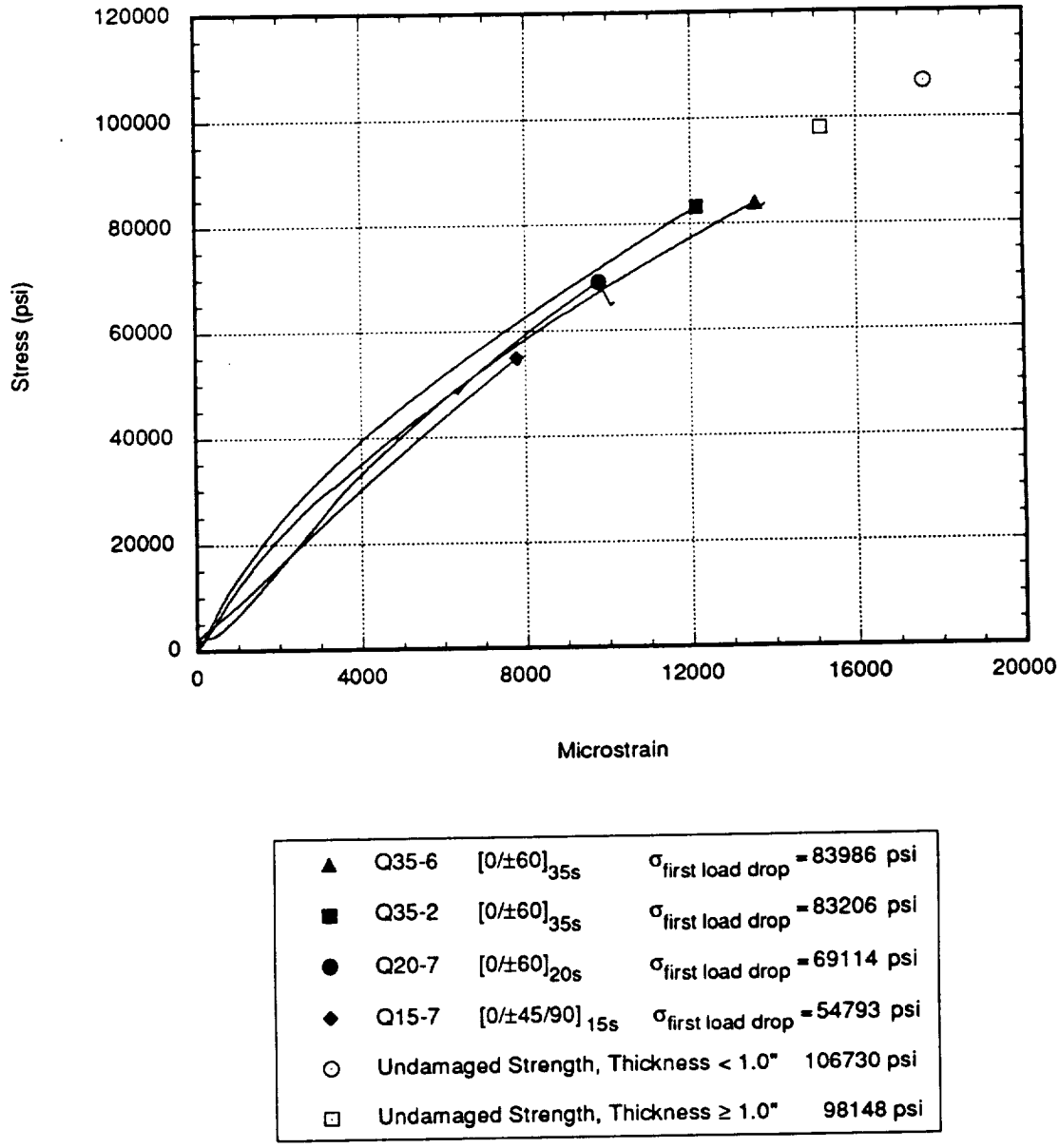

Figure 4.16 - Experimental compression relations for specimens with isolated delaminations near the surface, $[0/\pm45/90]_{15s}$, $[0/\pm60]_{20s}$, and $[0/\pm60]_{35s}$

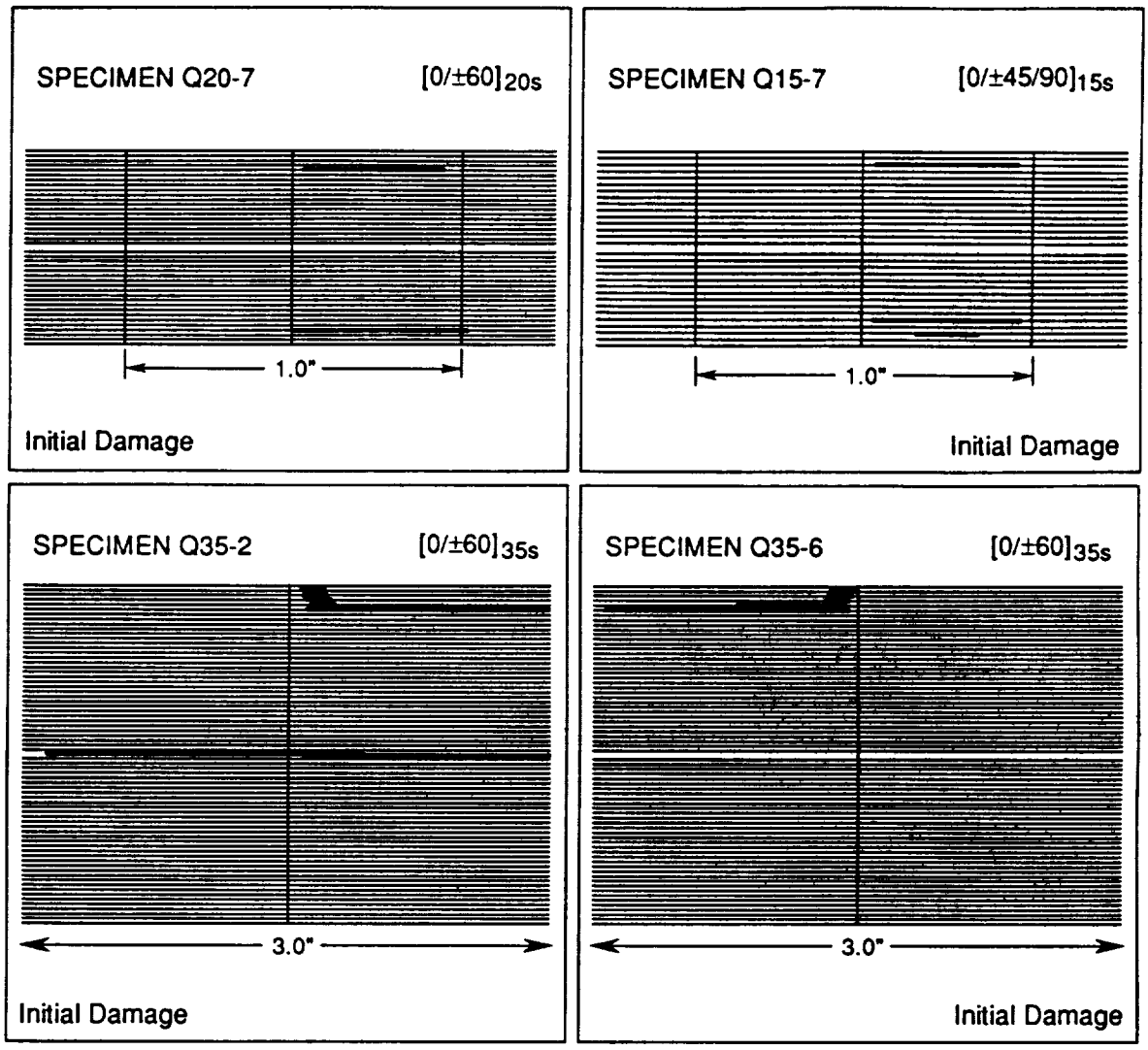

Figure 4.17 - Initial damage for specimens with isolated delaminations, $[0/\pm60]_{20s}$, $[0/\pm45/90]_{15s}$, and $[0/\pm60]_{35s}$

Notice (Figure 4.17) that the 15-ply sublaminates of both Q35-2 and Q35-6 contain matrix cracks and very short delaminations between the main delamination and the surface, which may have reduced the load at which their first failures occurred. Although specimen Q35-2 contains an additional delamination near its midplane when compared to specimen Q35-6, the delamination near the surface caused failure of the outer plies. Based on this observation, an examination of Figure 4.18 allows some comment on the interaction of isolated delaminations. Although the form of the compression stress-strain relations appear similar, specimen Q35-2, with a delamination at the midplane and another near the surface, fails at a lower stress than specimen Q35-6, with only a delamination near the surface. However, this difference is minimal.

4.4 Damage Near the Surface

Thick specimens and specimens with three point bend spans of 5.5 or 3.0 inches have damage that is generally restricted to the outermost plies of the laminate. Damage is located either in the first plies under the three-point bend loading nose or the last plies at the support points. The damage may be either balanced with respect to the load nose (damage on both sides of the centerline), or unbalanced (all damage on one side of the centerline). The form of damage also varies to include different combinations of matrix cracks, delaminations, and fiber breaks.

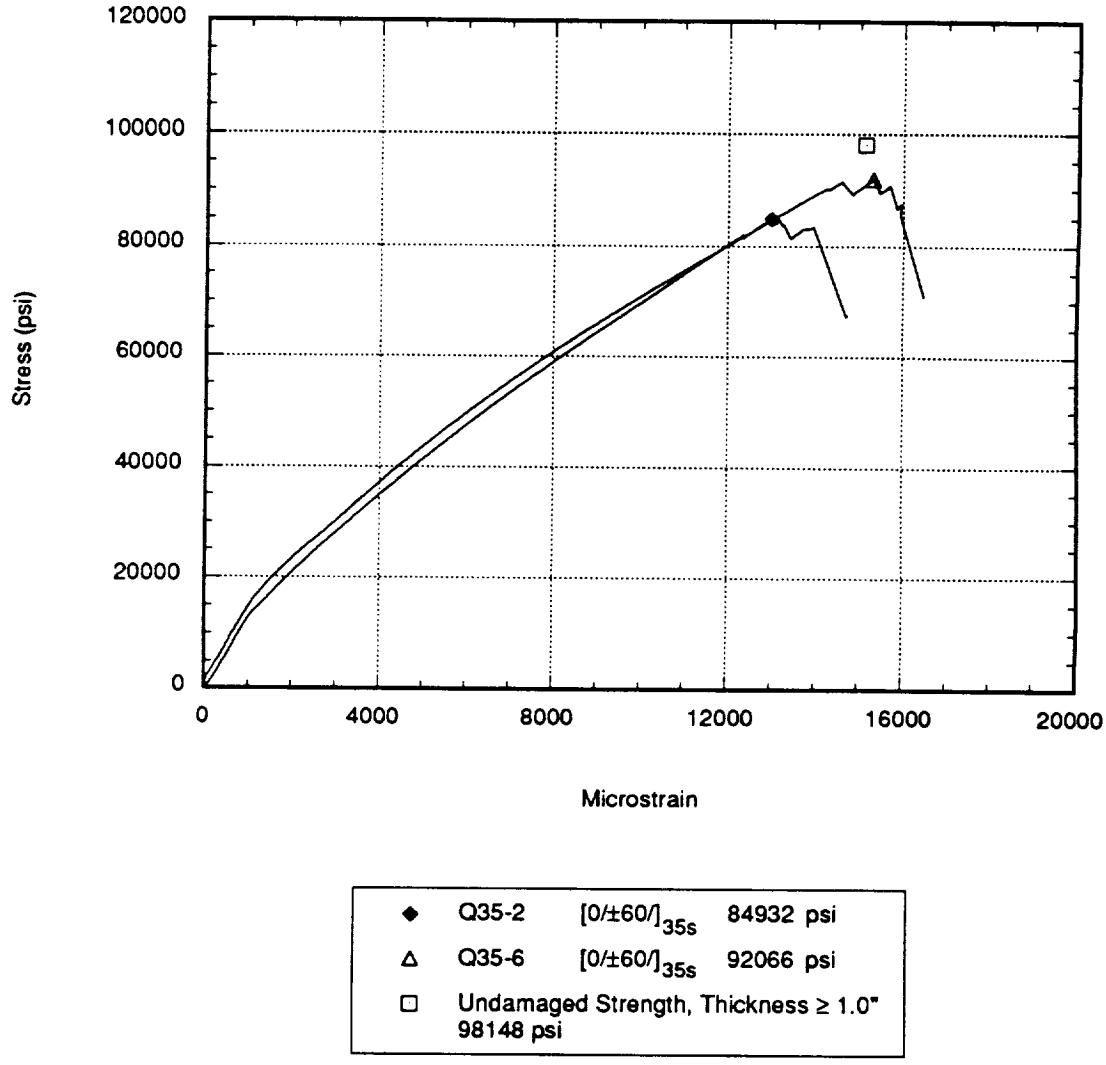

Figure 4.18 - Experimental compression relations for effect of delamination at the midplane, $[0/\pm60]_{35s}$

4.4.1 Compression Failure Modes

Of the twelve specimens tested with damage near the surface, eight contained balanced damage at both the load and support points and seven had unbalanced damage only at the load nose. Five of the seven unbalanced specimens had broken 0° fibers while all other specimens had only delaminations and/or matrix cracks. However, the compression failure modes varied not according to the specifics of the damage but according to the thickness of the specimens.

Except for the 48-ply, 0.24 inch thick specimens, failure of the initially damaged plies occurred prior to catastrophic failure. As loading progressed, the 120-ply, 0.60 inch thick specimens eventually failed completely with damage extending through the thickness of the specimen. The specimens with thicknesses of 1.0 inches or more and 200 or 210 plies, however, continued to fail from the outermost plies to the innermost. These thickest specimens never achieved loads significantly greater than the load at the first large load drop that occurred with the failure of the initially damaged plies. Testing was stopped for most of these specimens before catastrophic failure, leaving a base laminate still capable of carrying some load.

4.4.2 Failure of 48-Ply Specimens

The thinnest of the specimens tested, those with 48 plies and $[0/\pm45/90]_{6s}$ or $[0/\pm60]_{8s}$ stacking sequences, exhibited a unique initial damage mode for three-point bend spans of 3.0 and 5.5 inches. Damage is apparent under the load nose in the form of a crack across the width of the specimen which is visible from the upper surface. This crack is due to broken 0° fibers in the first layer beneath the load nose. Specimen Q8-1 (Figure 4.19), with a $[0/\pm60]_{8s}$ stacking

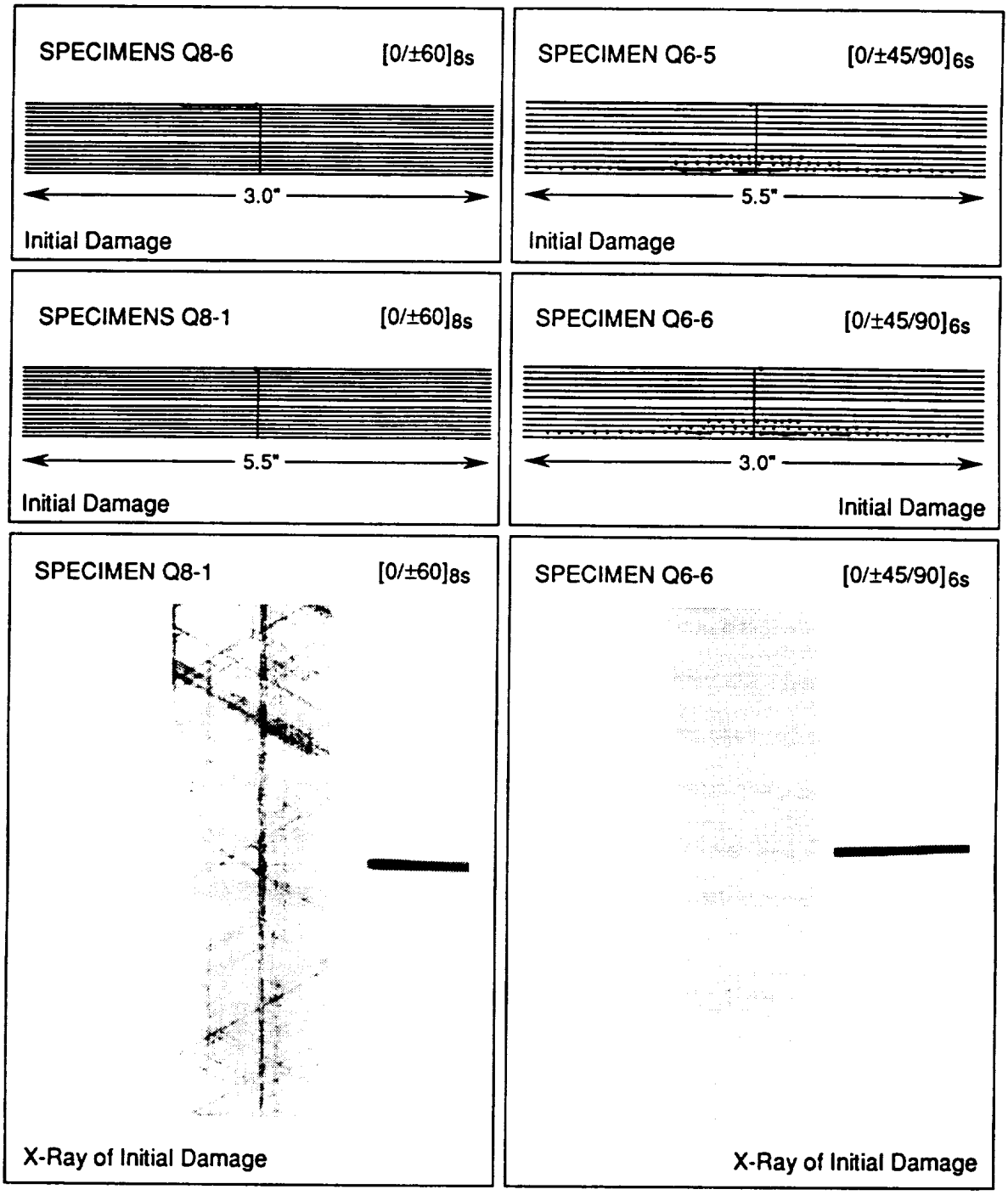

Figure 4.19 - Initial damage and failed specimens for symmetric damage near the surface, $[0/\pm45/90]_{6s}$ and $[0/\pm60]_{8s}$

sequence, contains this crack while specimen Q8-6 also contains a delamination beneath the damaged 0° ply. The x-rays of the initial damage contain this type of crack in addition to a distinct pattern of diagonal lines at angles of ±60°, as shown in Figure 4.19. All of the specimens cut from panel Q8 contain this same diagonal line pattern, although no matrix cracks can be discerned from the edges of the specimens. However, the specimens appear to have a very high quantity of voids (as indicated by the edge replicas) which may be so extensive as to cause the diagonal lines. The compressive strength of specimen Q8-6 is seen to be slightly lower than the strength of specimen Q8-1 (Figure 4.20) due the the additional delamination in specimen Q8-6.

Specimens Q6-5 and Q6-6, with $[0/\pm45/90]_{6s}$ stacking sequences, contain small cracks in the last few 90° plies on the tension side of the specimens in addition to the fiber breaks in the first 0° plies, as shown in Figure 4.19. After the cracks reach a critical density, they connect together not as delamination but within the plies in the x-direction. As indicated by the x-ray of specimen Q6-6 in Figure 4.19, the matrix cracks do not traverse the width of the specimen. Since the failure stress for these specimens (Figure 4.20) is consistent for the 0° fiber damage alone, it is believed that these cracks actually appear only on the edges of the specimens. It is also interesting to note that specimens with both stacking sequences, $[0/\pm45/90]_{6s}$ and $[0/\pm60]_{8s}$, fail at approximately the same stress.

4.4.3 Failure of 120-Ply, 200-Ply, and 210-Ply Specimens

Specimens that have thicknesses of 1.0 inches or greater with a 1.0 inch three-point bend span contain initial damage which is balanced about the centerline at the load nose and support points. Specimens from panel A, with a $[0/\pm45/90]_{25s}$ stacking sequence, were loaded under

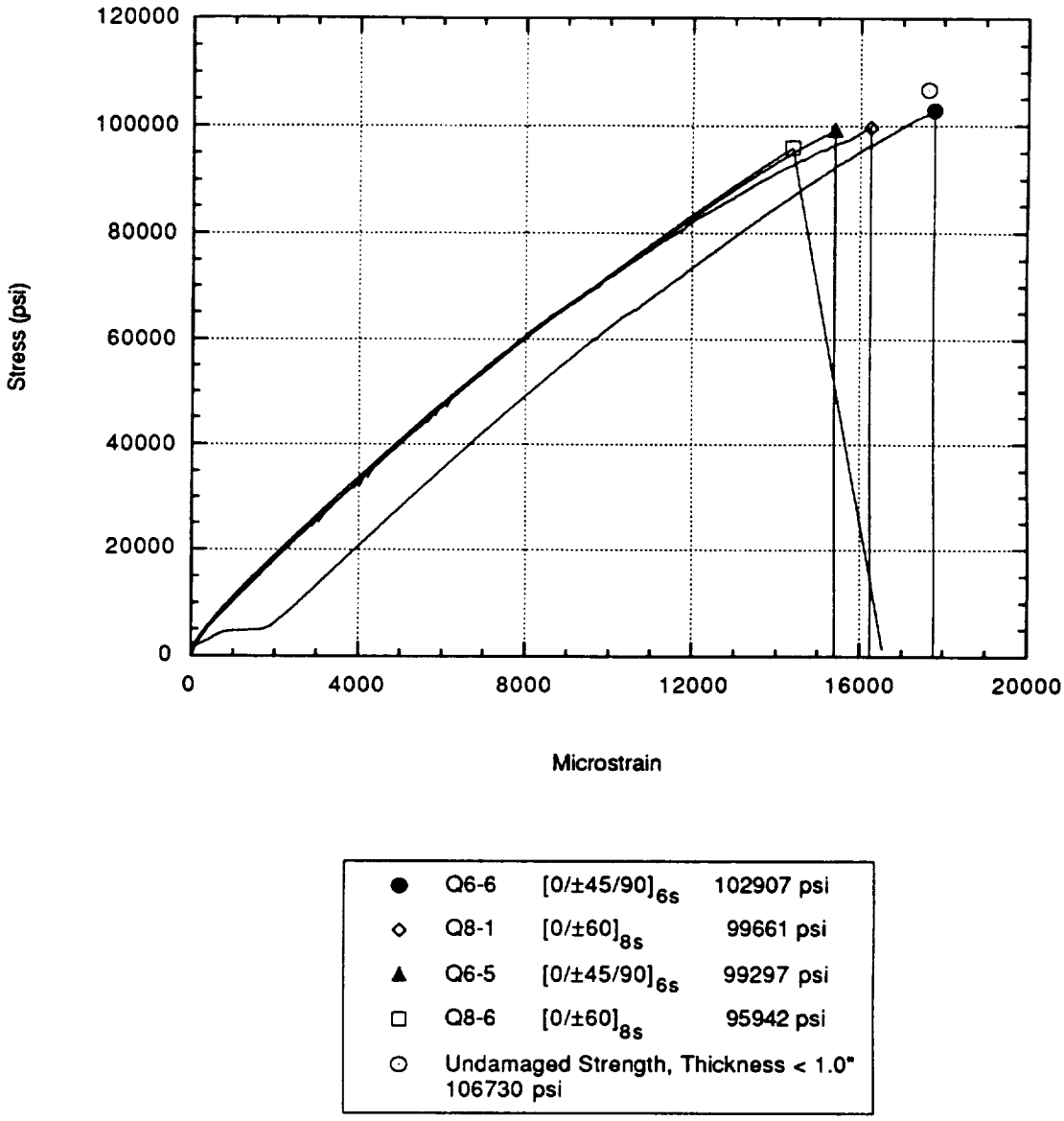

Figure 4.20 - Experimental compression relations for specimens with damage near the surface and back face matrix cracks, $[0/\pm45/90]_{6s}$ and $[0/\pm60]_{8s}$

three-point bending to different load levels all with the same span, as listed in Table 4.1. This was done to study the effects on compression strength of increasing amounts of initial damage. Specimen A4 has initial damage in the form of multiple through-thickness delaminations and is therefore discussed in Section 4.2.3. The resulting initial damage form for specimens A1, A2, A3, Q25-7 and Q35-7 is a combination of matrix cracks and delaminations as shown in Figures 4.21 and 4.22. This initial damage state is similar to the multiple through-thickness delamination classification in that the delaminations are on the order of 0.4 inches long. However, specimens with damage near the surface do not have delaminations that continue through the thickness of the specimens. As a result, these specimens experienced numerous small load drops prior to the end of testing. By stopping some of the tests for closer examination, this effect was attributed to the failure of small groups of plies at both of the outer faces of the specimens (front and back), similar to sublaminate buckling. A significant portion of each specimen remained intact after the outer ply failures, suggesting that further compressive loads could be carried.

By examining Figure 4.23, it can be seen that additional loading of specimens Q25-7, Q35-7, and A3 beyond their initial load drops did not result in significantly greater compression strengths. After the first load drop, load increases and falls off to form a sawtooth pattern, but the load never rises significantly above the level of the first peak. Specimens with both the $[0/\pm60]_{35s}$ and $[0/\pm45/90]_{25s}$ stacking sequences experienced similar initial damage states and final failure modes. The number of plies initially damaged caused an ordered reduction in compression strength, with a higher number of damaged plies causing a lower compressive strength.

Specimens on the order of 1.0 inches thick with three-point bend spans of 3.0 inches, exhibited a similar but less extensive damage pattern than the thick specimens with 1.0 inch spans. Specimen Q35-6, with a $[0/\pm60]_{35s}$ stacking sequence, has delaminations and matrix

Table 4.1 - Three-point bend loading levels for panel A specimens, $[0/\pm45/90]_{25s}$

Specimen	Stacking Sequence	Applied 3-Point Bend Loads (lbs)
A1	$[0/\pm45/90]_{25s}$	18045
A2	$[0/\pm45/90]_{25s}$	20047
A3	$[0/\pm45/90]_{25s}$	22009
A4	$[0/\pm45/90]_{25s}$	23965

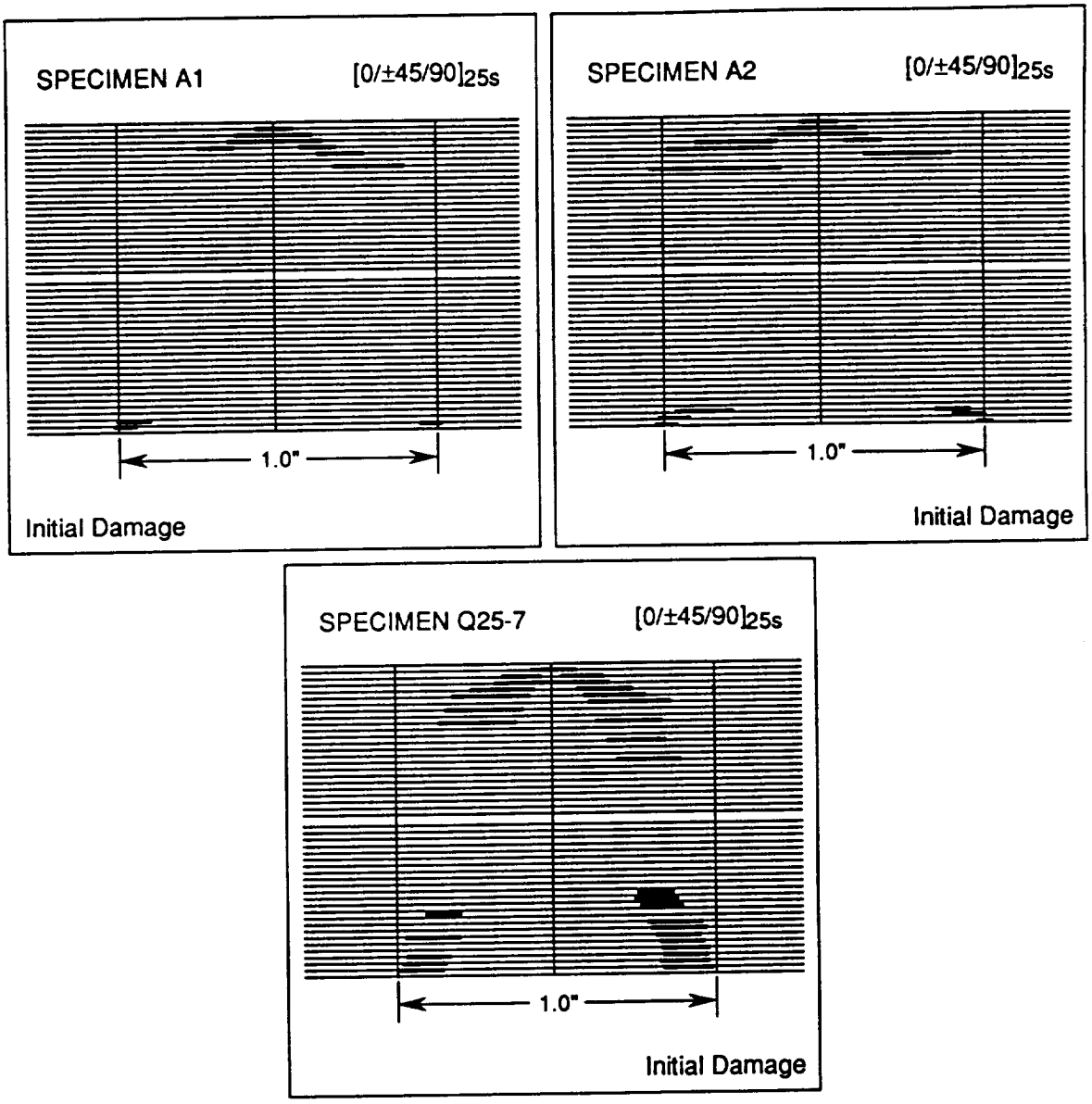

Figure 4.21 - Initial damage for balanced damage near the surface, $[0/\pm45/90]_{25s}$

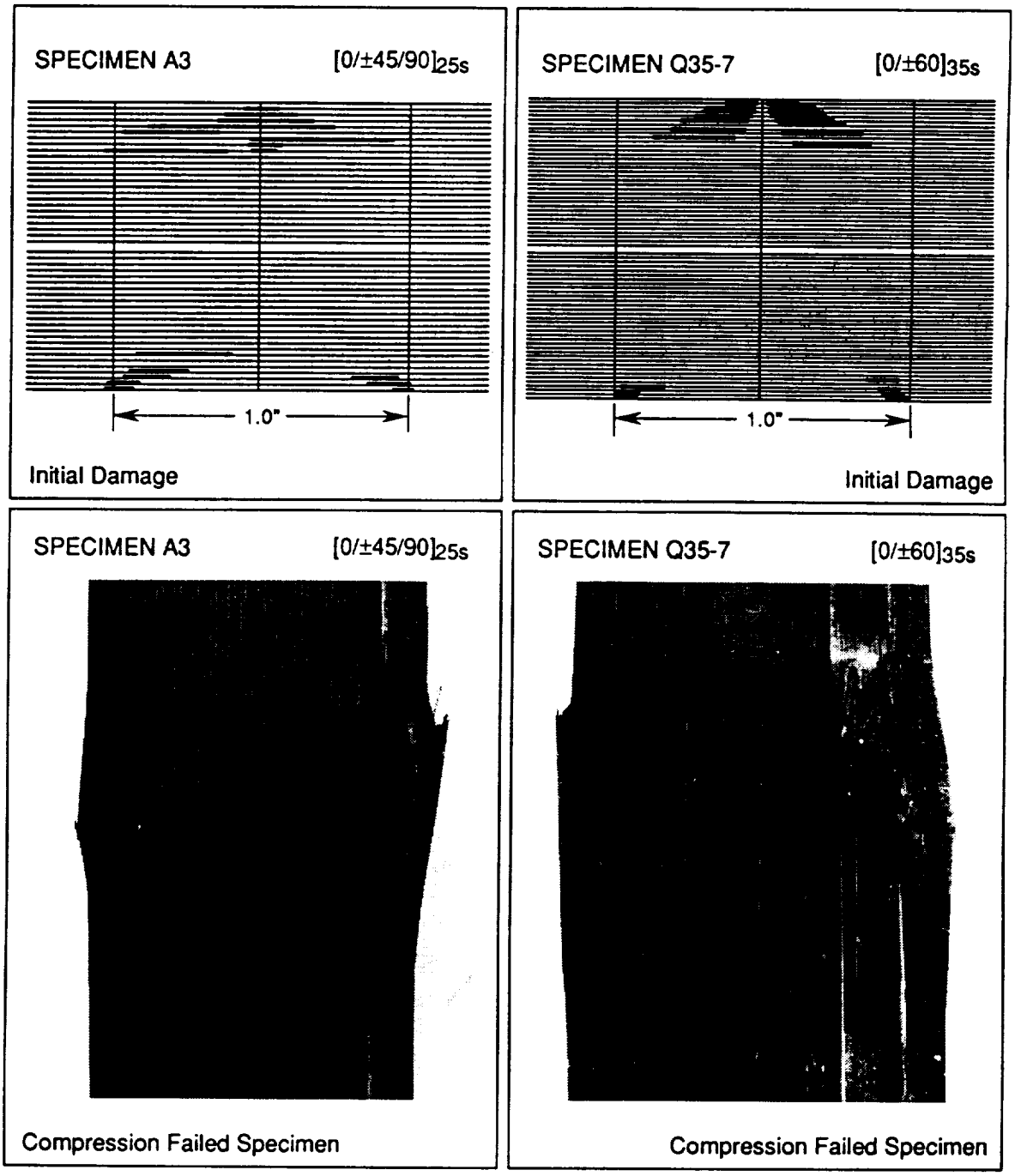

Figure 4.22 - Initial damage and failed specimens for balanced damage near the surface, $[0/\pm45/90]_{25s}$ and $[0/\pm60]_{35s}$

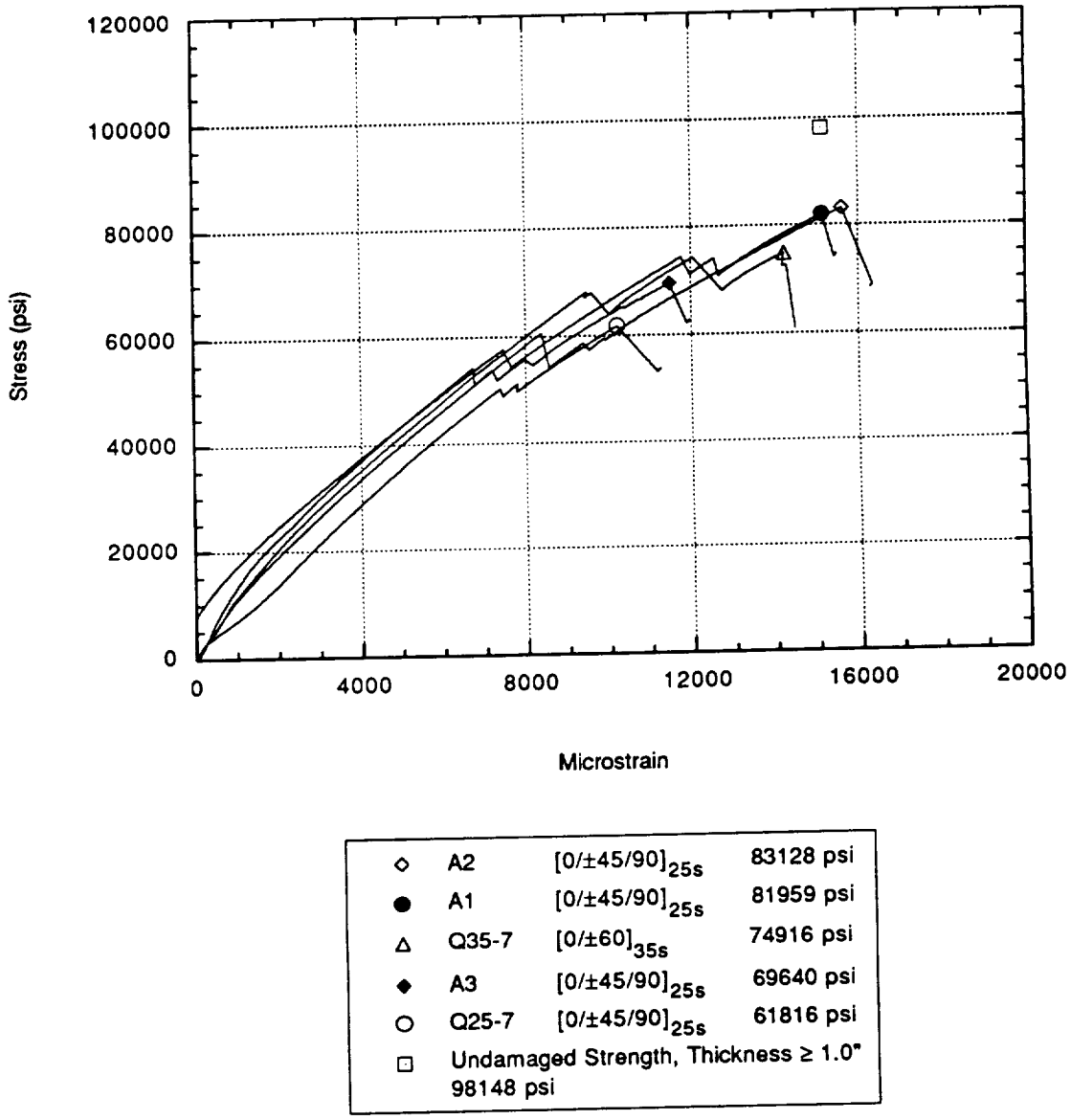

Figure 4.23 - Experimental compression relations for specimens with balanced damage near the surface, $[0/\pm45/90]_{25s}$ and $[0/\pm60]_{35s}$

cracks on one side of the centerline under the three-point bend load nose, as shown in Figure 4.24. Specimen Q25-6, shown in Figure 4.25, has the same type of initial damage as specimen Q35-6 but with a $[0/\pm45/90]_{25s}$ stacking sequence. No damage was visible at the support points for either specimen. By comparison of the compression stress-strain relations in Figures 4.26 and 4.23, it can be seen that the less extensive damage in specimen Q25-6 and Q35-6 resulted in higher compression strengths than for specimens Q25-7 and Q35-7. Also, loading proceeded relatively smoothly with few load drops prior to the end of testing, unlike the specimens with damage at both load and support points which experienced several small load drops throughout the loading procedure.

The other specimens of Figure 4.26 contain fiber breaks in addition to delaminations and matrix cracks on one side of the centerline under the load nose. These specimens, Q20-5, Q15-10, Q25-5, and Q35-5, are shown in Figures 4.24 and 4.25. The specimens all have three point bend spans which are long when compared to their thicknesses. Fiber breaks occur in the 0° plies beneath the load nose but slightly to one side of the centerline. Examination of Figure 4.25 shows that the failure mode for a specimen with (Q25-5) and without (Q25-6) fiber breaks is approximately the same. The compression strength of specimens with fiber breaks is slightly less than the strength of those specimens without fiber breaks, as can be seen by comparing the strengths of specimen Q35-5 with Q35-6 and specimen Q25-5 with Q25-6 in Figure 4.23.

For those specimens with fiber breaks, the compression strength generally decreases as the percentage of damaged plies to undamaged plies increases. Specimen Q35-5 cannot be directly compared to the others because the delaminations it contains are much longer than in the other specimens, thus causing a compression strength lower than might be expected from the fiber breaks alone.

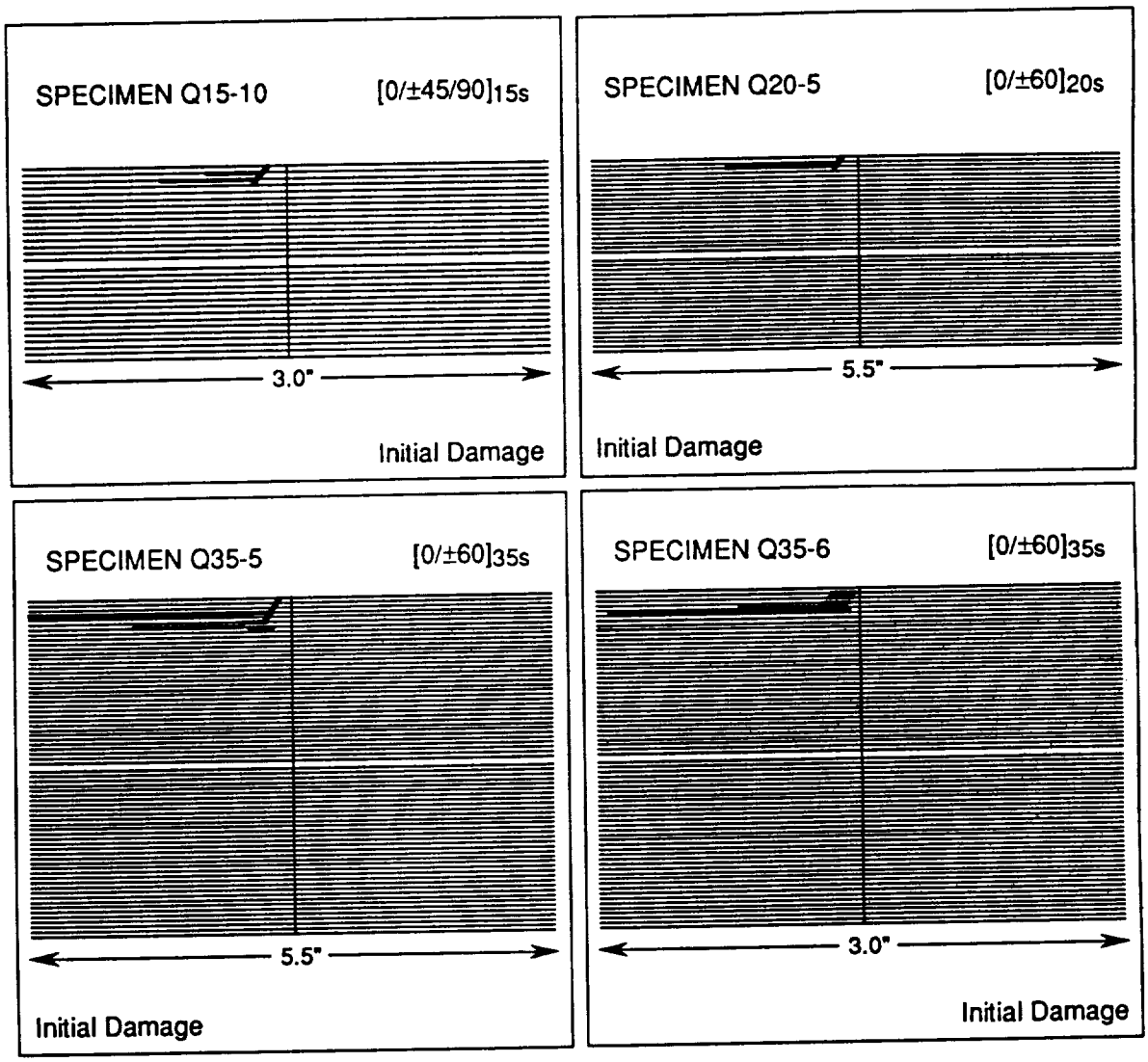

Figure 4.24 - Initial damage and failed specimens for unbalanced damage near the surface, $[0/\pm60]_{20s}$, and $[0/\pm60]_{35s}$

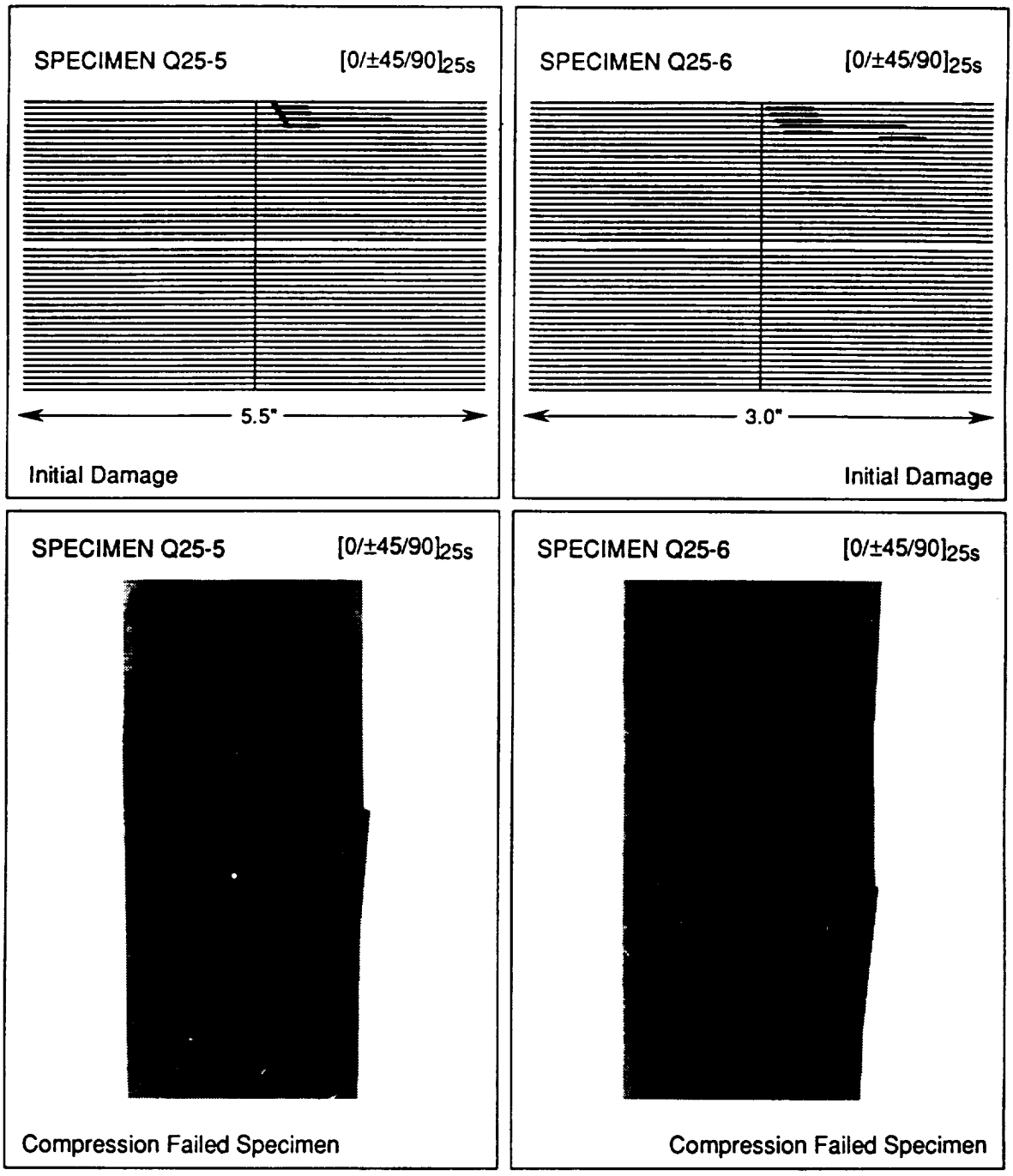

Figure 4.25 - Initial damage and failed specimens for unbalanced damage near the surface, $[0/\pm45/90]_{2s}$

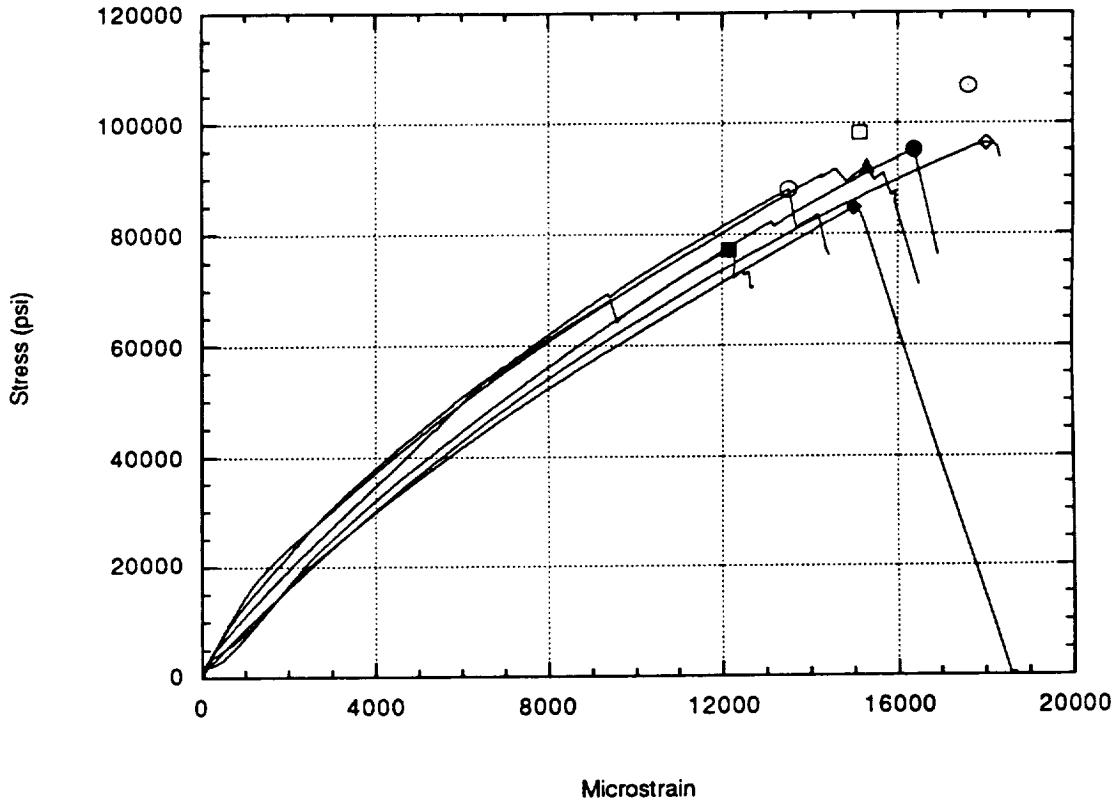

◇	Q20-5	$[0/\pm60]_{20s}$	96285 psi	◆	Q15-10	$[0/\pm45/90]_{15s}$	84579 psi
●	Q25-6	$[0/\pm45/90]_{25s}$	95117 psi	■	Q35-5	$[0/\pm60]_{35s}$	77122 psi
▲	Q35-6	$[0/\pm60]_{35s}$	92066 psi	○	Undamaged Strength, Thickness < 1.0" 106730 psi		
○	Q25-5	$[0/\pm45/90]_{25s}$	87931 psi	□	Undamaged Strength, Thickness ≥ 1.0" 98148 psi		

Figure 4.26 - Experimental compression relations for specimens with unbalanced damage near surface, $[0/\pm45/90]_{15s}$, $[0/\pm45/90]_{25s}$, $[0/\pm60]_{20s}$, and $[0/\pm60]_{35s}$

4.5 Grouped Ply Stacking Sequences

Two types of specimens with grouped stacking sequences, $[0_5/45_5/-45_5/90_5]_{5s}$ and $[0_5/60_5/-60_5]_{7s}$, were tested. Unlike the other specimens studied with interspersed stacking sequences, several plies of the same orientation were stacked together. Specimens were cut from three different panels with differences in layer compaction and initial matrix crack density due to differences and the manufacturing and curing procedures. The initial damage achieved after three-point bending includes a variety of modes depending on the span. Although the initial damage modes are somewhat similar to the modes noted in the interspersed stacking sequences, the compression failure modes are markedly different. However, regardless of the initial damage, the specimens with grouped stacking sequences tend to fail with approximately the same compression failure mode for all specimens of a given stacking sequence.

4.5.1 Initial Panel Differences

Specimens obtained from two different panels with a $[0_5/45_5/-45_5/90_5]_{5s}$ stacking sequence were tested. The first panel was part of the original study on three-point bending, and had a panel thickness of 1.0 inches with each ply approximately 0.005 inches thick. The second panel was manufactured at a later date, and has an overall thickness of 1.07 inches. This second panel, labeled B, contains matrix cracks from the manufacturing cycle with a density along the length of 6 per inch in the center 90° plies. The first panel, labeled Q5, contains matrix cracks with a density of only 1 per inch. Panel Q7, with a $[0_5/60_5/-60_5]_{7s}$ stacking sequence,

has 0.005 inch thick plies and no evidence of initial matrix cracks from the manufacturing process.

4.5.2 Compression Failure Modes, $[0_5/45_5/-45_5/90_5]_{5s}$

Regardless of the panel from which the specimens were taken, and independent of the initial damage mode, compression failure for $[0_5/45_5/-45_5/90_5]_{5s}$ type specimens was catastrophic with failure extending through the entire thickness of the specimen. Failure includes extensive matrix cracking in the ±45° layers. The cracks in the +45° layers appear to continue into the adjacent 0° plies, causing the 0° fibers to break along a 45° angle. The 0° plies are then shifted in the width direction, as explained in Section 4.1.3 in the discussion about undamaged specimens.

The effect of damage near the surface for panel B, with the higher density of initial matrix cracks, is shown in Figure 4.27. These specimens were all tested in three-point bend with a span of 1.0 inches. Panel B specimens were loaded to different three-point bend load levels in order to obtain different amounts of initial damage. These load levels are listed in Table 4.2, while the resulting initial damage can be seen in Figure 4.28. Specimens B2, B3, and B4 all have nearly the same compression strength even though the amount of damage is slightly greater for specimen B4. Specimen B5 has a slightly lower compression strength, corresponding to matrix cracks in one additional ply group beyond that in specimen B4. Likewise, specimen B6 has an even lower compression strength corresponding to a further increase in the amount of initial damage. All five B panel specimens, with three-point bend induced initial damage, show a small but significant reduction in compression strength below the compression strength of undamaged specimens.

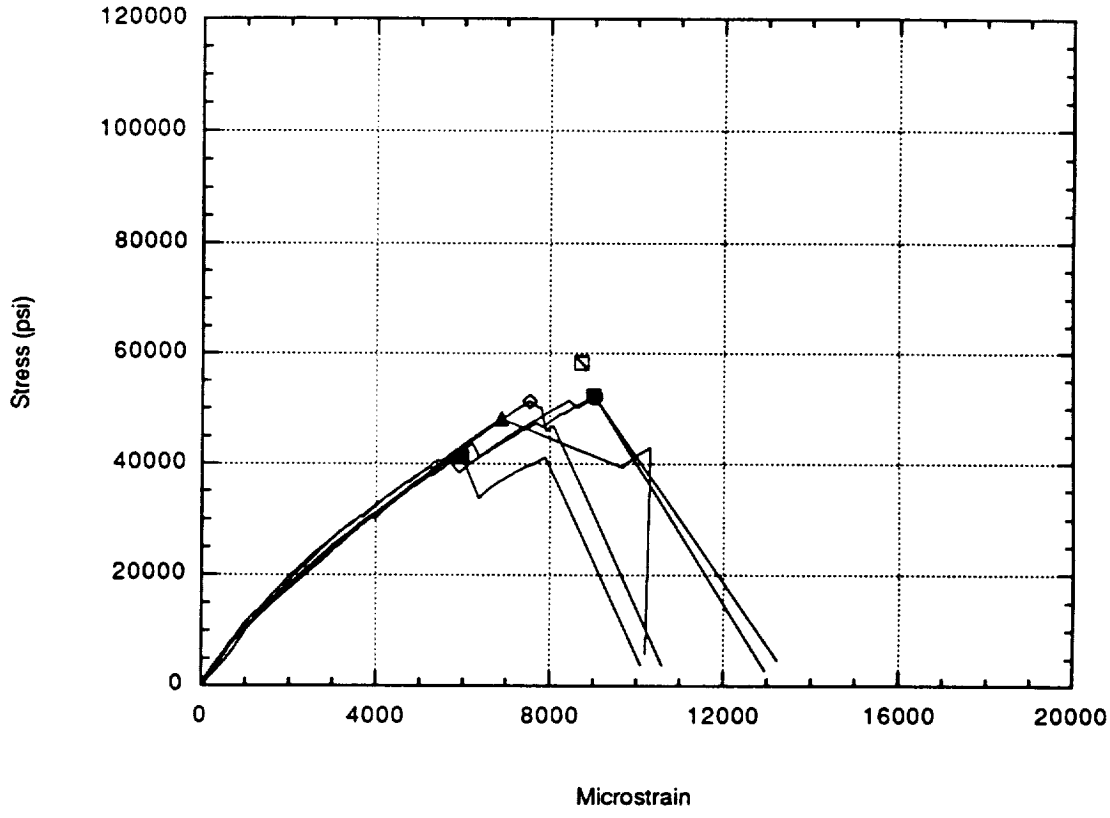

◇	B2	$[0_5/45_5/-45_5/90_5]_{5s}$	51329 psi
●	B3	$[0_5/45_5/-45_5/90_5]_{5s}$	52159 psi
□	B4	$[0_5/45_5/-45_5/90_5]_{5s}$	52339 psi
▲	B5	$[0_5/45_5/-45_5/90_5]_{5s}$	48192 psi
■	B6	$[0_5/45_5/-45_5/90_5]_{5s}$	41344 psi
⧅	Undamaged Strength, Panel B		58360 psi

Figure 4.27 - Experimental compression relations for B panel specimens, $[0_5/45_5/-45_5/90_5]_{5\,s}$

Table 4.2 - Three-point bend loading levels for panel B specimens, $[0_5/45_5/-45_5/90_5]_{5s}$

Specimen	Stacking Sequence	Applied 3-Point Bend Load (lbs)
B2	$[0_5/45_5/-45_5/90_5]_{5s}$	11883
B3	$[0_5/45_5/-45_5/90_5]_{5s}$	13632
B4	$[0_5/45_5/-45_5/90_5]_{5s}$	15072
B5	$[0_5/45_5/-45_5/90_5]_{5s}$	16602
B6	$[0_5/45_5/-45_5/90_5]_{5s}$	18148

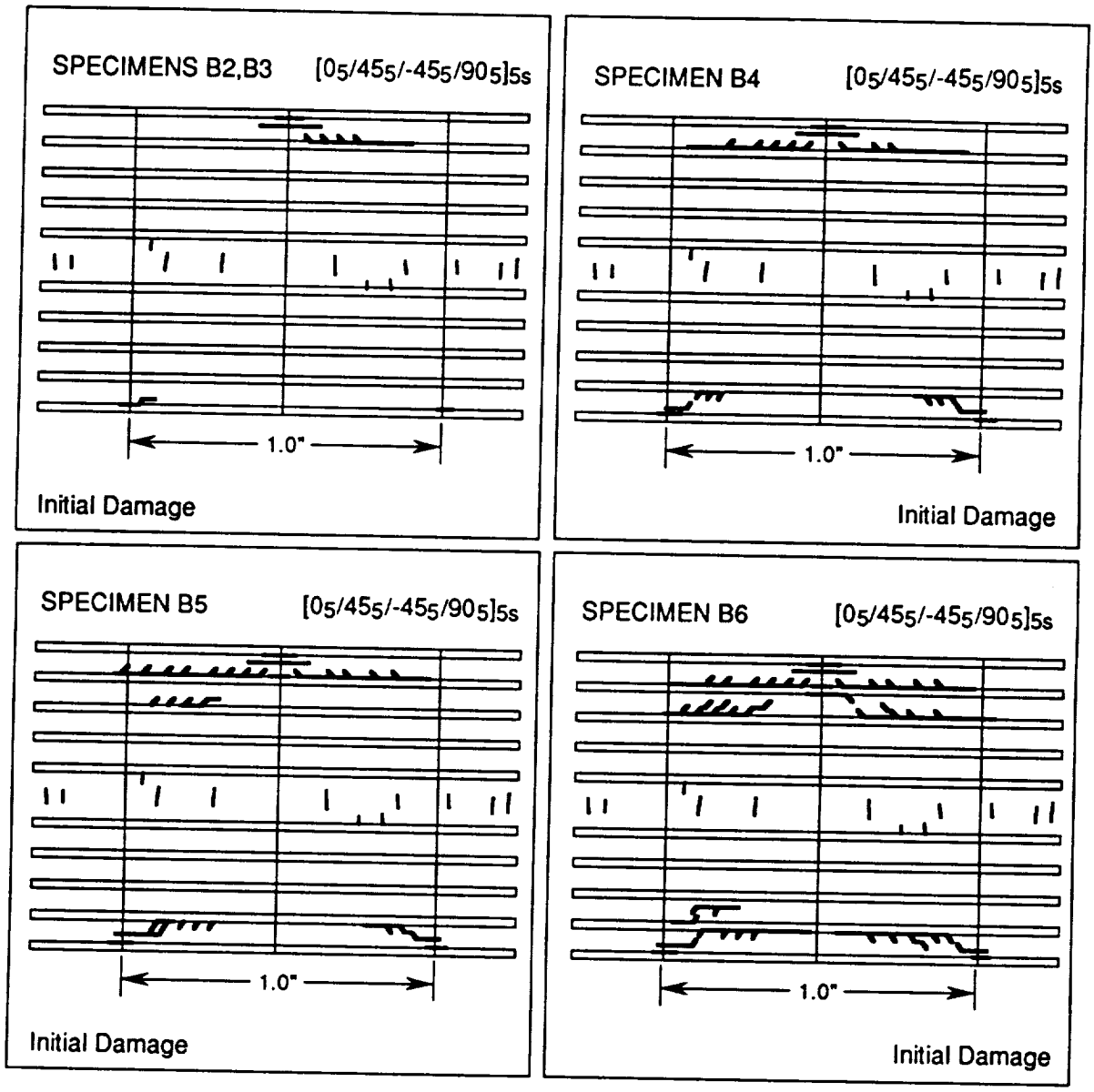

Figure 4.28 - Initial damage for B panel specimens, $[0_5/45_5/-45_5/90_5]_{5s}$

The compression stress-strain relations for specimens with similar initial damage states, but cut from panel Q5 with a $[0_5/45_5/-45_5/90_5]_{5s}$ stacking sequence, are shown in Figure 4.29. The initial damage states are shown in Figure 4.30. The initial damage in specimen Q5-8 is essentially the same as that in specimens B2 and B3 with the exception of the initial matrix cracks that appeared at the center of the B panel specimens. The compression strength of specimen B2 is lower than that of Q5-8, as can be seen in Figure 4.29. This can be attributed to the corresponding difference in undamaged compression strengths for the two panels due to the initial matrix crack density.

Both initial and final stress-strain relations for specimens Q5-8 and Q5-9 are shown in Figure 4.29. The initial relation was obtained by stopping the loading to observe the damage that occurred after the first load drop, as explained in Chapter 3. The specimen was returned to the fixture and reloaded to obtain the final loading relation. Specimen Q5-9 is very similar to specimen Q5-8 except that the initial damage for specimen Q5-9 is concentrated closer to the centerline due to the 0.5 inch three-point bend span. An examination of the specimens stopped after the first load drop reveals an increase in the number of matrix cracks in the center plies. Additionally, edge replicas taken after the first load drop show broken 0° fibers in the first ply group, which is probably the cause of the load drop. Correspondingly, the slopes (and therefore stiffnesses) of the final compression loading relations for Q5 panel specimens are more in line with the slopes of the B panel specimens. The difference in damage location between specimens Q5-8 and Q5-9 appears to have no effect on the compression strength.

Specimens Q5-4 and Q5-7 have damage which continues through the thickness of the specimens, as shown in Figure 4.31. At first glance, this damage appears to be the same as the multiple through-thickness delamination classification encountered in interspersed stacking sequences and discussed in Section 4.2. However, the damage in the grouped ply specimens

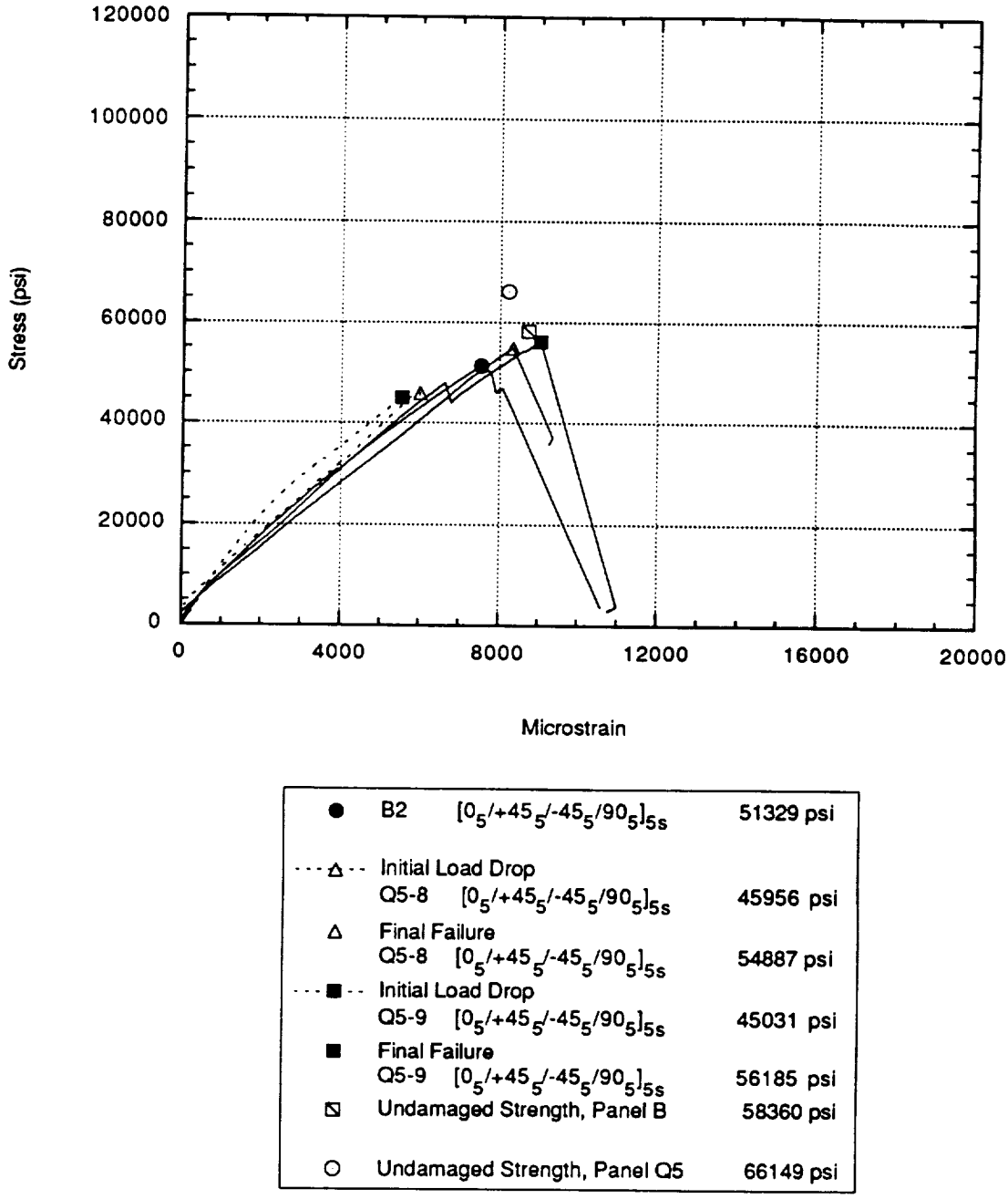

Figure 4.29 - Experimental compression relations for grouped ply specimens with matrix cracks near the surface, $[0_5/45_5/-45_5/90_5]_{5s}$

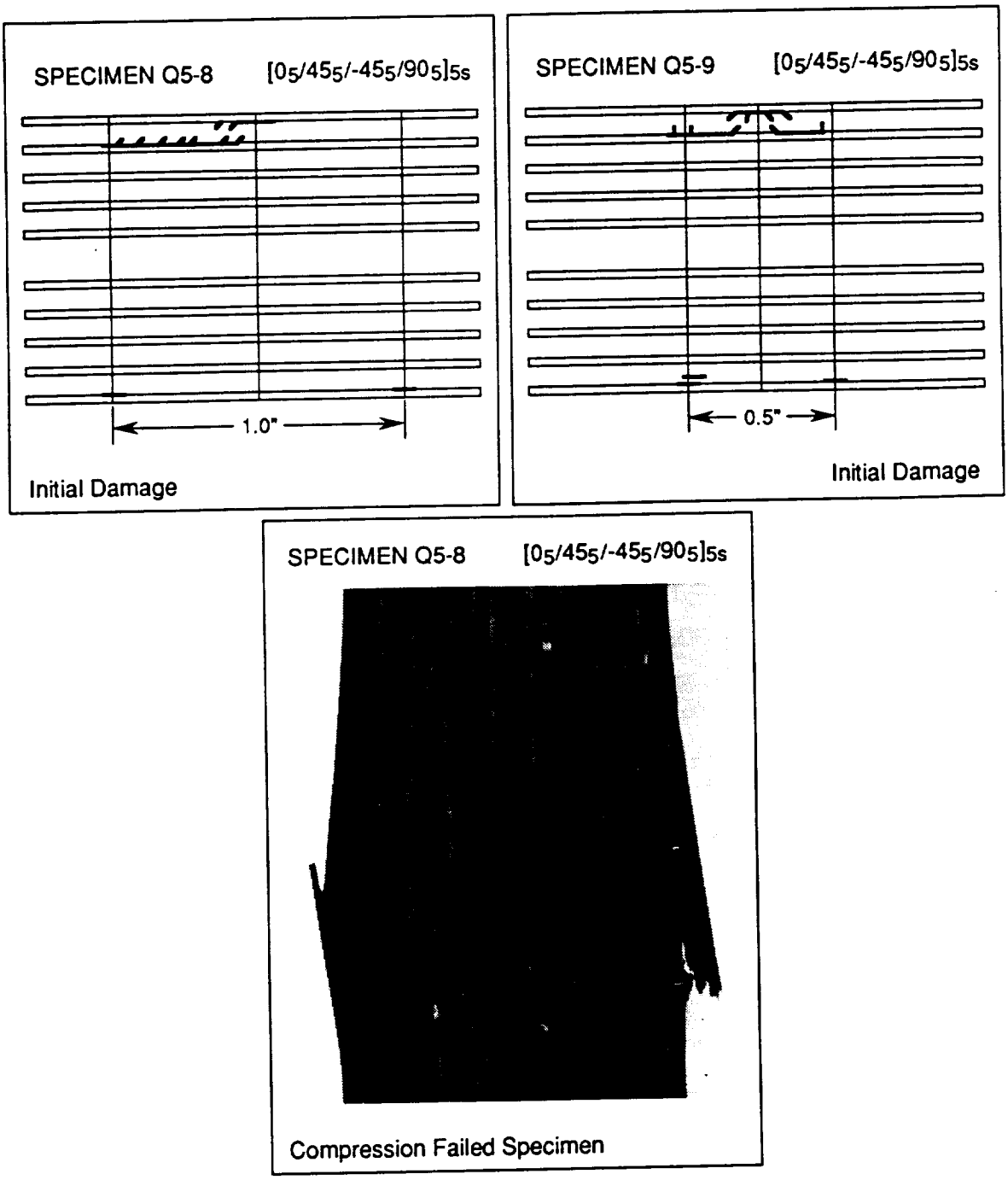

Figure 4.30 - Initial damage and failed specimen for grouped ply specimens with matrix cracks near the surface, $[0_5/45_5/-45_5/90_5]_{5s}$

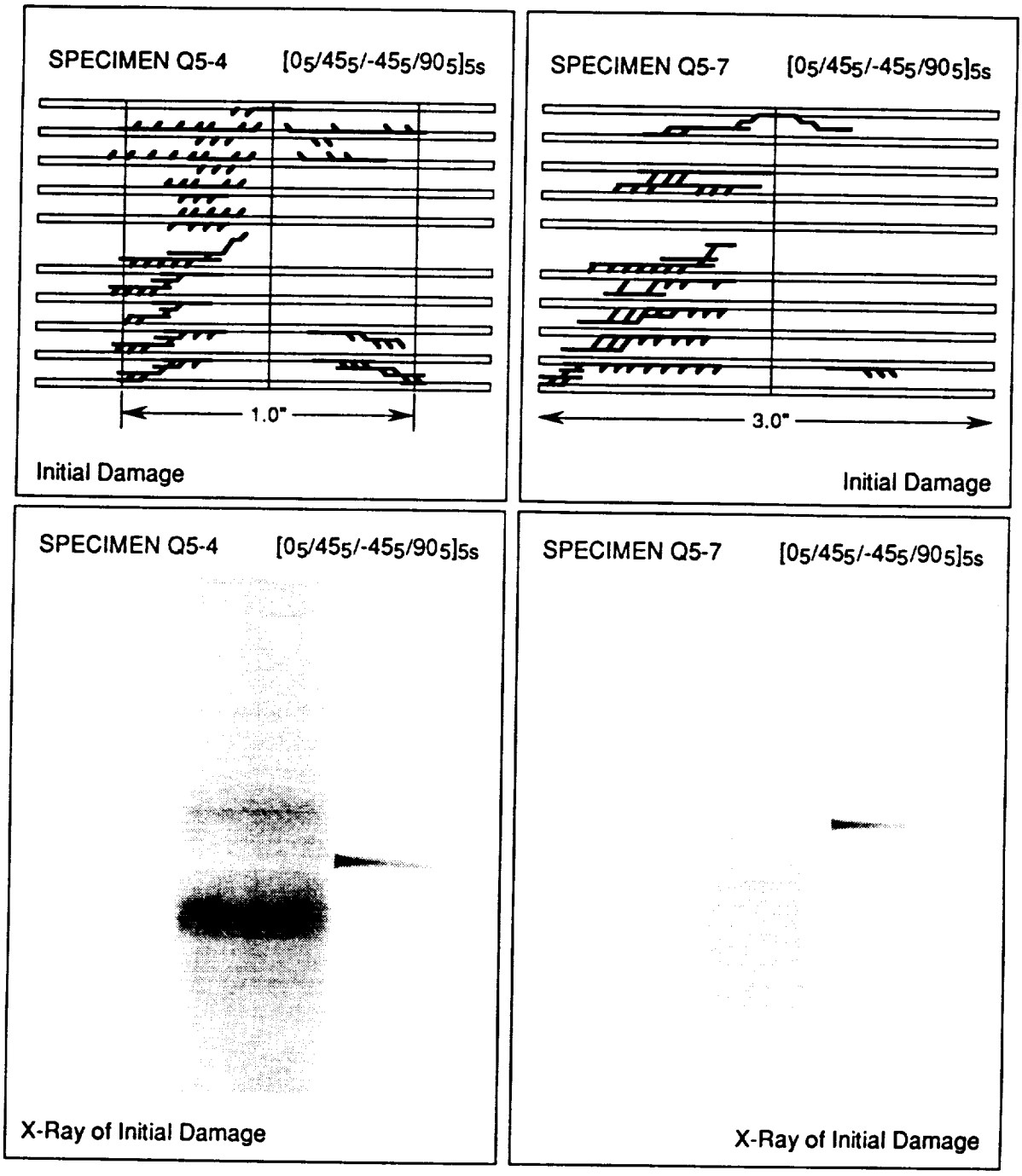

Figure 4.31 - Initial damage and x-rays of initial damage for grouped ply specimens with damage through the thickness, $[0_5/45_5/-45_5/90_5]_{5s}$

contains predominantly matrix cracks with few delaminations. Additionally, the failure mode for all of the $[0_5/45_5/-45_5/90_5]_{5s}$ specimens looks like the photo of specimen Q5-8 shown in Figure 4.30, which is quite different than the failure mode of specimen A4 ($[0/\pm45/90]_{25s}$ stacking sequence), shown in Figure 4.12.

Examination of the x-rays taken after three-point bend lead to an additional observation about the difference between the specimens Q5-4 and Q5-7. Specimen Q5-4 has damage which is balanced with respect to the centerline, while specimen Q5-7 has damage which is concentrated on one side of the centerline only. As expected, the compression strength of specimen Q5-4 is much lower than the undamaged strength for panel Q5, as shown in Figure 4.32. However, specimen Q5-7 does not show as great a reduction. Perhaps this is due to the unbalanced nature of the initial damage, although one specimen is not enough on which to base such a conclusion.

The final specimen from panel Q5 is specimen Q5-6, shown in Figure 4.33. The initial damage for this specimen is concentrated at the midplane and back face. The midplane of the specimen has a large matrix crack/delamination combination that continues throughout the unsupported gage length of the specimen. The back face has a series of tension cracks in the 90° ply, some of which are connected along the edge in the length direction. As illustrated in Figure 4.32, the initial slope of the compression failure relation for this specimen is notably different than the slope for the other Q5 specimens. This may be due to the lower number and density of matrix cracks in the initial damage state. Again, one specimen is not enough from which to draw significant conclusions.

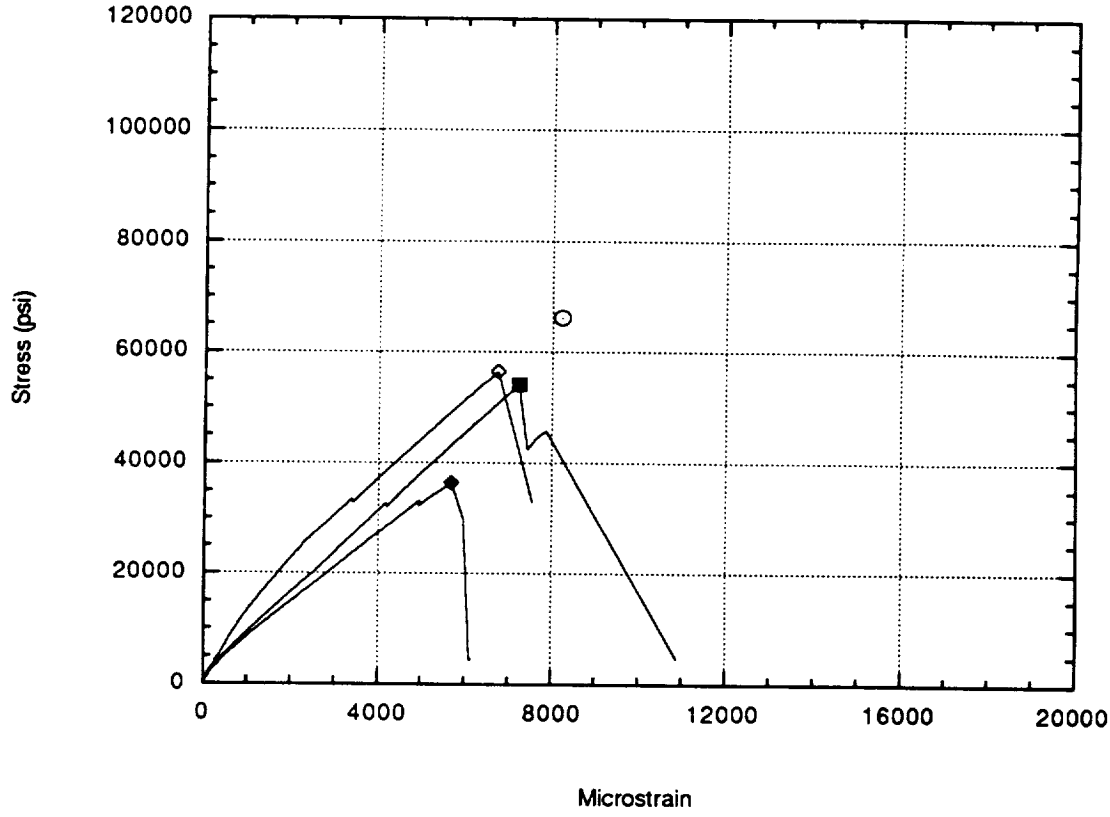

Figure 4.32 - Experimental compression relations for grouped ply specimens with damage through the thickness, $[0_5/45_5/-45_5/90_5]_{5s}$

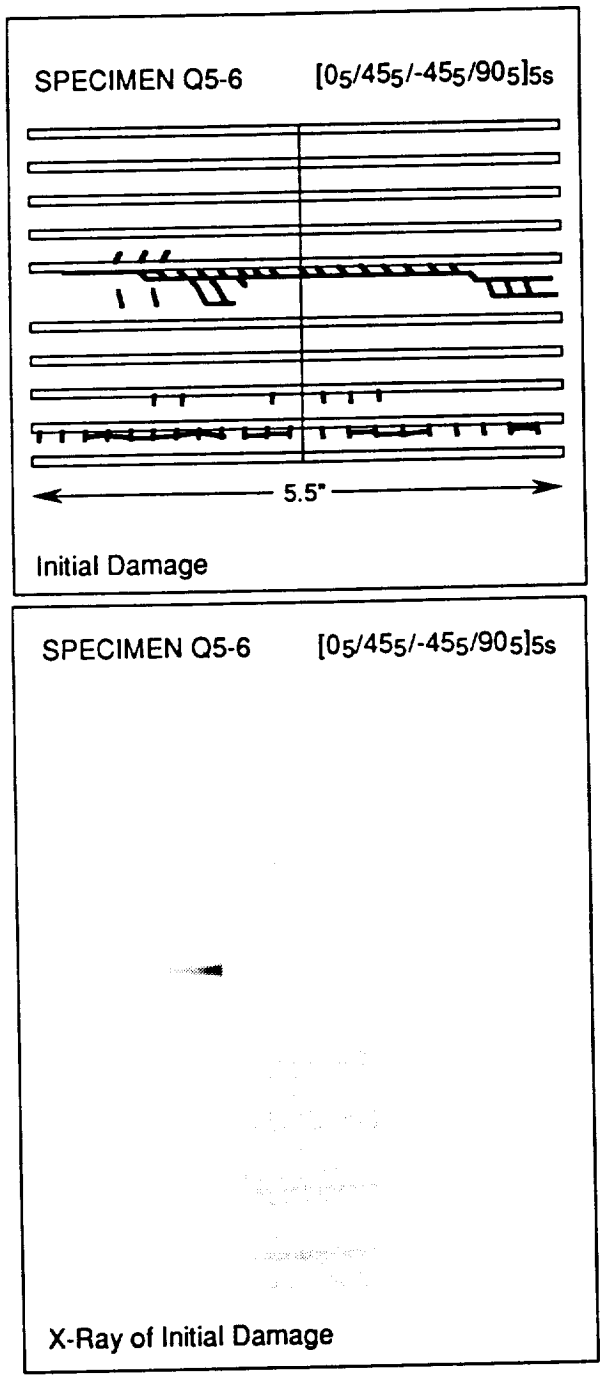

Figure 4.33 - Initial damage and x-ray of initial damage for grouped ply specimen with damage at the midplane, $[0_5/45_5/-45_5/90_5]_{5s}$

4.5.3 Compression Failure Modes, $[0_5/60_5/-60_5]_{7s}$

Panel Q7 has a stacking sequence of $[0_5/60_5/-60_5]_{7s}$. Both the undamaged compression strength and the subsequent compression strength of initially damaged specimens is higher than that reported for the $[0_5/45_5/-45_5/90_5]_{5s}$ specimens. Additionally, the compression failure mode for the $[0_5/60_5/-60_5]_{7s}$ type specimens consisted of damage restricted to the first and last ply groups. This compression failure mode was consistent for all four of the specimens tested from this panel, including the undamaged specimen.

Specimens Q7-2 and Q7-6 have essentially the same initial damage state and compression strength. The compression strength is shown in the compression stress-strain relations of Figure 4.34 and the initial damage is shown in Figure 4.35. Initial damage consists of matrix cracks in the plies near the midplane, a few matrix cracks under the load nose, and tension matrix cracks in the last ply group near the back face. In specimen Q7-6, the last ply group also contains a number of delaminations. Both specimen compression tests were stopped after the first load drop and the specimens were examined for new damage. This examination revealed that 0° fibers had broken in the first and last ply groups of both specimens. The different slope for the final loading relation of specimen Q7-2 can be attributed to an increase in the number of midplane matrix cracks after the first compression loading.

Specimen Q7-7, shown in Figure 4.35, had a three-point bend span of 1.0 inches with initial damage restricted to the first 15 plies. However, the compression strength is significantly higher than that reported for the $[0_5/45_5/-45_5/90_5]_{5s}$ specimens with similar initial damage states (specimens Q5-8,Q5-9, B2, B3, and B4). The reduction in strength due to this type of initial damage is approximately the same for both grouped ply stacking sequences, ranging from

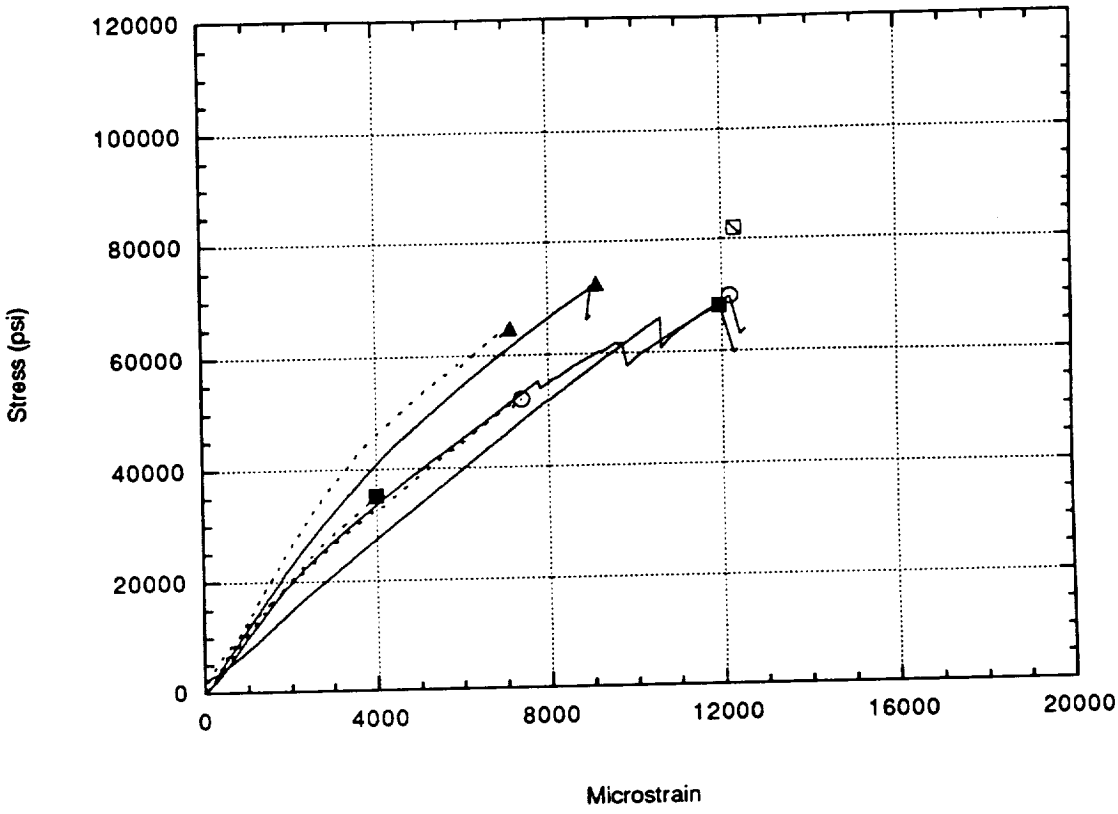

Figure 4.34 - Experimental compression relations, grouped ply specimens with damage near the surface and matrix cracks, $[0_5/60_5/-60_5]_{7s}$

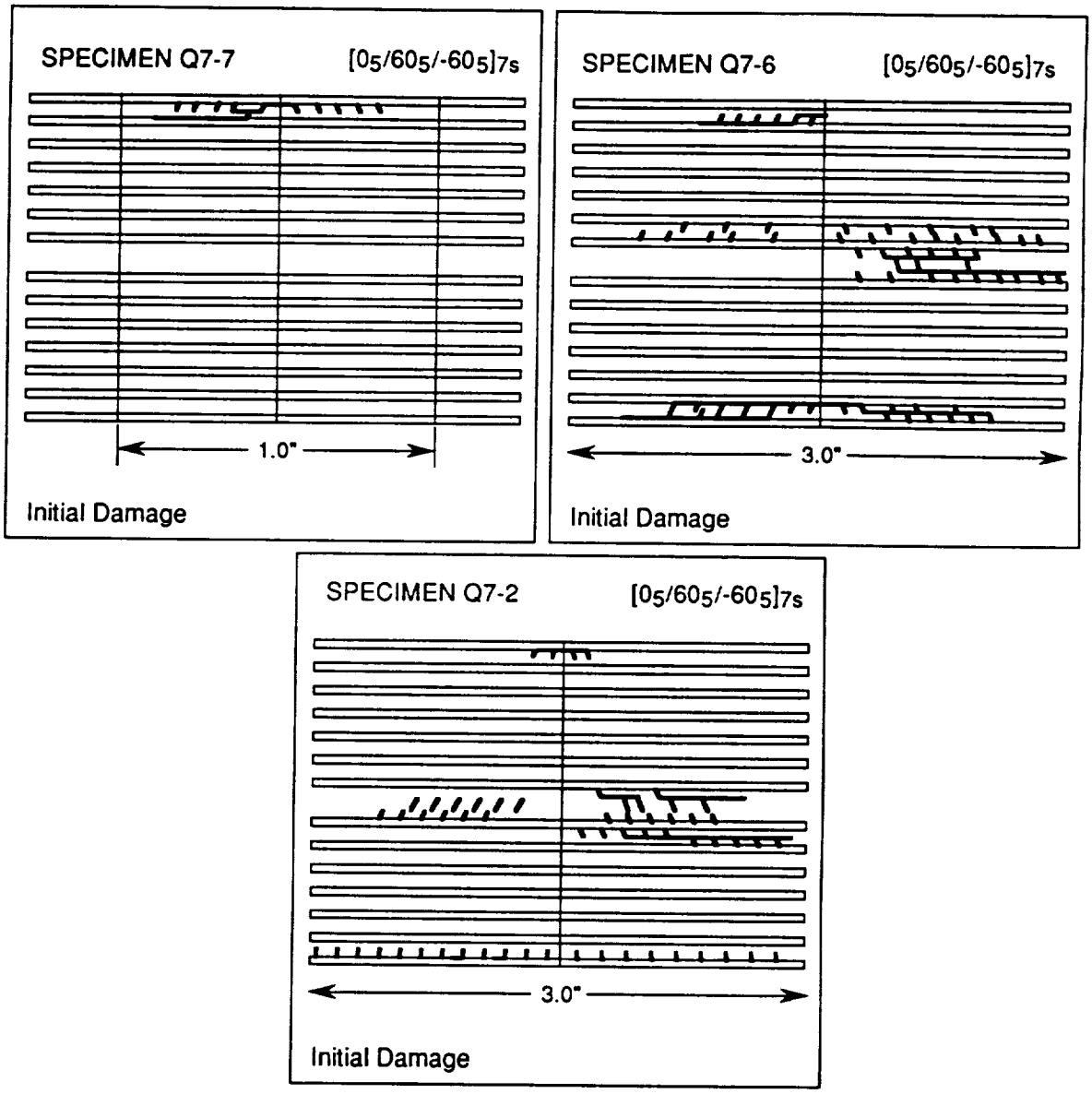

Figure 4.35 - Initial damage and failed specimen for grouped ply specimens with damage near the surface and matrix cracks, $[0_5/60_5/-60_5]_{7s}$

a 12% to 17% reduction. Note also the difference between the initial slope of Q7-7 and the initial slopes of the other Q7 specimens. This difference (increased stiffness) is likely due to the lack of midplane matrix cracking in specimen Q7-7. When the specimen was stopped and examined after the first load drop, the 0° fibers in the first and last ply groups were damaged.

Chapter 5
Numerical Analysis

There is a wide body of literature on the analysis of initially damaged composites, including numerous techniques to predict compression failure. The failure of the specimens that are tested in the present study can be explained in part through qualitative comparison with published literature. For example, the specimens with damage near the surface failed primarily due to sublaminate buckling. This phenomenon has been studied extensively for both through-the-width delaminations [21,31,32,34,36] and embedded delaminations [26,33,36-39]. Multiple through-the-thickness delaminations typically occur during impact events [18-20,22-25]. This type of initial damage has been of recent interest in studies by Davidson [29,39], Dost, et al. [37], Ilcewicz,et al. [38], Avery [26], and Lee, et al. [40]. Because analysis for these two types of damage is already available, and because each represents a significant body of research, additional analysis of these failures is not included here. However, the effect of isolated delaminations far from the surface cannot be thoroughly explained using sublaminate buckling theory since the sublaminates are no longer thin, and therefore are less prone to failure by buckling. Likewise, compression failure of laminates with grouped ply

stacking sequences and matrix cracks cannot be described by current sublaminate buckling techniques from the literature, which neglect laminate edge effects. A linear static, 2-dimensional finite element analysis to predict compression failure of specimens with isolated delaminations is presented in the next section. The same finite element analysis is also used to explain the discrepancy in compression strengths between interspersed and grouped stacking sequences. Effects of the compression fixture are included when possible, with additional information available in reference [2].

5.1 Finite Element Analysis

A 2-dimensional finite element code developed at Virginia Tech was used to conduct analyses of specimens with isolated delaminations and specimens with grouped ply stacking sequences. The program, called CLFE2D [41], uses a generalized plane strain assumption with displacements given by:

$$\begin{aligned} u(x,y,z) &= U(y,z) + \varepsilon_x^{\circ}\, x \\ v(x,y,z) &= V(y,z) \\ w(x,y,z) &= W(y,z) \end{aligned} \qquad (5.1)$$

The term ε_x° represents the applied normal (axial) strain and the terms U(x,y), V(x,y), and W(x,y) represent the unknown nodal displacements. The generalized plane strain assumption restricts all quantities except axial displacement to be independent of the axial coordinate x. The global coordinates x, y, and z along with the fiber coordinates 1, 2, and 3 are shown in Figure 5.1. The

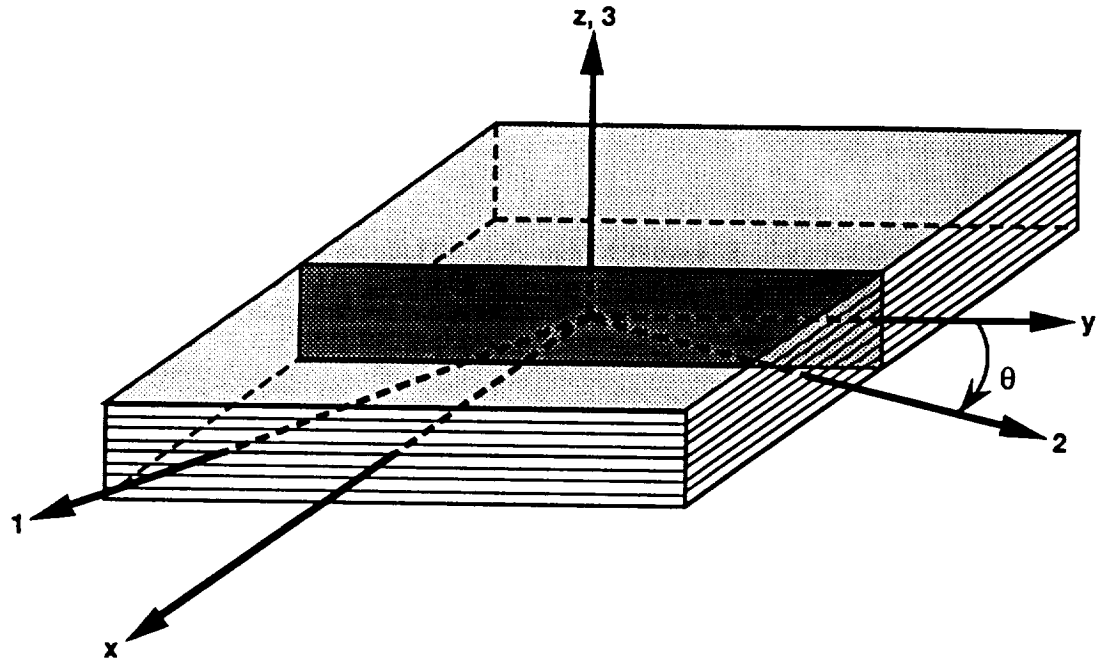

Figure 5.1 - Coordinate axes as defined for finite element analysis

program uses 4-node quadrilateral elements. The details of the finite element formulation can be found in reference [42].

The stress output was modified to give stresses at the Gauss quadrature points. Output in the form of deformed shapes (displacements) and stresses were examined using PATRAN.

5.1.1 Stiffness Matrix Modification

The values of the material properties required by the finite element code were obtained from reference [1] and are listed in Table 5.1. The properties are used for calculation of the stiffness matrix C_{ij} (of equation 5.2) which relates fiber coordinate stresses and strains for an orthotropic material. In order to simulate initial damage, the code was modified to allow for different stiffnesses at each gauss point. By reducing the stiffnesses at distinct locations and in specified directions, the model can simulate the stiffness approximately as though damage were present.

$$\begin{Bmatrix} \sigma_{11} \\ \sigma_{22} \\ \sigma_{33} \\ \tau_{23} \\ \tau_{31} \\ \tau_{12} \end{Bmatrix} = \begin{bmatrix} C_{11} & C_{12} & C_{13} & 0 & 0 & 0 \\ C_{12} & C_{22} & C_{23} & 0 & 0 & 0 \\ C_{13} & C_{23} & C_{33} & 0 & 0 & 0 \\ 0 & 0 & 0 & C_{44} & 0 & 0 \\ 0 & 0 & 0 & 0 & C_{55} & 0 \\ 0 & 0 & 0 & 0 & 0 & C_{66} \end{bmatrix} \begin{Bmatrix} \varepsilon_{11} \\ \varepsilon_{22} \\ \varepsilon_{33} \\ \gamma_{23} \\ \gamma_{31} \\ \gamma_{12} \end{Bmatrix} \quad (5.2)$$

For example, in order to represent broken fibers, C_{11} , C_{12} , C_{13}, C_{55}, and C_{66} are set equal to zero to yield $\sigma_{11} = \tau_{31} = \tau_{12} = 0$.

Table 5.1 - Material properties for AS4/3501-6 as obtained from Starbuck et al.[1]

AS4/3501-6 Material Properties	
E_1	21 Msi
E_2	1.5 Msi
E_3	1.5 Msi
G_{12}	0.8 Msi
G_{13}	0.8 Msi
G_{23}	0.4 Msi
υ_{12}	0.3
υ_{13}	0.3
υ_{23}	0.55

$$\begin{Bmatrix} 0 \\ \sigma_{22} \\ \sigma_{33} \\ \tau_{23} \\ 0 \\ 0 \end{Bmatrix} = \begin{bmatrix} 0 & 0 & 0 & 0 & 0 & 0 \\ 0 & C_{22} & C_{23} & 0 & 0 & 0 \\ 0 & C_{23} & C_{33} & 0 & 0 & 0 \\ 0 & 0 & 0 & C_{44} & 0 & 0 \\ 0 & 0 & 0 & 0 & 0 & 0 \\ 0 & 0 & 0 & 0 & 0 & 0 \end{bmatrix} \begin{Bmatrix} \varepsilon_{11} \\ \varepsilon_{22} \\ \varepsilon_{33} \\ \gamma_{23} \\ \gamma_{31} \\ \gamma_{12} \end{Bmatrix} \tag{5.3}$$

Delaminations are represented by setting C_{13} , C_{23} , C_{33}, C_{44}, and C_{55} equal to zero to yield $\sigma_{33} = \tau_{31} = \tau_{23} = 0$.

$$\begin{Bmatrix} \sigma_{11} \\ \sigma_{22} \\ 0 \\ 0 \\ 0 \\ \tau_{12} \end{Bmatrix} = \begin{bmatrix} C_{11} & C_{12} & 0 & 0 & 0 & 0 \\ C_{12} & C_{22} & 0 & 0 & 0 & 0 \\ 0 & 0 & 0 & 0 & 0 & 0 \\ 0 & 0 & 0 & 0 & 0 & 0 \\ 0 & 0 & 0 & 0 & 0 & 0 \\ 0 & 0 & 0 & 0 & 0 & C_{66} \end{bmatrix} \begin{Bmatrix} \varepsilon_{11} \\ \varepsilon_{22} \\ \varepsilon_{33} \\ \gamma_{23} \\ \gamma_{31} \\ \gamma_{12} \end{Bmatrix} \tag{5.4}$$

This stiffness reduction method was also utilized by Ozden and Engblom [43].

5.1.2 Failure Criteria

Stress-based failure criteria were included in the program to check for compression failure at each Gauss point. One of the criteria used was developed by Hashin [44] to predict matrix tension failure. When a specimen is loaded in compression, the matrix experiences tension stresses due to the Poisson effect. Hashin's failure criterion is given by

$$\frac{1}{Y_t^2}(\sigma_{22} + \sigma_{33})^2 + \frac{1}{S^2}\left(\tau_{23}^2 + \tau_{12}^2 + \tau_{31}^2 - \sigma_{22}\sigma_{33}\right) \geq 1 \tag{5.5}$$

where Y_t is the maximum tensile strength perpendicular to the fibers (in the 2-direction) and S is the maximum shear strength. Strength values used in this analysis were obtained from

Hercules [45]. The value for the maximum shear strength is obtained by averaging the strengths from the 0° short beam shear test and the inplane ±45° tensile shear test.

$$Y_t = 7.8 \text{ ksi}$$

$$S = 15.0 \text{ ksi}$$

A maximum stress failure criterion was used to predict compression failure in the 0° plies. The value used for longitudinal compression strength was obtained from Hercules [45] as

$$X_C = 250 \text{ ksi}$$

Failure was predicted whenever $\sigma_{11} > X_C$.

5.2 Isolated Long Delaminations

Specimens with initial damage described as isolated long delaminations were discussed in Section 4.3 of Chapter 4. The goal of the analysis presented in this section is to understand the failure mechanisms of those specimens with delaminations far from the surface, when sublaminate buckling is no longer a failure mode.

Analysis is conducted using the two-dimensional finite element program described previously. The cross section of the specimen chosen for the model and the applied boundary conditions are shown in Figure 5.2. The model includes the entire length of the specimen and is symmetric with respect to the midplane. The mesh includes one element per layer and 200 elements along the length of the specimen. Layers are assumed to be 0.005 inches thick. Boundary conditions are applied for symmetry, to represent the compression fixture, and to apply a constant displacement to one end of the model. The initial modelling of a delamination

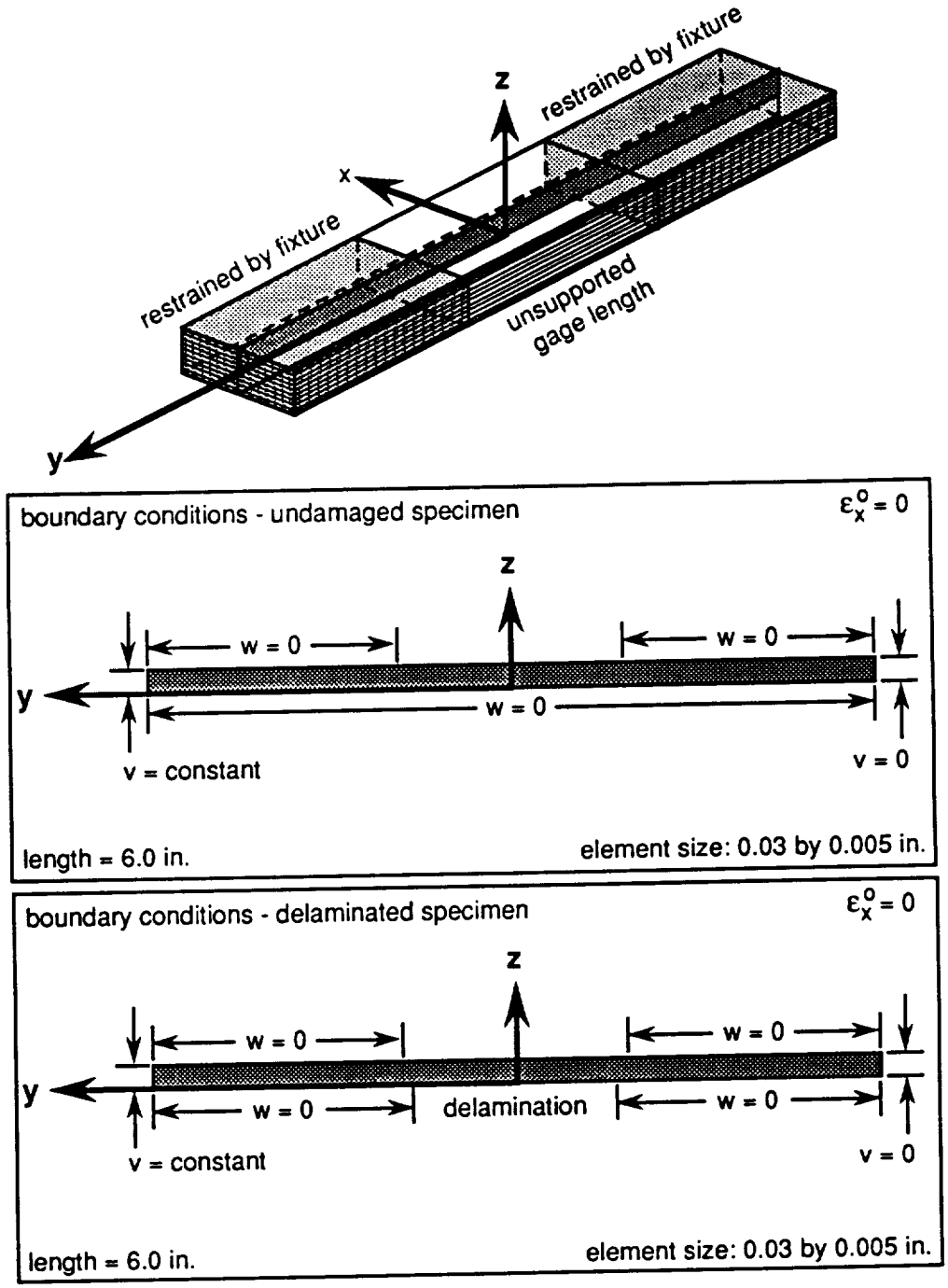

Figure 5.2 - Model and boundary conditions for isolated long delaminations

at the midplane was accomplished by removing the symmetry boundary condition for the center 1.44 inches of the model.

An outline of the deformed mesh (displacements are scaled 20 times) and a more detailed view of the region of the undamaged specimen at the edge of the grips is shown in Figure 5.3. Analysis results indicated that the highest stress occurred in the 0° layer closest to the edge of the grips. This compares qualitatively with the experimental results, which show failure initiating at the grips. This failure location also concurs with the results of Camponeschi [2]. The strain at failure according to the maximum stress failure criterion is 10470 microstrain (μ), which is significantly below the average failure strain of 17686 μ found experimentally. However, the finite element program used was linear, and a close examination of the plots in Chapter 4 suggests that the compression loading is not linear. Therefore, failure strains for damaged specimens will be normalized according to the undamaged failure strains for either analysis or experiments, respectively. That is, analysis strains are normalized by 10470 μ, and experimental strains are normalized by 17686 μ.

5.2.1 Effect of Delamination

The model for a specimen with a midplane delamination is shown in Figure 5.2. The results from this model were kinematically inadmissible, as shown in Figure 5.4, indicating that the delaminated surfaces crossed over each other. Therefore, a second numerical analysis was conducted with the same boundary conditions as the undamaged specimens, but with reduced stiffness (C_{13} , C_{23} , C_{33}, C_{44}, and C_{55}) in the elements along the bottom of the model according to equation 5.4. This simulated delamination was the same length as the delamination created with boundary conditions. The more acceptable deformed mesh from this

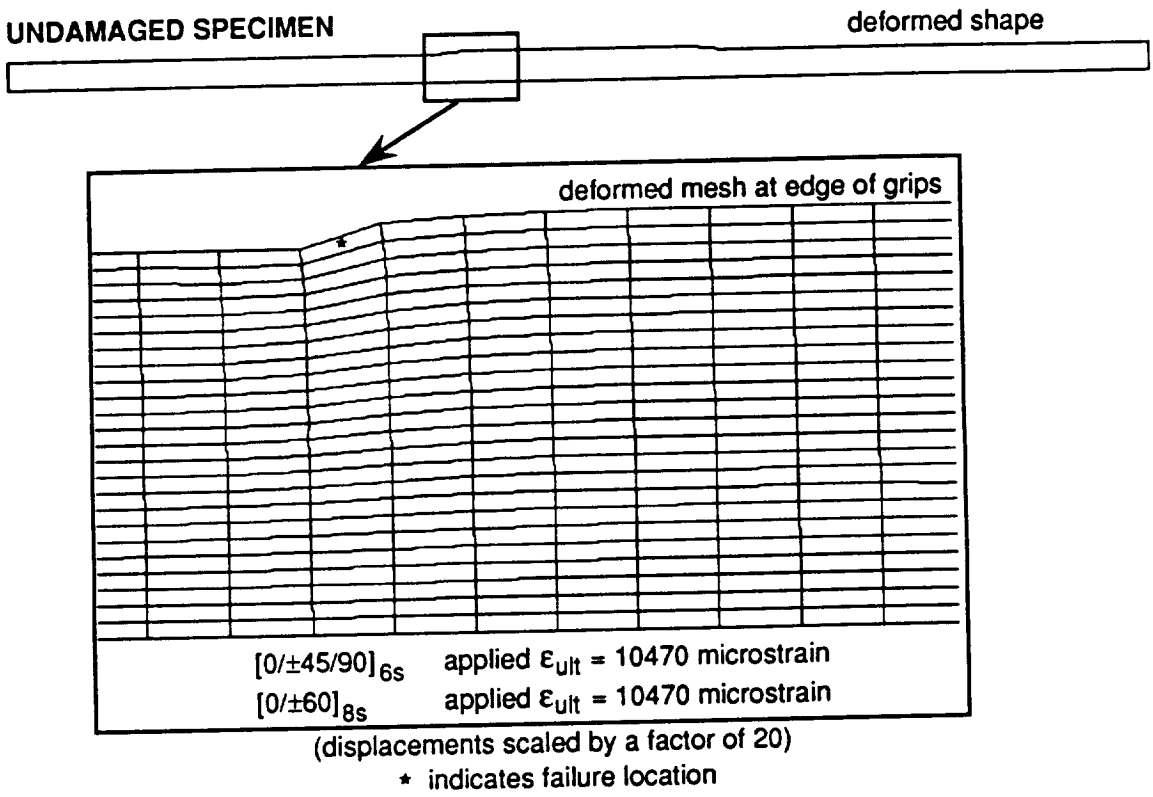

Figure 5.3 - Analysis results for undamaged, 48 ply specimens

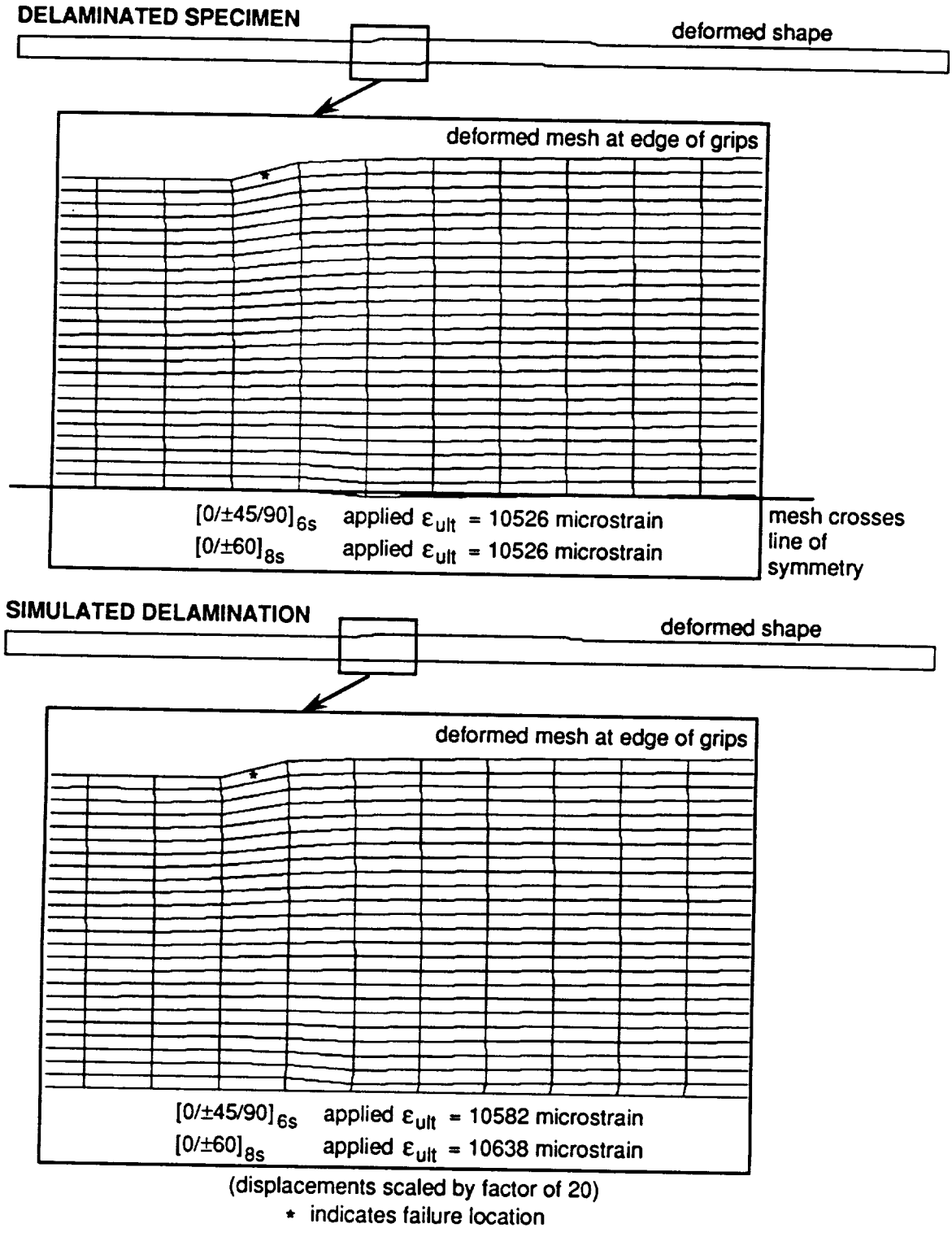

Figure 5.4 - Analysis results for 48-ply specimens, delamination at midplane

model is shown in Figure 5.4. Although both delamination models gave very similar failure strain results, neither model indicated a loss in failure strain as seen in the experiments.

Pavier and Chester [29] noted a similar result using a two-dimensional finite element analysis. They noted that an unsymmetric sublaminate, created when a symmetric laminate delaminates, did not experience significant deflection. Although the unsymmetric laminate has bend/stretch coupling effects, these effects were suppressed by the clamped specimen boundary conditions. Without significant deflection, no loss in failure strain was observed.

5.2.2 Effect of Broken 0° Fibers

Careful examination of initial damage states in the specimens indicated the presence of damage in addition to the isolated delaminations. Fibers were broken in the first 0° ply under the load nose of the three-point bend fixture. The effects of this type of damage were examined using a model similar to that for the undamaged specimen, but with the addition of a simulated broken fiber at the top center where the experiments indicated fiber breaks. The simulation was accomplished using equation 5.3.

Deformed mesh results are shown in Figure 5.5. The failure strain for the model with a damaged 0° ply was significantly lower than for the undamaged case. Also, the location of the failure was no longer at the edge of the grips, but instead in the next 0° ply below the failed ply. An additional analysis was conducted using a model with simulated fiber breaks in the first two 0° plies to determine if failure would progress. The failure strains for two failed 0° plies were lower than for the one failed ply case, indicating that failure would progress through the thickness of

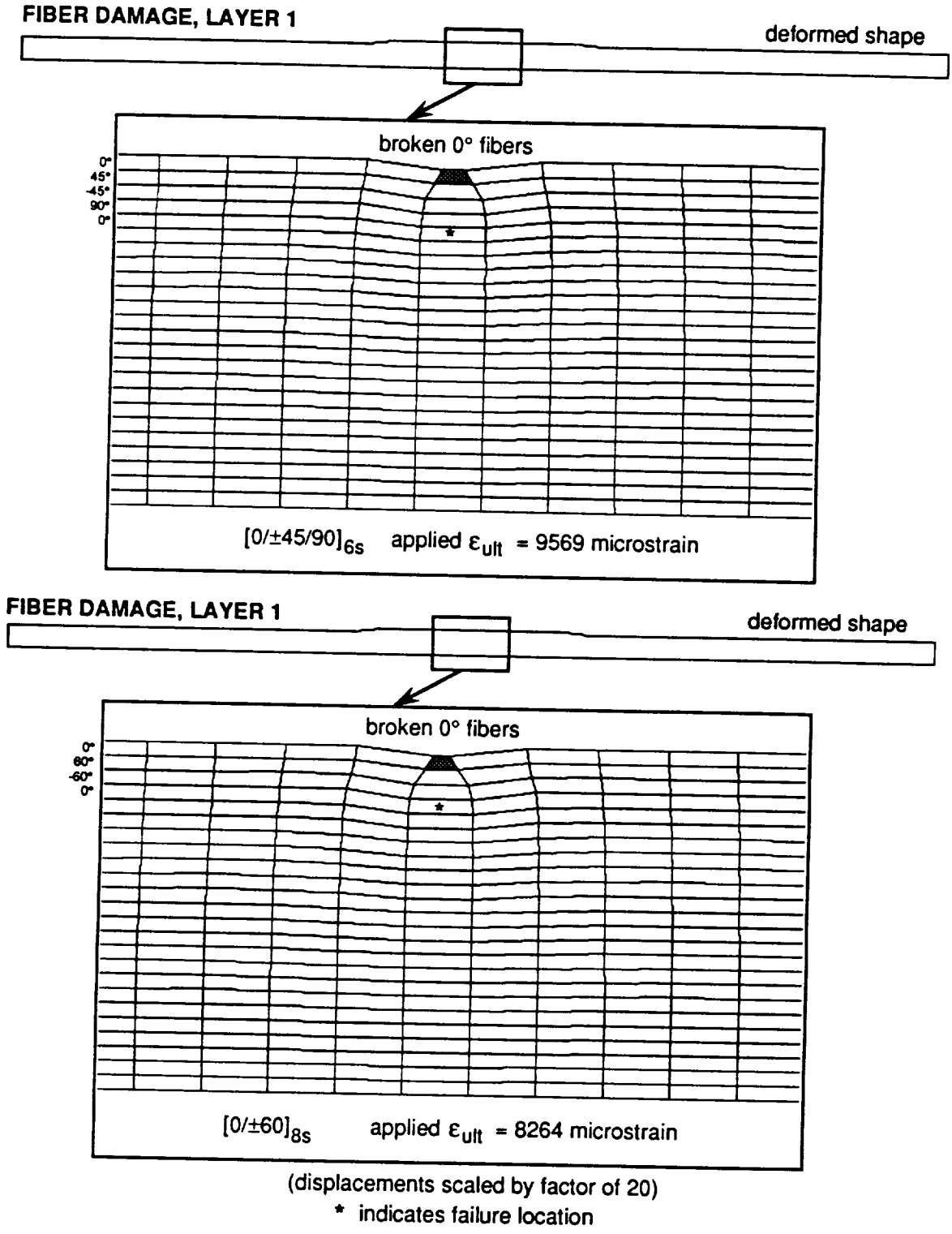

Figure 5.5 - Analysis results for 48 ply specimens, broken fibers first 0° ply

the specimen without additional applied displacement. The results for this second case can be seen in Figure 5.6.

Although the broken 0° fibers seemed to be the cause of the reduced failure strain, experimental results indicated a similar failure strain for both [0/±60] and [0/±45/90] type stacking sequences, while analysis results showed a difference. Therefore, analysis was conducted using models with both broken 0° fibers and a simulated delamination at the midplane. The addition of the midplane delamination only increased the difference between the stacking sequences, as shown in Table 5.2. Experimental observation suggests that a fiber break in the first 0° ply initiates a delamination between that 0° ply and the layer directly beneath it. Since the available set of point stress failure criteria are incapable of predicting failure by delamination initiation, this phenomenon could not be verified.

However, a delamination could be simulated beneath the fiber break using equation 5.4. For a very short delamination, 0.09 in., the failure strains for both stacking sequences were found to increase, but by differing amounts. Final models were evaluated with all three initial damage components, the broken fibers, the delamination beneath the 0° layer, and a simulated delamination at the midplane. Resulting failure strain show only a small difference between stacking sequences, which would not be detectable in the experimental results. All of the numerical results are summarized in Table 5.2.

The experimental results for those specimens with fiber breaks in the first 0° layer and/or isolated long delaminations are shown in Table 5.3. Normalized failure strains for the final analytical model and the experimental results agree fairly well. The reduction in failure strain, and therefore failure stress, can be attributed primarily to the presence of fiber damage in the

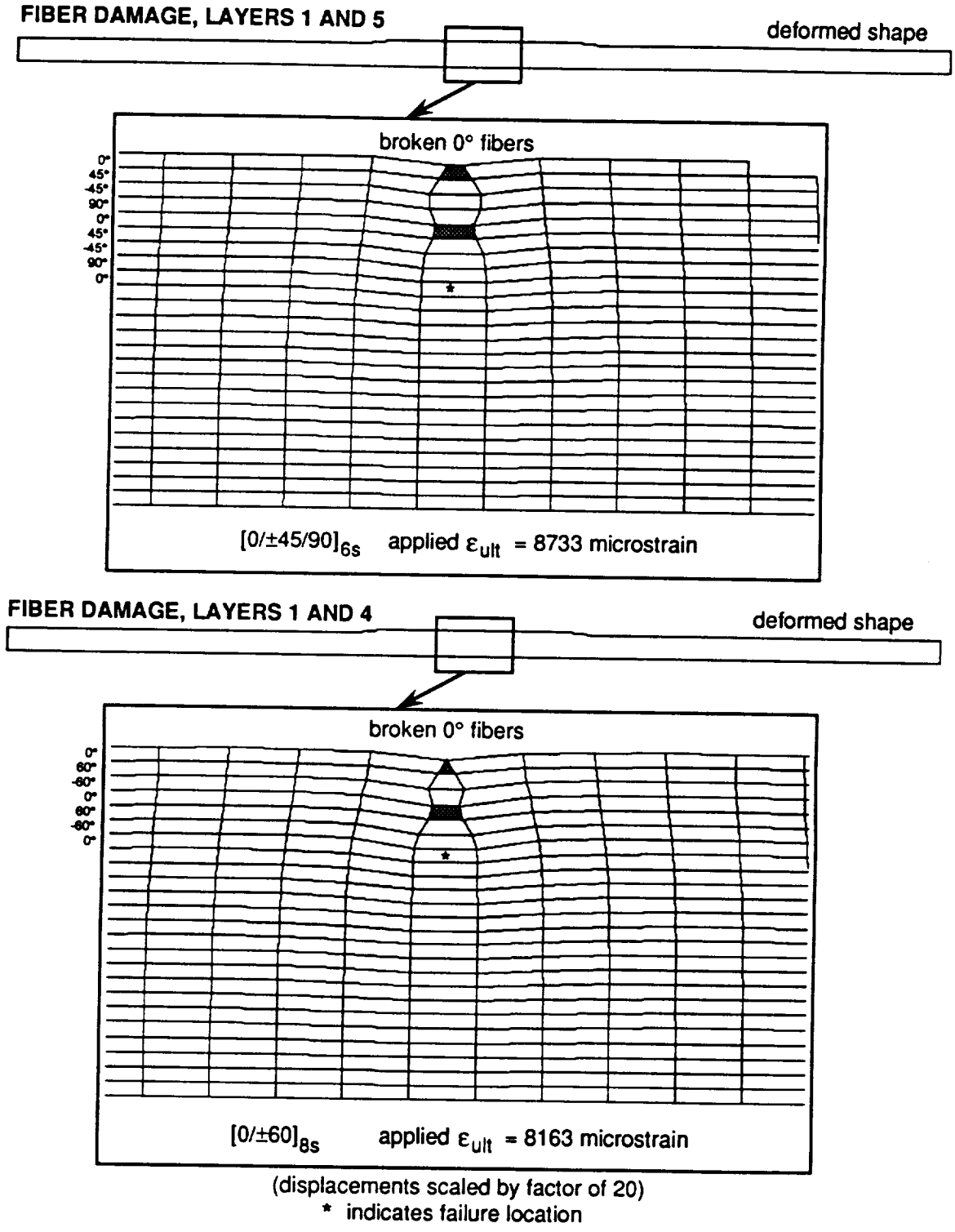

Figure 5.6 - Analysis results for 48-ply specimens, broken fibers two 0° plies

Table 5.2 - Analysis results for 48-ply specimens, $[0/\pm45/90]_{6s}$ and $[0/\pm60]_{8s}$

Damage Description	$[0/\pm45/90]_{6s}$ Normalized Failure Strain	$[0/\pm60]_{8s}$ Normalized Failure Strain
delamination at midplane	1.0	1.0
simulated delam. at midplane	1.0	1.0
broken fiber, first 0° layer	0.91	0.79
broken fibers, first and second 0° layers	0.83	0.78
broken fiber, first 0° layer simulated delam. at midplane	0.88	0.75
broken fiber, first 0° layer delamination after first 0° layer	0.91	0.83
broken fiber, first 0° layer delamination after first 0° layers simulated delam. at midplane	0.85	0.78

Table 5.3 - Experimental results for 48-ply and 60-ply specimens, $[0/\pm45/90]_{6s}$, $[0/\pm45/90]_{15s}$, and $[0/\pm60]_{8s}$

Specimen		Damage Description	Normalized Failure Strain
Q8-7	$[0/\pm60]_{8s}$	delamination at midplane	0.83
Q15-2	$[0/\pm45/90]_{15s}$	delamination at midplane	0.86
Q15-6	$[0/\pm45/90]_{15s}$	delamination at midplane matrix cracks under load nose, first 4 ply groups	0.90
Q6-7	$[0/\pm45/90]_{6s}$	delamination at midplane delamination 12 plies from bottom	0.66
Q8-3	$[0/\pm60]_{8s}$	delamination 15 plies from top delamination 15 plies from bottom	0.75
Average		**specimens with isolated delaminations**	**0.80**
Q8-1	$[0/\pm60]_{8s}$	broken fibers, first 0° layer	0.92
Q8-6	$[0/\pm60]_{8s}$	broken fibers, first 0° layer delamination after first 0° layer	0.81
Q6-5	$[0/\pm45/90]_{6s}$	broken fibers, first 0° layer *	0.87

* This specimen also contains matrix tension cracks at the edges of the specimen in the last 9 plies

outermost 0° ply. The midplane delamination seems to have little or no effect on the predicted failure strain.

5.3 Grouped Ply Stacking Sequences

Experimental results show a decrease in strength for undamaged specimens when the stacking is changed from interspered, ($[0/\pm60]_{3S}$ and $[0/\pm45/90]_{2S}$), to grouped ($[0_5/60_5/-60_5]_{7s}$ and $[0_5/45_5/-45_5/90_5]_{5s}$). Both interspersed sequences have similar undamaged strengths, as shown in Table 5.4. The $[0_5/60_5/-60_5]_{7s}$ grouped stacking sequence has a slightly lower undamaged strength (12%) while the $[0_5/45_5/-45_5/90_5]_{5s}$ grouped stacking sequence has an even lower undamaged strength (33%). These results are also shown in Figures 4.3 and 4.5.

An analysis comparing the grouped and interspersed cases was conducted using the same finite element program as for the isolated long delamination case. The cross section and boundary conditions are the same as the undamaged specimen from Figure 5.2. The symmetric model has 200 elements along its 6 in. length, with one element per layer. Rather than modelling all 200 to 210 layers, models with a reduced number of layers were employed. For the [0/±60] family, 30 layers were modelled with stacking sequences of $[0/\pm60]_{10s}$ and $[0_5/60_5/-60_5]_{2s}$. A slightly larger model with 40 layers was used to study the [0/±45/90] family, with stacking sequences of $[0/\pm45/90]_{10s}$ and $[0_5/45_5/-45_5/90_5]_{2s}$.

The first attempt to model the undamaged strength produced the same failure strain for all four cases. Returning to the experimental observations, it was noted that 0° fibers begin breaking off of the corners of the specimens at strains of about 13000 μ. However, since these fibers fail

Table 5.4 - Experimental results for comparison of grouped and interspersed ply undamaged laminate strengths

Specimen	Stacking Sequence	Failure Stress (psi)	Failure Strain (μ)
Q35-9	$[0/\pm60]_{35s}$	93650	13367
Q35-10	$[0/\pm60]_{35s}$	92222	13427
Q7-10	$[0_5/60_5/-60_5]_{7s}$	82019	12268
Q25-9	$[0/\pm45/90]_{25s}$	100437	15042
Q25-10	$[0/\pm45/90]_{25s}$	97711	15664
A5	$[0/\pm45/90]_{25s}$	100825	15771
Q5-10	$[0_5/45_5/-45_5/90_5]_{5s}$	64381	7545
Q5-11	$[0_5/45_5/-45_5/90_5]_{5s}$	67918	9222

Note:

- Specimen Q35-11 is not included because its width is significantly less than the other specimens, yielding a greater failure stress and strain.
- Specimen B7 is not included due to its high percentage of initial matrix cracks.

due to bending in both the y and z directions, the two-dimensional analysis used here is unable to predict this failure. Additionally, the effect of individual 0° fiber failure on the redistribution of stresses and the progression of damage is also beyond the capabilities of this two-dimensional analysis. That is, whether load is transferred to fibers next to the failure in the y-direction or the z-direction cannot be determined.

An analysis was conducted with the properties of one 0° element at the edge of the grips reduced according to equation (5.3) for the $[0_5/60_5/-60_5]_{2s}$ and $[0_5/45_5/-45_5/90_5]_{2s}$ models. For both cases, the next failure was located in the 0° element directly below the fiber failure at a strain of 0.62%.

5.3.1 $[0_5/60_5/-60_5]_{2s}$ vs. $[0/\pm60]_{10s}$ Stacking Sequences

An assumption was made that the fiber failure which initiated at the specimen corners continued through and across the outside 0° ply at a strain of 6200 μ. A numerical analysis was conducted using a model with the stiffness of the outside 0° layer reduced (C_{11} , C_{12} , C_{13}, C_{55}, and C_{66}) at the edge of the grips, to represent fiber breakage according to equation (5.3), for the $[0/\pm60]_{10s}$ case. All five outside 0° layers were reduced in a second model for the $[0_5/60_5/-60_5]_{2s}$ case. These models are shown in Figure 5.7. Results indicated that the next failure for the interspersed $[0/\pm60]_{10s}$ case occurred in the next 0° ply below the initial fiber damage. However, for the grouped $[0_5/60_5/-60_5]_{2s}$ case, failure was located in the 60° ply adjacent to the broken fiber 0° layers. The actual strains at which these failures occurred is known to be inaccurate due to the two-dimensional representation of this three dimensional problem, but the trend is significant. Failure of the 0° ply in the interspersed case occurred at a strain of 8400 μ, while failure of the 60° ply in the grouped case occurred at a strain of 7700 μ.

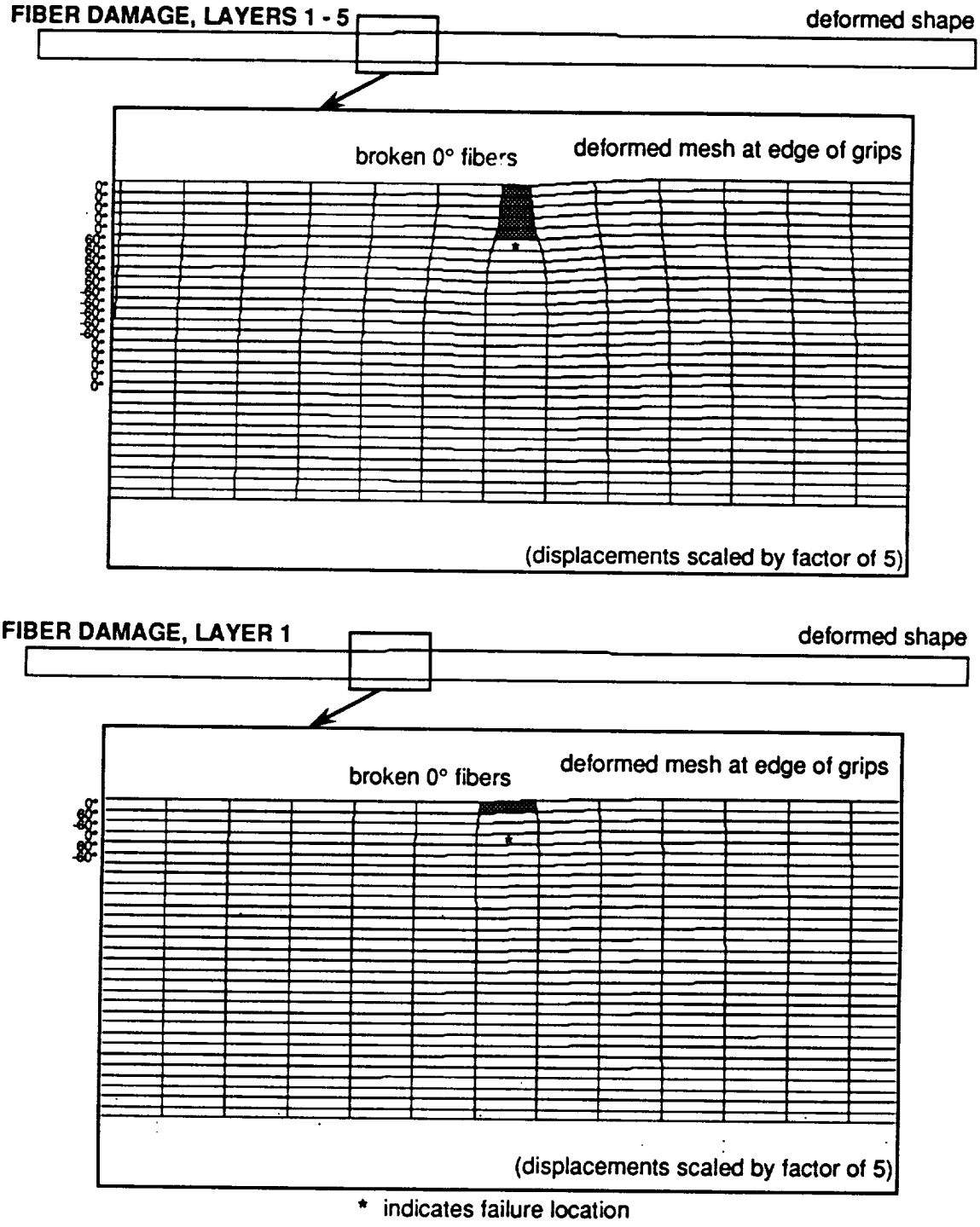

Figure 5.7 - Analysis results for $[0_5/60_5/\text{-}60_5]_{2s}$ and $[0/\pm60]_{10s}$ specimens, broken fibers outside 0° plies

This follows the experimental data which indicates a lower failure strain for the grouped ply laminate. According to this analysis, the reduction is due to a loss of five outside 0° plies for the grouped case versus one outside 0° ply for the interspersed case, all due to the fixture effects at the edge of the grips.

5.3.2 $[0_5/45_5/-45_5/90_5]_{2s}$ vs. $[0/\pm45/90]_{10s}$ Stacking Sequences

The same assumption that was made for the [0/±60] type cases was made here. That is, fiber failure which initiated at the corners of the specimens was assumed to traverse through and across the outside 0° plies at a stress of 6200 μ. The model for the interspersed $[0/\pm45/90]_{10s}$ case included one reduced element with reduced stiffness (C_{11} , C_{12} , C_{13}, C_{55}, and C_{66}) in the outside 0° layer. The model for the grouped case included five reduced elements to represent fiber failure in the first five outside 0° layers. These models are shown in Figure 5.8. Similar to the results for the [0/±60] family, the location of the next failure differed for the grouped and interspersed cases. For the $[0/\pm45/90]_{10s}$ case, failure proceeded to the 0° ply below the outside, damaged 0° ply. This occurred at a strain of 9700 μ, although again the actual value is inaccurate due to the two-dimensional representation. For the grouped $[0_5/45_5/-45_5/90_5]_{2s}$ case, failure occurred in the 45° layer directly adjacent to the broken 0° fibers. This occurred at a much lower strain of 5100 μ, indicating that as soon as the five outside 0° plies failed, so did the 45° ply immediately below. This again follows the trend of the experimental data, which suggests a lower failure strain for the grouped ply case. Moreover, the analysis also suggests a lower failure strain for the $[0_5/45_5/-45_5/90_5]_{2s}$ case than the $[0_5/60_5/-60_5]_{2s}$ case, which is also noted in the experimental results.

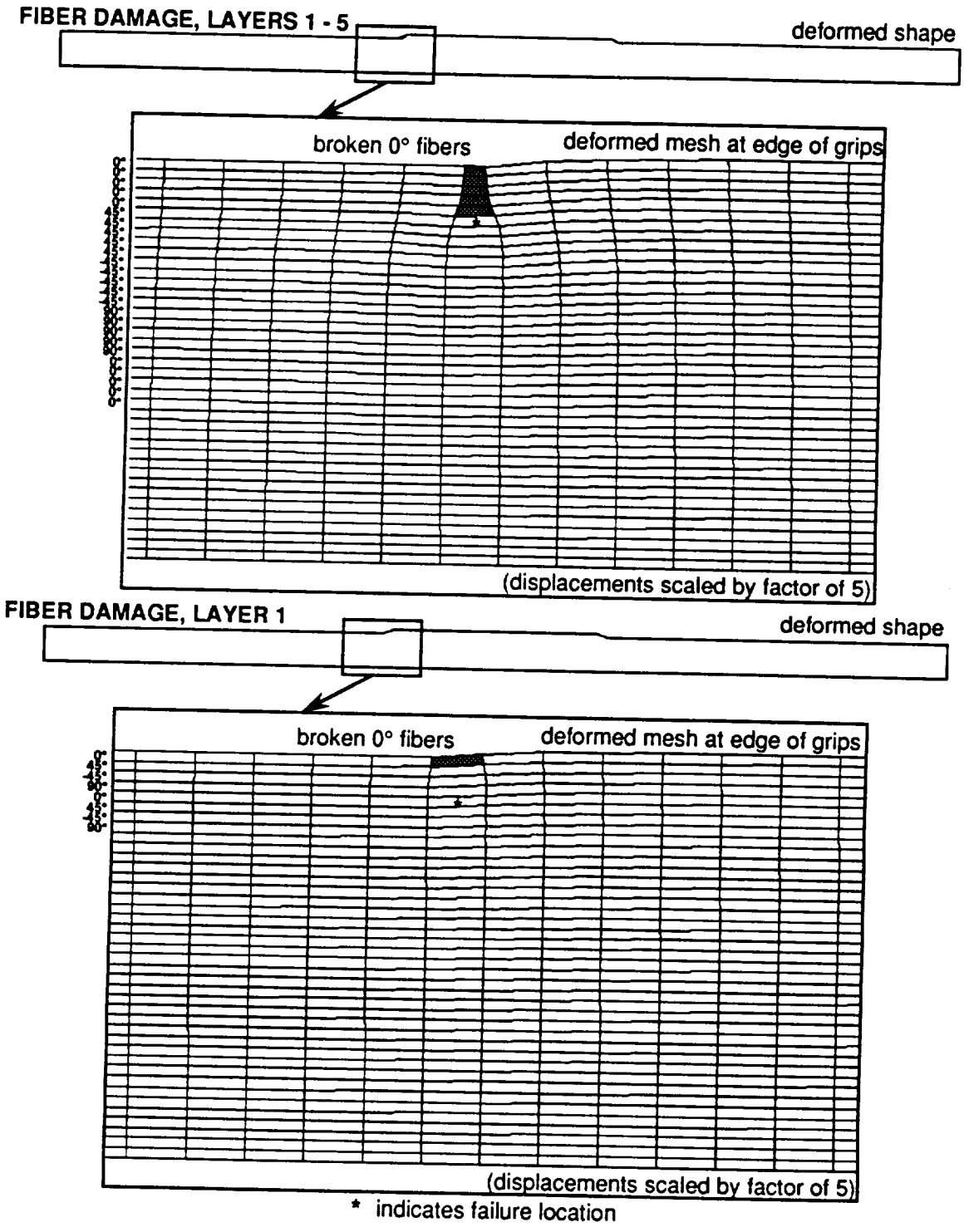

Figure 5.8 - Analysis results for $[0_5/45_5/-45_5/90_5]_{2s}$ and $[0/\pm45/90]_{10s}$ specimens, broken fibers outside 0° plies

5.3.3 Free Edge Effects

Herakovich [46, 47] studied the effects of grouped or clustered plies on the interlaminar shear stresses near the free edge. Maximum shear and normal interlaminar stresses (τ_{yz}, τ_{zx} and σ_z) were found to increase for greater ply thickness. These effects were studied using the finite element program CLFE2D [41] with a unit value for ε_x^o. It was noted that the magnitudes of the interlaminar shear stresses, as determined by finite element analysis, are a function of the selected finite element grid. However, relative comparisons can be made between different stacking sequences evaluated with the same grid. Looking specifically at the effects of interlaminar stresses on compression strength, Vizzini and Mueller [48] noted experimentally that compression strength was reduced for a $[45_n/\text{-}45_n/0_n]_s$ stacking sequence as n was increased. They suggested that this was due to the corresponding increase in interlaminar stresses.

In order to study this phenomenon for the present case, a quarter plane symmetric finite element model was constructed of the y-z cross section, as shown in Figure 5.9. According to Whitcomb and Raju [49], the distribution of interlaminar stresses for a thick laminate consisting of stacked, repeating units is insensitive to total laminate thickness. Therefore, only one repeating unit was modeled for the grouped ply laminate cases, $[0_5/45_5/\text{-}45_5/90_5]_s$ and $[0_5/60_5/60_5]_s$. For the specimens used for comparison from the experimental work, the width and thickness were approximately equal. Therefore, the width of these models is equal to the thickness of 20 plies, or 0.1 in., corresponding to the thickness of the $[0_5/45_5/\text{-}45_5/90_5]_s$ case. The mesh consisted of elements 0.0025 in. in the z-direction and 0.005 in. in the y direction. This corresponded to two elements per layer.

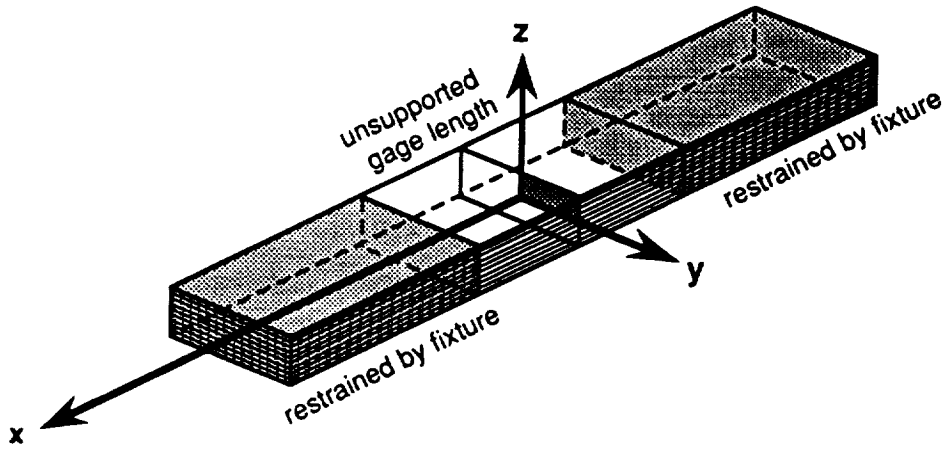

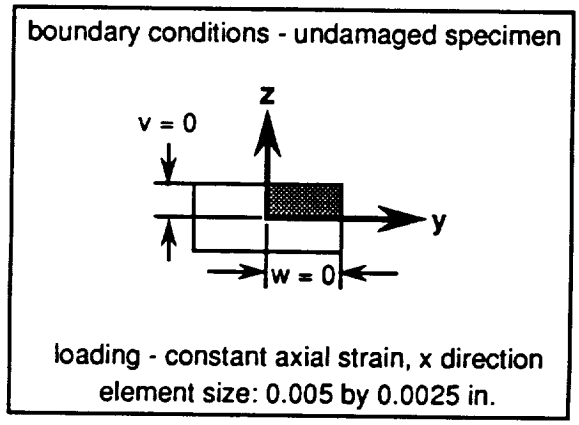

Figure 5.9 - Model and boundary conditions for study of edge effects

The deformed meshes for the [0/±45/90] family are shown in Figure 5.10, while the deformed meshes for the [0/±60] type cases are shown in Figure 5.11. The interlaminar normal stress (σ_z) should be positive for mesh expansion ($+\varepsilon_z$) and negative for mesh contraction ($-\varepsilon_z$). The deformations near the free edge are significantly greater for the [0/±45/90] family than for the [0/±60] cases, indicating a likely difference in the interlaminar normal stresses. The interlaminar stresses near the free edge, τ_{yz}, τ_{zx} and σ_z, are shown in Figure 5.12 and 5.13. The curves are somewhat irregular due to the coarseness of the grid. However, the maximum interlaminar stresses have a greater magnitude of the [0/±45/90] stacking than for the [0/±60] stacking, which corresponds to the deformed mesh predictions. This was explained by Herakovich [47] as being due to the greater difference in coefficients of mutual influence ($\eta_{xy,x}$) for +45/-45 interfaces than for +60/-60 interfaces.

Hashin's [44] failure criterion for matrix tension failure (equation 5.4) was used due to the criterion's dependence on the transformed interlaminar stresses σ_{33}, τ_{31},and τ_{23}. Failure for the $[0/\pm45/90]_{5s}$ case was predicted at 7250 μ while failure for the $[0_5/45_5/-45_5/90_5]_s$ case was predicted at 6000 μ. Recall that the actual magnitudes of the predicted failure strain are a function of finite element grid size, and are therefore not suitable for direct comparison with experiment. However, the 17% reduction in strength for the grouped case does follow the experimental trend. Meanwhile, failure for the [0/±60] type cases was not predicted even for strains greater than 11000 μ, indicating that failure does not occur due to matrix tension.

In addition to the experimentally noted reduction in strength for grouped ply laminates, an overall difference was noted in the failure modes of [0/±45/90] and [0/±60] type laminates. The [0/±45/90] family failed instantaneously through the entire thickness of the specimens, while the [0/±60] family failed in the outer plies first. The analysis results for free edge interlaminar

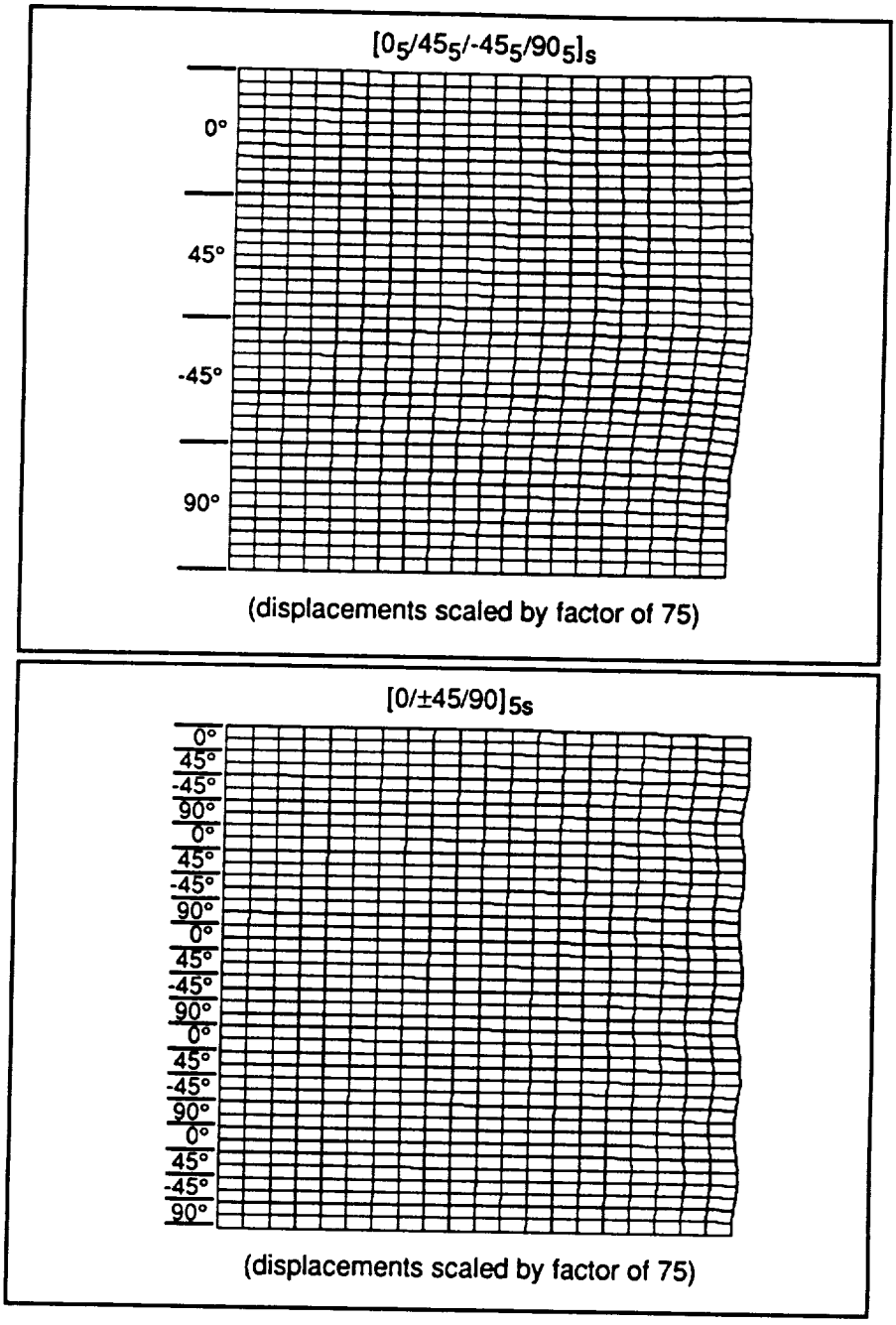

Figure 5.10 - Analysis results for $[0_5/45_5/-45_5/90_5]_s$ and $[0/\pm45/90]_{5s}$ specimens, deformations at free edge

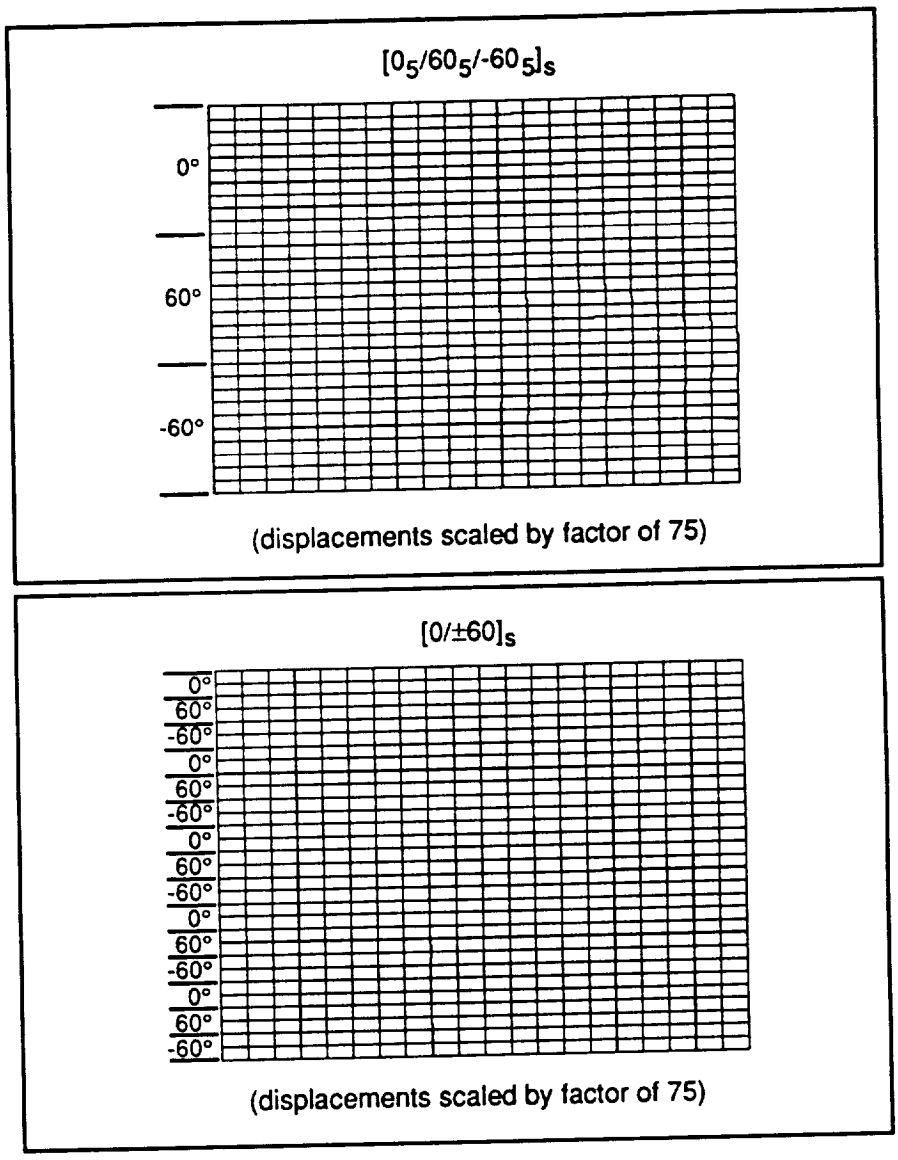

Figure 5.11 - Analysis results for $[0_5/60_5/\text{-}60_5]_s$ and $[0/\pm60]_{5s}$ specimens, deformations at free edge

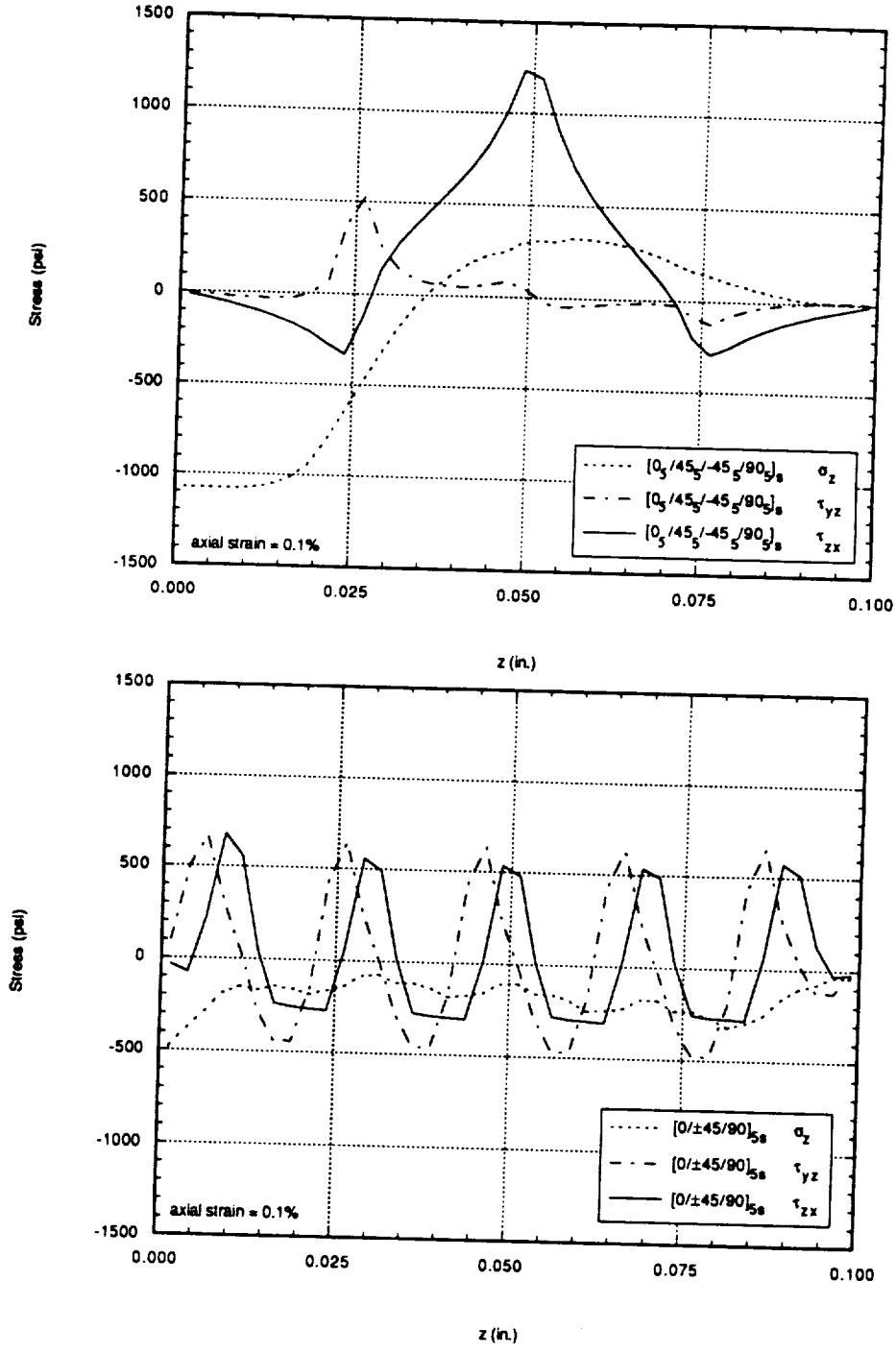

Figure 5.12 - Free edge stresses through the thickness, $[0_5/45_5/-45_5/90_5]_s$ and $[0/\pm45/90]_{5s}$ stacking sequences

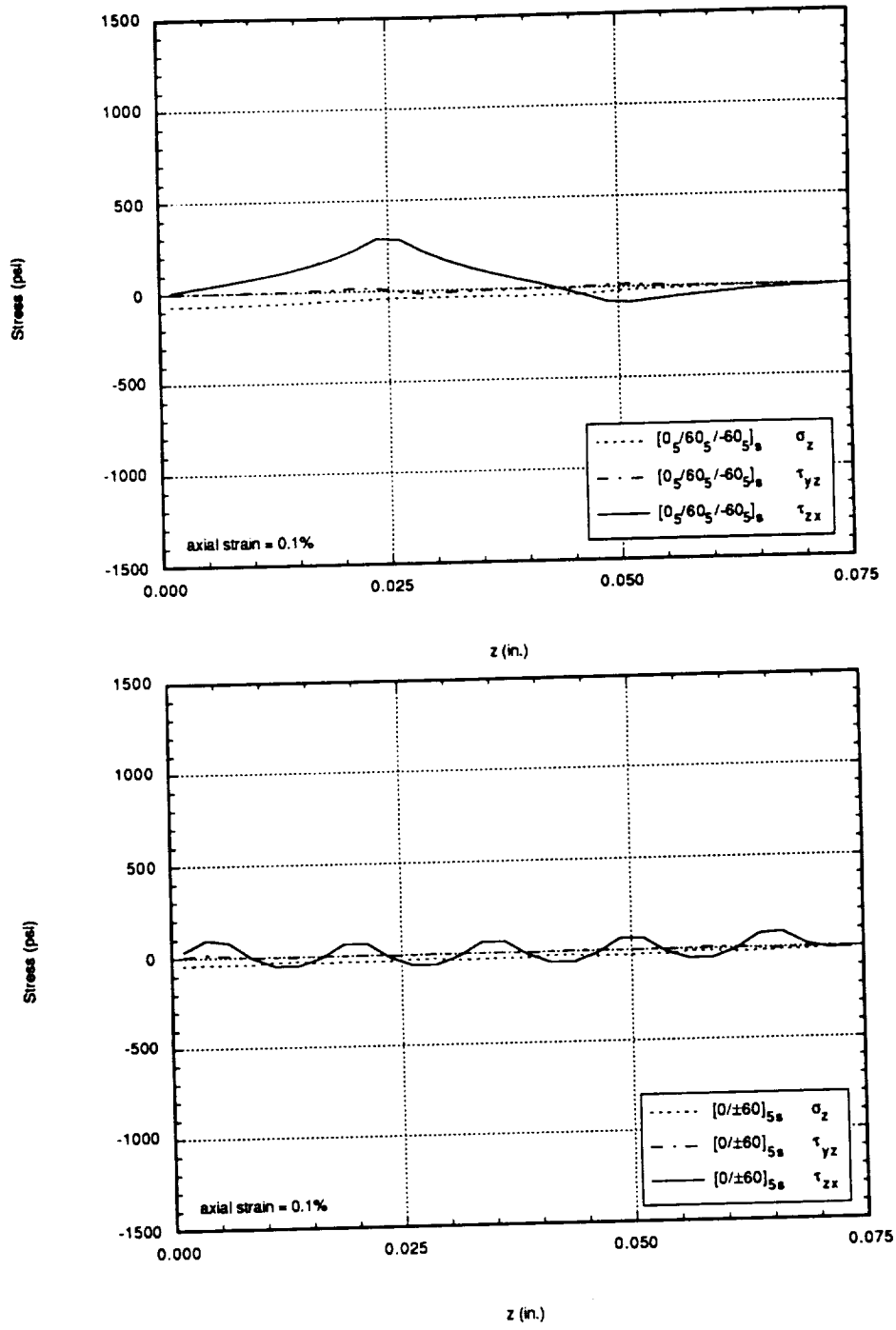

Figure 5.13 - Free edge stresses through the thickness, $[0_5/60_5/-60_5]_s$ and $[0/\pm60]_{5s}$ stacking sequences

stresses suggest that this trend may be due to the significant interlaminar edge stresses in the [0/±45/90] type specimens.

Chapter 6
Summary and Conclusions

The main objective of this research was to determine the effect of initial damage on compression strength and failure modes of beam-like specimens with various stacking sequences. The study included eight different stacking sequences, $[0/\pm45/90]_{6s}$, $[0/\pm45/90]_{15s}$, $[0/\pm45/90]_{25s}$, $[0_5/45_5/-45_5/90_5]_{5s}$, $[0/\pm60]_{8s}$, $[0/\pm60]_{20s}$, $[0/\pm60]_{35s}$, and $[0_5/60_5/-60_5]_{7s}$. The stacking sequences resulted in four thicknesses, ranging from 0.24 to 1.1 inches. Initial damage was induced during a previous study [1] conducted to evaluate the effects of various geometric and lamination parameters on the damage initiation and progression in three-point bend specimens. The stacking sequence, thickness, and three-point bend span was varied by Starbuck et al. [1] during the previous study. During the present study, more detailed damage descriptions were obtained beyond the examination and identification conducted by Starbuck. A thorough examination of the specimens using edge replicas and x-rays yielded four different initial damage modes, which were categorized as multiple through-thickness delaminations, isolated delaminations, damage near the surface, and matrix cracks in grouped ply laminates. A compression testing fixture was selected to

account for varying specimen thickness at a constant length and width, and quasi-static compression testing was conducted. Experimental compression results were compared according to the initial damage modes. A finite element analysis was conducted to further understand the experimental findings that were not addressed by previous analytical work in the literature.

6.1 Summary of Results Based On Initial Damage States

6.1.1 Compression of Undamaged Specimens

(1) The compression strength of undamaged specimens is the same for both $[0/\pm60]_{ns}$ and $[0/\pm45/90]_{ns}$ stacking sequences. This can be attributed to the fact that both sequences have 0° plies on the outer surface, which causes failure to initiate at fiber breakage at the edges of the compression fixture grips.

(2) Specimens with $[0/\pm45/90]_{ns}$ and $[0_5/+45_5/-45_5/90_5]_{5s}$ stacking sequences exhibit compression failure modes with failure extending through the thickness of the specimen. Meanwhile, specimens with $[0/\pm60]_{ns}$ ($n\geq20$) and $[0_5/60_5/-60_5]_{7s}$ stacking sequences have compression failure modes which include only the outside plies where failure first initiates. This is most likely due to the presences of high interlaminar stresses near the edges in the [0/±45/90] type specimens, which are insignificant in the [0/±60] type specimens.

6.1.2 Multiple Through-Thickness Delaminations

(3) The compression strength of specimens with one delamination per ply set was from 50% to 75% below the compression strength of similar undamaged specimens. For delaminations of equal length (approximately 0.2 inches) and density (one delamination per ply set), the reduction in compression strength was approximately the same for specimens with $[0/\pm45/90]_{6s}$, $[0/\pm45/90]_{15s}$, and $[0/\pm45/90]_{25s}$ stacking sequences. This implies that the thickness of the sublaminates, and not the thickness of the specimens, determines the value of the compression strength for multiple through-thickness delaminations of similar length.

(4) The compression failure mode changed according to the length of the delaminations. For delaminations of length 0.4 in. or less, failure was antisymmetric, as descried by Lee et al. [40]. This failure mode was experimentally noted by Williams and Rhodes [22] and termed a transverse shear mode failure. Longer delaminations, between 0.4 and 0.6 in. in length, failed in a symmetric mode. This was also described in the analysis by Lee et al. [40].

6.1.3 Isolated Long Delaminations

(5) A damage state consisting only of delaminations was not actually achieved from three-point bend testing. Instead, a damage state which consisted of both delaminations and fiber damage from the three-point bend load nose was achieved. For delaminations far from the surface, the combination of isolated delamination and localized fiber breaks

resulted in experimental compression strengths that were approximately 20% below the undamaged compression strengths. This loss was apparent for all specimens with 1 or 2 delaminations located far from the top or bottom surfaces of the specimen.

(6) Two-dimensional, generalized plane strain finite element analysis indicated that the majority of the loss in compression strength could be attributed to the broken 0° fibers in the first layer where the load nose of the three-point bend fixture contacted the specimen.

(7) The two-dimensional finite element analysis also verified the result noted by Pavier and Chester [29]. That is, the unsymmetric sublaminates that are generated due to the delamination of symmetric laminates did not experience significant deflection. The bend/stretch coupling effects of the unsymmetric laminate were prevented from causing deflection due to the clamped boundary condition of the specimen.

6.1.4 Damage Near the Surface

(8) The failure mode for thick specimens (thickness $\geq$ 1.0 in.) was sublaminate buckling, as noted in [19,20,22,23,24,27,28,29]. Analysis to verify this can by found in [21,30-39]. Although the failure of thin specimens (thickness < 1.0 in.) may have initiated as sublaminate buckling, specimens failed through their entire thickness before the testing could be stopped.

6.1.5 Grouped Stacking Sequences

(9) The failure strength of undamaged $[0_5/60_5/-60_5]_{7s}$ specimens was approximately 12% below the strength of the interspersed specimens with the same thickness. This could not be attributed to increased interlaminar stresses at the free edges since these stresses were insignificant. The loss is attributed to the presence of five 0° plies at each surface of the specimen. When failure initiates due to the fixture grip, failure of the outside 0° plies occurs. The finite element analysis indicated that the loss of these five 0° plies versus only one 0° ply for the interspersed case causes the failure strength to be lower for the grouped ply case.

(10) The compression failure modes appear to be the same for all the $[0_5/+45_5/-45_5/90_5]_{5s}$ specimens, regardless of the initial damage. This is believed to be due to the presence of increased interlaminar stresses near the free edges of the specimen. The undamaged failure strength is approximately 33% below the strength of the interspersed specimens with the same thickness. This difference is believed to be due to both the interlaminar stresses and the concentration of 0° plies at the outside surfaces.

6.2 Concluding Remarks

The damage mode that caused the greatest loss in compression strength was multiple through-thickness delaminations, with a strength loss of 50-75%. This suggests, as noted previously in

[23], that damage area is not a reliable method of predicting compression strength. The isolated delaminations were longer, and thus covered a greater area as viewed from the top by x-ray, but the strength loss was only about 20%. And, in fact, even this loss cannot be conclusively attributed to the presence of delamination. The damage that occurred in the outside 0° plies was found to cause strength loss due to damage from three-point bend testing or due to stress concentrations at the edges of the grips. The compression strength loss of the $[0_5/60_5/-60_5]_{7s}$ specimens may be due entirely to the presence of 0° plies at the outside surfaces. A combination of 0°, 60°, and -60° plies that did not include 0° plies at the outside may not have shown this strength loss.

The strength loss for specimens with less through-the-thickness damage than the multiple through-thickness type specimens showed compression strengths that varied according to the amount of initial damage. As the damage involved more and more ply sets near the surface, the strength continued to decrease until the case of delaminations in every ply set was reached and the 50-75% strength loss was attained. Analysis in the literature has been concentrating on the idea of sublaminate buckling for specimens with multiple delaminations, however these experimental results suggest the need for further work which does not assume separate sublaminate buckling.

The initial damage mode most like impact damage, as reported in Refs. [19,22,23], was multiple through-thickness delaminations. Compression failure of these laminates is best explained by Lee et al. [40], suggesting the need for further work in combining multiple delamination buckling analyses with experimental results as a way of understanding compression after impact.

References

1. Starbuck, J. M., Gürdal, Z., Pindera, M., and Poe, C.C. "Damage States in Laminated Composite Three-Point Bend Specimens - An Experimental/Analytical Correlation Study," CCMS-90-06, VPI-E-90-11, Virginia Polytechnic Institute and State University, July 1990.

2. Camponeschi, E. T. Jr. "Compression Response of Thick-Section Composite Materials," David Taylor Research Center Report, DTRC-SME-90/60, October 1990.

3. Shuart, M. J. "Short Wavelength Buckling and Shear Failures for Compression-Loaded Composite Laminates," NASA-TM-87640, Nov. 1985.

4. Adams, D. F. "A Comparison of Composite Material Compression Test Methods in Current Use," *Proceedings of the 34th International SAMPE Symposium*, May 1989, pp. 1422-1433.

5. Schoeppner, G. A. and Sierakowski, R. L. "A Review of Compression Test Methods for Organic Matrix Composites," *Journal of Composites Technology & Research*, Vol. 12, No. 1, Spring 1990, pp. 3-12.

6. "Compressive Properties of Unidirectional or Crossply Fiber-Resin Composites," ASTM Standard D 3410-87, American Society for Testing and Materials, Philadelphia, Pennsylvania.

7. "Price List and Specifications Brochures: Composite Material Mechanical Test Fixtures," Wyoming Test Fixtures, Inc., Laramie, Wyoming, May 1989.

8. Clark, R. K., and Lisagor, W. B. "Compression Testing of Graphite/Epoxy Composite Materials," *Test Methods and Design Allowables for Fibrous Composites*, ASTM STP 734, C. C. Chamis, Ed., American Society for Testing and Materials, 1981, pp. 34-53.

9. Gürdal, Z., and Starbuck, J. M. "Compressive Characterization of Unidirectional Composite Materials," *Analytical and Testing Methodologies for Design with Advanced Materials*, 1988, pp. 337-347.

10. Shuart, M. J. "Failure of Compression-Loaded Multidirectional Composite Laminates," *AIAA Journal*, Vol. 27, No. 9, September 1989, pp. 1274-1279.

11. Adams, D. F. and Lewis, E. Q. "Influence of Specimen Gage Length and Loading Method on the Axial Compressive Strength of a Unidirectional Composite Material," submitted for publication in *Experimental Mechanics*.

12. Smoot, M.A. "Compressive Response of Hercules AS1/3501-6 Graphite/Epoxy Composites," CCM Report 82-16, University of Delaware, June 1982.

13. Rosen, B. W. "Mechanics of Composite Strengthening," *Fiber Composite Materials*, American Society for Metals, Metals Park, OH, 1965, pp. 37-75.

14. Argon, A. S. "Fracture of Composites," *Treatise on Materials Science and Technology*, Vol. 1, 1972, pp. 106-114.

15. Budiansky, B. "Micromechanics," *Computers and Structures*, Vol. 16, No. 1-4, 1983, pp. 3-12.

16. Wass, A. M., Babcock, C. D. Jr., and Knauss, W. G. "A Mechanical Model for Elastic Fiber Microbuckling," *Transactions of the ASME Journal of Applied Mechanics*, Vol. 57, March 1990, pp. 138-149.

17. Gürdal, Z. and Hafka, R. T. "Compressive Failure Model for Anisotropic Plates with a Cutout," *AIAA Journal*, Vol. 25, No. 11, 1987, pp. 1476-1481.

18. Starnes, J. H. Jr., Rhodes, M. D. and Williams, J. G. "Effect of Impact Damage and Holes on the Compressive Strength of a Graphite/Epoxy Laminate," *Nondestructive Evaluation and Flaw Criticality for Composite Materials*, ASTM STP 696, R. B. Pipes, Ed., American Society for Testing and Materials, 1979, pp. 145-171.

19. Rhodes, M. D. , Williams, J. G. , and Starnes, J. H. Jr. "Low-Velocity Impact Damage in Graphite-Fiber Reinforced Epoxy Laminates," Presented and the 34th Annual Conference Reinforced Plastics/Composite Institute, The Society of the Plastics Industry, Inc., New Orleans, Louisiana, Jan. 29-Feb. 2, 1979.

20. Starnes, J. H. Jr. and Williams, J. G. "Failure Characteristics of Graphite-Epoxy Structural Components Loaded in Compression," NASA TM-84552, Sept. 1982.

21. Chai, H., Babcock, C. D., and Knauss, W. G. "One-Dimensional Modelling of Failure in Laminated Plates by Delamination Buckling," *International Journal of Solids and Structures*, Vol. 17, No. 11, 1981, pp. 1069-1083.

22. Williams, J. G. and Rhodes, M D. "Effect on Resin on Impact Damage Tolerance of Graphite/Epoxy Laminates," *Composite Materials: Testing and Design (Sixth Conference)*, ASTM STP 787, I.M. Daniels, Ed., American Society for Testing and Materials, 1982, pp. 450-480.

23. Guynn, E. G. and O'Brien, T. K. "The Influence of Lay-up and Thickness on Composite Impact Damage and Compression Strength," *Proceedings of the 26th AIAA/ASME/ASCH/AHS Structures, Structural Dynamics and Materials Conference*, Orlando, Florida, April 1985, pp. 187-196.

24. Dost, E. F., Ilcewicz, L. B., Avery, W. B., and Coxon, B. R. "The Effects of Stacking Sequence on Impact Damage Resistance and Residual Strength for Quasi-Isotropic Laminates," submitted for publication, ASTM,1990.

25. Gosse, J. H. and Mori, P. B. Y. "Impact Damage Characterization of Graphite/Epoxy Laminates," *Proceedings of the American Society for Composites, 3rd Technical Conference on Composite Materials*, Sept. 1988, pp. 344-353.

26. Avery, W. B. "A Semi-Discrete Approach to Modeling Post-Impact Compression Strength of Composite Laminates," *Proceedings of the 21st International SAMPE Technical Conference*, Vol. 21, Sept. 1989, pp. 141-151.

27. Wang, J. T. and Whitcomb, J. D. "The Effects of Base Laminate Damage on Instability-Related Delamination Growth," *AIAA-90-1021-CP*, pp. 1201-1207

28. Davidson, B.D. " An Experimental Investigation of Delamination Buckling and Growth," *Proceedings of the 31st AIAA/ASME/ASCE/AHS/ASC Structures, Structural Dynamics, and Materials Conference*, April 1990, pp. 1281-1226.

29. Davidson, B. D. "On Modelling the Residual Strength of Impact Damaged, Compression Loaded Laminates," *Proceedings of the 21st International SAMPE Technical Conference*, Vol. 21, Sept. 1989, pp. 109-119.

30. Pavier, M. J. and Chester, W. T. "Compression Failure of Carbon Fibre-Reinforced Coupons Containing Central Delaminations," *Composites*, Vol. 21, No. 1, January 1990, pp. 23-31.

31. Sallam, S. and Simitses, G. J. "Delamination Buckling and Growth of Flat, Cross-Ply Laminates," *Composite Structures*, Vol. 4, 1985, pp. 361-381.

32. Yin, W. L., Sallam, S. N. and Simitses, G. J. "Ultimate Load Carrying Capacity of Delaminated Beam-Plates" *AIAA Journal*, Vol. 24, No. 1, January 1986, pp. 123-128.

33. Shivakumar, K.N. and Whitcomb, J.D. "Buckling of a Sublaminate in a Quasi-Isotropic Composite Laminate," *Journal of Composite Materials*, Vol. 19, Jan 1985, pp. 2-18.

34. Shaw, D. and Tsai, M.Y. "Analysis of Delamination in Compressively Loaded Laminates," *Composites Science and Technology*, Vol. 34, 1989, pp. 1-17.

35. Jones, R. and Callinan, R. J. "Analysis of Compression Failure in Composite Materials," *Progress in Science and Engineering of Composites*, T. Hayashi, K. Kawata and S. Umecawa, Eds. ICCM-IV, Vol. 1, 1982, pp. 447-454.

36. Whitcomb, J. D. "Mechanics of Instability-Related Delamination Growth," NASA-TM 100622, May 1988.

37. Dost, E. F., Ilcewicz, L. B., and Gosse, J. H. "Sublaminate Stability Based Modeling of Impact-Damaged Composite Laminates," *Proceedings of the American Society for Composites, 3rd Technical Conference on Composite Materials*, Sept. 1988, pp. 354-363.

38. Ilcewicz, L. B., Dost, E. F., and Coggeshall, R. L. "A Model for Compression After Impact Strength Evaluation," *Proceedings of the 21st International SAMPE Technical Conference*, Vol. 21, Sept. 1989, pp. 130-140.

39. Davidson, B. D. "An Analysis to Predict Local Buckling in Composite Laminates Containing Multiple Delaminations," to be published, *Journal of Composite Materials.*

40. Lee, J., Gürdal, Z., and Griffin, O. H.," A Layer-wise Approach for the Bifurcation Problem in Laminated Composites with Delaminations," to be published, *Proceedings of the 33th AIAA/ASME/ASCH/AHS Structures, Structural Dynamics and Materials Conference,* Dallas, Texas, April 1992.

41. Buczek, M. B., Gregory, M. A., and Herkovich, C. T. "CLFE2D - A Generalized Plane Strain Finite Element Program for Laminated Composites Subjected to Mechanical and Hygrothermal Loading," VPI-E-83-40, College of Engineering, Virginia Polytechnic Institute and State University, Blacksburg, VA, October 1983.

42. Renieri, G. D. and Herkovich, C. T. "Nonlinear Analysis of Laminated Fibrous Composites," VPI-E-76-10, College of Engineering, Virginia Polytechnic Institute and State University, Blacksburg, VA, October 1976.

43. Ozden, O. O. and Engblom, J. J. "Analysis of Progressive Failure in Composites," *Composites Science and Technology*, Vol. 28, 1987, pp. 87-102.

44. Hashin, Z. "Failure Criteria for Unidirectional Fiber Composites," *Journal of Applied Mechanics*, Vol. 47, June 1980, pp. 329-334.

45. Hercules Prepreg Tape Materials Characterization Data Package. Hercules Composite Products Group, February 1989.

46. Herakovich, C.T. "Influence of Layer Thickness on the Strength of Angle-Ply Laminates," *Journal of Composite Materials*, Vol. 16, May 1982, pp. 216-227.

47. Herakovich, C. T. "Free Edge Effects in Laminated Composites," *Handbook of Composites Vol. 2 - Structures and Design*, Herakovich, C. T. and Tarnopol'skii, Y. M., Eds. 1989, pp. 187-230.

48. Vizzini, A. J. and Mueller, N. L. "The Effects of Thickness on Notched Laminated Composites under Uniaxial Compression," *ASC Proceedings*, 1989, pp. 859-867.

49. Whitcomb, J. D. and Raju, I. S. "Analysis of Interlaminar Stresses in Thick Composite Laminates With and Without Edge Delamination," *Delamination and Debonding of Materials,* ASTM STP 876, W. S. Johnson, Ed., American Society for Testing and Materials, Philadelphia, 1985, pp. 69-94.

BIBLIOGRAPHIC DATA SHEET	1. Report No. VPI-E-92-15; CCMS-92-16	2.	3. Recipient's Accession No.
4. Title and Subtitle Compression of Thick Laminated Composite Beams With Initial Impact-Like Damage			5. Report Date June 1992 6.
7. Author(s) N.L. Breivik, Z. Gürdal, and O.H. Griffin, Jr.			8. Performing Organization Rept. No. VPI-E-92-15, CCMS-92-16
9. Performing Organization Name and Address Virginia Polytechnic Institute and State University Department of Engineering Science and Mechanics Blacksburg, VA 24061-0219			10. Project/Task/Work Unit No. 11. Contract/Grant No. NAG-1-343 NASA-Va. Tech Composites Prog.
12. Sponsoring Organization Name and Address Mechanics of Materials Branch National Aeronautics and Space Administration Langley Research Center Hampton, VA 23665-5225			13. Type of Report & Period Covered Interim Report 90 1/90-12/91 14.

15. Supplementary Notes
Support was provided through the NASA-Virginia Tech Composites Program.
The grant monitor was C.C. Poe, Jr. of the Mechanics of Materials Branch.

16. Abstract

While the study of compression after impact of laminated composites has been under consideration for many years, the complexity of the damage initiated by low velocity impact has not lent itself to simple predictive models for compression strength. The damage modes due to non-penetrating, low velocity impact by large diameter objects can be simulated using quasi-static three-point bending. The resulting damage modes are less coupled and more easily characterized than actual impact damage modes.

This study includes the compression testing of specimens with well documented initial damage states obtained from three-point bend testing. Compression strengths and failure modes were obtained for quasi-isotropic stacking sequences from 0.24 to 1.1 inches thick with both grouped and interspersed ply stacking. Initial damage prior to compression testing was divided into four classifications based on the type, extent, and location of the damage. These classifications are multiple through-thickness delaminations, isolated delaminations, damage near the surface, and matrix cracks. Specimens from each classification were compared to specimens tested without initial damage in order to determine the effects of the initial damage on the final compression strength and failure modes. A finite element analysis was used to aid in the understanding and explanation of the experimental results.

It was found that specimens with multiple through-thickness delaminations experienced the greatest reduction in compression strength, from 50 to 75% below the strength of undamaged specimens. All the sublaminates formed by the delaminations failed at the same time. Individual sublaminate buckling was observed for isolated delaminations near the surface of the laminate. Delaminations far from the specimen surface had little effect on the final compression strength. Damage occurring in the outside 0° plies caused a 10 to 20% strength reduction according to both analytical and experimental results. The effects of increased interlaminar stresses near the specimen edges caused a reduction in undamaged strength of $[0_5/45_5/-45_5/90_5]_{5s}$ specimens, while having little effect on the $[0_5/60_5/-60_5]_{7s}$ specimens.

17. Key Words and Document Analysis. 17a. Descriptors
Compression, Laminated Composite, Damage, Delaminations, Simulated Impact

17b. Identifiers/Open-Ended Terms

17c. COSATI Field/Group

18. Availability Statement	19. Security Class (This Report) UNCLASSIFIED	21. No. of Pages 168
	20. Security Class (This Page) UNCLASSIFIED	22. Price

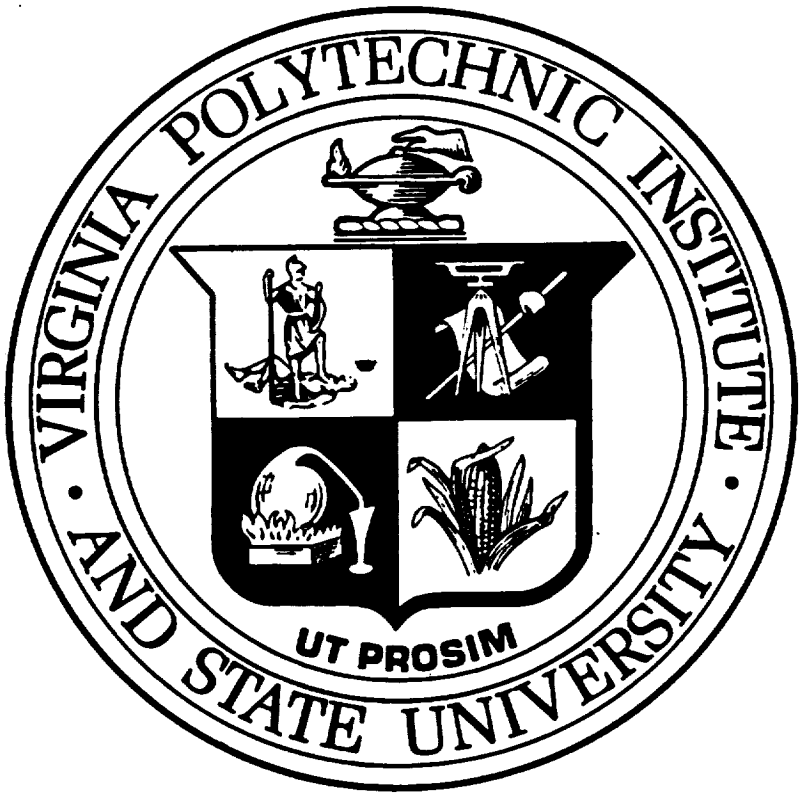

VIRGINIA TECH CENTER FOR COMPOSITE MATERIALS AND STRUCTURES

The Center for Composite Materials and Structures is a coordinating organization for research and educational activity at Virginia Tech. The Center was formed in 1982 to encourage and promote continued advances in composite materials and composite structures. Those advances will be made from the base of individual accomplishments of the sixty-five full and associate members who represent eleven different departments in three colleges.

The Center functions through an Administrative Board which is elected yearly and a Director who is elected for a three-year term. The general purposes of the Center include:

- collection and dissemination of information about composites activities at Virginia Tech,
- contact point for other organizations and individuals,
- mechanism for collective educational and research pursuits,
- forum and agency for internal interactions at Virginia Tech.

The Center for Composite Materials and Structures is supported by a vigorous program of activity at Virginia Tech that has developed since 1963. During 1988-89 and 1989-90 fiscal years sponsored research project expenditures for investigation of composite materials and structures have totalled approximately five million dollars annually.

Various Center faculty are internationally recognized for their leadership in composite materials and composite structures through books, lectures, workshops, professional society activities, and research papers.

Research is conducted in a wide variety of areas including design and analysis of composite materials and composite structures, chemistry of materials and surfaces, characterization of material properties, development of new material systems, and relations between damage and response of composites. Extensive laboratories are available for mechanical testing, nondestructive testing and evaluation, stress analysis, polymer synthesis and characterization, material surface characterization, component fabrication, and other specialties.

Educational activities include ten formal courses offered at the undergraduate and graduate levels dealing with the physics, chemistry, mechanics, and design of composite materials and structures. As of 1991, 129 Doctoral and 172 Master's students have completed graduate programs and are now active in industry, government, and education in the United States and abroad. The Center averaged 125 active student members during 1989-90 and 1990-91. Many Bachelor-level students have been trained in various aspects of composite materials and structures.

The Center has invested in the development of an administrative database (now fully operational for Center members) and a composite material properties database (now ready for data entry).

In addition to the CCMS Report Series, the Center sponsers a bi-monthly Seminar Series attended by faculty, staff, and students and the Center jointly sponsors a sesqui-annual Technical Review with the Center for Adhesive and Sealant Science which is well attended by government and corporate contacts.

MEMBERS OF THE CENTER

Aerospace and Ocean Engineering

Raphael T. Haftka
Eric R. Johnson
Rakesh K. Kapania

Chemical Engineering

Donald G. Baird
Garth L. Wilkes

Chemistry

John G. Dillard
Harry W. Gibson
James E. McGrath
Thomas C. Ward
James P. Wightman

Civil Engineering

Richard M. Barker
Richard E. Weyers

Clothing and Textiles

Jeanette M. Cardamone

Electrical Engineering

Ioannis M. Besieris
Richard O. Claus
Douglas K. Lindner

Engineering Science and Mechanics

Robert Czarnek
David A. Dillard
Normal E. Dowling
John C. Duke, Jr.
Daniel Frederick
O. Hayden Griffin, Jr.
Zafer Gurdal
Robert A. Heller
Edmund G. Henneke, II
Michael W. Hyer
Robert M. Jones
Ronald D. Kriz
Liviu Librescu
Alfred C. Loos
Don H. Morris
John Morton
Ali H. Nayfeh
Daniel Post
J. N. Reddy
Kenneth L. Reifsnider
C. W. Smith
Wayne W. Stinchcomb
Surot Thangjitham

Industrial and Systems Engineering

Joel A. Nachlas

Materials Engineering

Jesse J. Brown, Jr.
Seshu B. Desu
Ronald S. Gordon
D. P. H. Hasselman
Robert W. Hendricks
Ronald G. Kander

Mathematics

Werner E. Kohler

Mechanical Engineering

Charles E. Knight
Craig A. Rogers
Curtis H. Stern

Inquiries should be directed to:
Center for Composite Materials and Structures
Virginia Tech
Blacksburg, VA 24061-0257
Phone: (703) 231-4969
Fax: (703) 231-9452